Modulation of TRPV1 function by phosphorylation and site-directed mutagenesis: from structure to biophysics

Die Modulation der TRPV1 Funktion durch Phosphorylierung und ortsspezifische Mutagenese: von der Struktur zur Biophysik

Dissertation zur Erlangung des Doktorgrades der Naturwissenschaften

(Dr. rer. nat.)

Der Fakultät für Biologie und Vorklinischen Medizin

der Universität Regensburg

vorgelegt von

Thomas Jendryke

aus

Hagen

Im Jahr

2016

Das Promotionsgesuch wurde eingereicht am:

18.03.2016

Die Arbeit wurde angeleitet von:

Prof. Dr. C. H. Wetzel

Unterschrift:

Table of contents

1 Zusammenfassung

Der TRPV1 Rezeptor ist ein polymodal aktivierbarer Kationenkanal, der eine besondere Rolle in der Nozizeption einnimmt. Es ist bekannt, dass die positive Modulation der TRPV1 Funktion durch Proteinkinase-vermittelte Phosphorylierungsprozesse zur Ausbildung von Hyperalgesie und/oder Allodynie beiträgt. Die vorliegende Studie hat das Ziel, die funktionellen Auswirkungen der Cdk5-vermittelten Phosphorylierung des TRPV1 Rezeptors an Position Threonin-406 aufzuklären. Mit Hilfe von elektrophysiologischen Messungen konnten wir zeigen, dass die Koexpression von TRPV1 und Cdk5 in CHO Zellen eine Ca^{2+}-abhängige Desensitisierung des TRPV1 Ionenkanals verhindert. Um den Zusammenhang zwischen Struktur und Funktion der TRPV1 Phosphorylierung durch die Cdk5 zu untersuchen, haben wir verschiedene $TRPV1_{T406}$ Mutanten erstellt, welche durch Einfügen negativ geladener Aminosäurereste die Cdk5-abhängige Phosphorylierung am Threonin-406 imitieren, oder diese durch Ersetzen des Threoninrests mit Alanin inhibieren. Mit Hilfe elektrophysiologischer Ganz-Zell und Einzelkanal Messungen, sowie mit Ca^{2+}-imaging und TIRF Mikroskopie, haben wir die Funktion dieser $TRPV1_{T406}$ Mutanten durch ihre Reaktion auf verschiedene Stimuli, wie Capsaicin, Hitze oder Protonen umfassend charakterisiert. Die Funktionsanalyse ergab, dass die Modifikation an Position T406 weitreichende Folgen für die Funktion des TRPV1 Ionenkanals haben kann. Das einbringen einer negativ geladenen Aminosäure, wie z.B. Asparaginsäure, veränderte die Ligandensensitivität, die Aktivierungs- und Desensitisierungskinetik sowie die Spannungsabhängigkeit des TRPV1 Ionenkanals. Die Einzelkanal Eigenschaften von $TRPV1_{T406D}$ Ionenkanälen zeigten ebenfalls deutliche Veränderungen, die auf einen veränderten Gating-Mechanismus des Rezeptors hindeuten. Unter Berücksichtigung der publizierten hochaufgelösten 3D Struktur des TRPV1 haben wir einen möglichen (mechanistischen) Übertragungsweg unter Beteiligung der Position 406 identifiziert und diesen Weg durch gezieltes Einbringen von Alanin-Resten und elektrophysiologischer Charakterisierung der TRPV1 Mutationen überprüft. Eine Störung des Übertragungsweges führte ebenfalls zu einer veränderten Funktion des TRPV1 Ionenkanals. Die Ergebnisse zeigen, dass die Position T406 des TRPV1 eine funktionelle Schlüsselrolle einnimmt und durch Phosphorylierung an der Modulation der Kanalfunktion beteiligt ist.

2 Summary

The TRPV1 receptor is a polymodally activated cation channel acting as key receptor in nociceptive neurons. Its function is modulated by kinase-mediated phosphorylation, which contributes to the development of hyperalgesia and allodynia. In the present study, we demonstrate that TRPV1 function is strongly modulated by the Cdk5-mediated phosphorylation at amino acid residue T406. We observed that co-expression of TRPV1 and Cdk5 prevents the Ca^{2+}-dependent desensitization of the ion channel and has therefore severe consequences on receptor function. In order to understand the structural/functional consequences of TRPV1 phosphorylation in detail, we generated various $TRPV1_{T406}$ receptor variants to mimic or inhibit the Cdk5-mediated phosphorylation. The function of these newly generated $TRPV1_{T406}$ mutants was analyzed in a detailed characterization by means of electrophysiological whole-cell and single-channel experiments as well as Ca^{2+}-imaging and TIRF microscopy. TRPV1-mediated currents were induced by challenging TRPV1 expressing CHO or HEK293 cells with capsaicin, low pH or heat. Our results revealed that the function of TRPV1 receptors highly depends on position T406. The introduction of negatively charged amino acids (Asp or Glu) modulates the ligand-sensitivity, activation and desensitization kinetics as well as the voltage-dependence of TRPV1. Moreover, the analysis of the single-channel properties of $TRPV1_{WT}$ and $TRPV1_{T406D}$ revealed that the introduction of Asp at position T406 alters the ion channel gating mechanism. In order to investigate this gating mechanism in detail, we considered the high resolution 3D structure of TRPV1 and found a potential transition pathway putatively involved in the mechanistic processes provoking a conformational change of the protein and leading to the opening of the channel pore. By mutating various amino acid residues lining this transition pathway and electrophysiological analysis of the recombinant receptors, we could show that the introduction of a negative charge at position T406 induces conformational changes in the TRPV1 linker domain which influence the gating mechanism of the TRPV1 receptor. Therefore, we conclude that the Cdk5-mediated phosphorylation of TRPV1 at position T406 is an important molecular switch that influences the TRPV1-mediated nociception.

3 Introduction

3.1 Nociception and pain

The appropriate perception of noxious or potentially painful stimuli by nociceptors is crucial for life, since it prevents harm and injuries. Nociceptors are specialized sensory neurons of the trigeminal ganglion (TG) or the dorsal root ganglion (DRG). The free nerve endings in the periphery perceive noxious stimuli and transmit the information to specific nuclei in the central nervous system (Kandel et al. 2000). Trigeminal sensory neurons and dorsal root ganglion neurons are functionally and morphologically homologous, but the regions they innervate are different. Trigeminal sensory neurons innervate cranial structures such as face, lips, oral cavity, conjunctiva, and dura mater, whereas DRG neurons transmit information from the limbs and trunk (Kandel et al. 2000).

Based on the stimulus type three classes of nociceptors can be distinguished: mechanical, thermal and polymodal nociceptors. Mechanical nociceptors are excited by tactile stimuli such as pinch or squeezing. Thermal nociceptors can be subdivided into nociceptors excited by noxious heat (temperatures above 45 °C) or noxious cold (temperatures below 5 °C). Polymodal receptors were excited by various stimuli such as pinch, puncture, noxious heat or cold as well as irritant chemicals (Kandel et al. 2000). However, the nerve fiber that transmits the potential painful stimulus classifies the type of pain. Myelinated Aδ-fiber axons conduct the pain signal with an action potential speed of 20 meters/second and induce the *first* or *cutaneous pricking pain*. The *first pain* has a high spatial resolution, is well localized and easily tolerated. The much slower conducting non-myelinated C-fiber neurons only allow velocities of two meters/second inducing the *second pain* or *burning pain* which is poorly localized and poorly tolerated. In addition, pain arising from viscera, musculature and joints is called *third* or *deep pain*. *Deep pain* is also poorly localized and can be chronic or is associated with referred pain (Kandel et al. 2000; Haslwanter et al. 2013). Moreover, several substances such as histamine, K^+, bradykinin, substance P, protons, ATP, serotonin, and acetylcholine were released by injured and/or inflamed tissue, inducing the direct or indirect activation of nociceptors (Kandel et al. 2000).

In order to develop new medical active substances, that may help to relieve from pain, it is necessary to understand the molecular mechanism of pain transduction in detail. Therefore it is mandatory to investigate the molecular sensor, which initiates the signal transduction in nociceptors. A milestone that improved the understanding of signal transduction in nociceptive neurons was the cloning and characterization of the capsaicin receptor *transient receptor potential vanilloid 1* (TRPV1) by Caterina et al. (Caterina et al. 1997).

3.2 **Transient receptor potential (TRP) ion channels**

The TRPV1 ion channel belongs to the transient receptor potential (TRP) ion channel superfamily. The first experiments that lead to the identification of the transient receptor potential family were done by Cosens and Manning. In the electroretinogram (ERG) of *Drosophila melanogaster* mutants, they found a short transient response during bright light exposure (Cosens & Manning 1969). But it took another 20 years to identify the mutated gene locus, finally Montell and Rubin cloned the gene containing the mutation and termed it *transient receptor potential* (TRP) (Montell & Rubin 1989). Until today, 28 different mammalian TRP ion channels were identified and constitute one of the largest ion channel family, the TRP superfamily (Fig. 1).

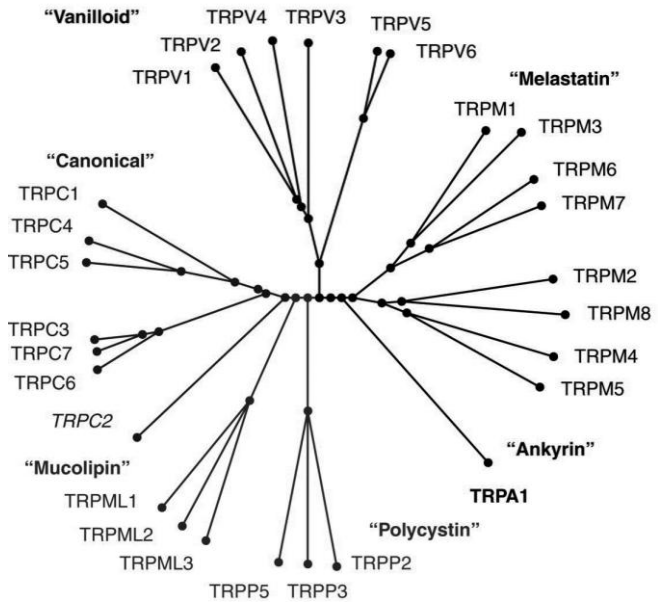

Figure 1. Phylogenetic tree of the mammalian TRP-superfamily by Gees et al. including six subfamilies and 28 ion channels (Gees et al. 2010).

The mammalian TRP superfamily can be subdivided into six subfamilies: the TRPC1-7 (canonical), TRPV1-6 (vanilloid), TRPM1-8 (melastatin), TRPA1 (ankyrin), TRPP1-3 (polycystin) and TRPML1-3 (mucolipin) (Clapham 2003). All TRP channels consist of four subunits and each subunit includes six transmembrane domains (S1-S6), with a pore-forming loop between the fifth and sixth transmembrane domain and cytoplasmatic located amino (N-) and carboxyl (C-) termini (Minke & Cook 2002). These regions are well known and include domains and motifs that are involved in channel assembly, activation, and regulation. TRP ion channels are non-selective cation channels that respond to a variety of physical and chemical stimuli such as temperature, mechanical force, osmolality, and chemical components (Minke & Cook 2002). Additionally, is the TRP channel function and expression triggered by several modifications such as phosphorylation, dephosphorylation, G-protein-coupling or phosphateidylinositol-4,5-biphosphate (PIP2) binding (Venkatachalam & Montell 2007). The polymodal activation and regulation of the TRP ion channels is very important in the sensory system of animals, espacially the thermal and chemical activation of TRPV1-TRPV4, TRPM8 and TRPA1 (Dhaka et al. 2006).

3.3 **TRPV ion channel subfamily**

The TRPV1 is the first member of the TRPV subfamily which includes six ion channels (TRPV1-TRPV6) (Gunthorpe et al. 2002). Characteristic for the TRPV subfamily members is the large N-terminal domain, which contains six Ankyrin repeat domains (ARD) (Latorre et al. 2009; Jung et al. 2002) and the polymodal activation by several physical and chemical (*vanilloids*) stimuli. Interestingly, TRPV1-TRPV4 ion channels are also molecular thermosensors with different thermal thresholds. Several studies using DRG or TG neurons or the overexpression of TRPV ion channels in HEK, CHO cells or frog oocytes revealed the different threshold temperatures of TRPV1 (~42°C), TRPV2 (~52°C), TRPV3 (~33°C) and TRPV4 (~27°C) (Patapoutian et al. 2003). The activation of TRPV1-TRPV4 receptors induces the non-selective influx of cations through the ion channel pore, whereas the activation of TRPV5 and TRPV6 receptors leads to an highly selective Ca^{2+} influx (Vennekens et al. 2000; Yue et al. 2001). The polymodal activation and modification of TRPV ion channels in nociceptors, particularly the TRPV1 receptor, qualifies them as pharmacological targets.

3.4 Structural and functional features of the TRPV1 receptor

The structure of the TRPV1 ion channel was investigated for a long time, but due to technical limitations the resolution of the TRPV1 3D structure was very low (Moiseenkova-Bell et al. 2008). Only the 3D structure of the N-terminal located ankyrin repeat domain (ARD) was provided at relative high-resolution by Lishko et al. (Lishko et al. 2007). However, the further development of the electron cryo-microscopy facilitated Cao et al. and Liao et al. to provide a high-resolution 3D structure of TRPV1 in the closed and open state as well as in an intermediate state (Cao et al. 2013; Liao et al. 2013). Based on these detailed 3D structures of the TRPV1 (Fig. 2), the following is a description of the most important structures and domains of the TRPV1 ion channel.

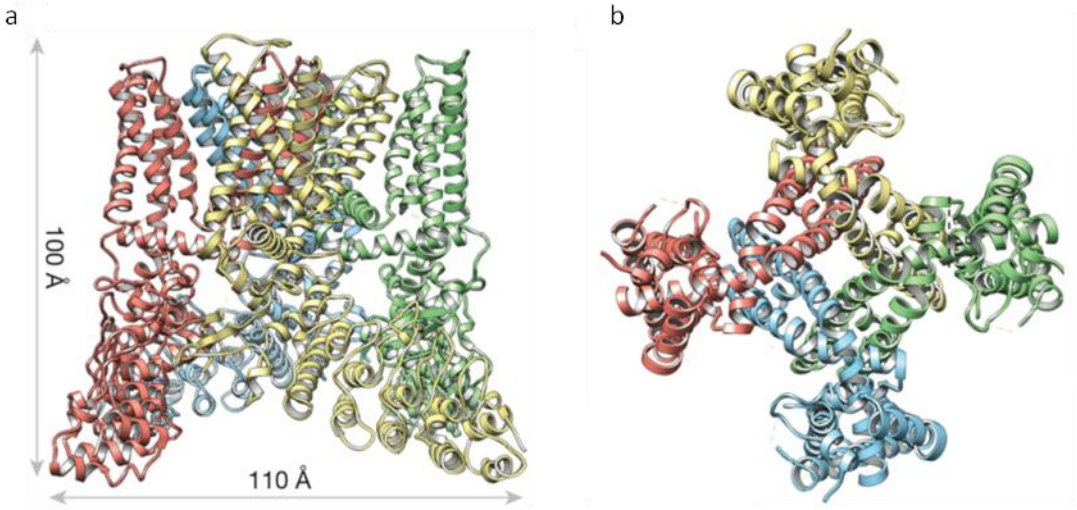

Figure 2. 3D structure of the TRPV1 ion channel by Liao et al. presented as ribbon diagram. (**a**) Side view on the four subunits, each subunit consisting of six transmembrane domains and intracellular located N- and C- termini (**b**) Bottom view on the six transmembrane domains (TMD) including TMD 1-4 and TMD 5-P-6 with the central pore (Liao et al. 2013).

The intracellular N-terminus of the TRPV1 includes six ankyrin repeats and the linker domain (P360-V415), which connects the ARD to the pre-TMD 1 helix. Ankyrin repeats are characterized by 33-residues that form two α-helices which were connected by loops. It is assumed that the TRPV1 ankyrin repeat domains are involved in ion channel assembly and subunit-subunit interaction (Erler et al. 2004; Hellwig 2005), which was verified by the high resolution structure of the TRPV1.

Cao et al. have shown that an atypical extended loop and two helices of ankyrin repeats 3 and 4 interact with a C-terminal β-strand (Cao et al. 2013). Additionally, the ARD surface forms an extensive cytoplasmic area that is proposed to facilitate the binding and interaction with calmodulin and ATP (Lishko et al. 2007). The linker domain connects the ARD to the pre-TMD 1 helix and includes β-strands as well as α-helices. The tightly packed domain is located between the six ankyrin repeats on the N-terminal side and the pre-TMD 1 helix and TRP domain on the C-terminal side. The interaction of two β-strands from the linker domain with two ankyrin repeats of an adjacent C-terminal subunit indicates that the linker domain is important for TRPV1 ion channel assembly. Furthermore, the linker domain contains an extended and kinked helix, which has equivalent characteristics as the TRP domain. This helix probably affects the ion channel gating since it is strategically located to interact with the TMD 4-5 linker and the pre-TMD1 helix (Fig. 3) (Liao et al. 2013). The six transmembrane domains of TRPV1 are structured into two sections, the surrounding transmembrane domains 1-4 and the central pore forming TMD 5-P-6 section.

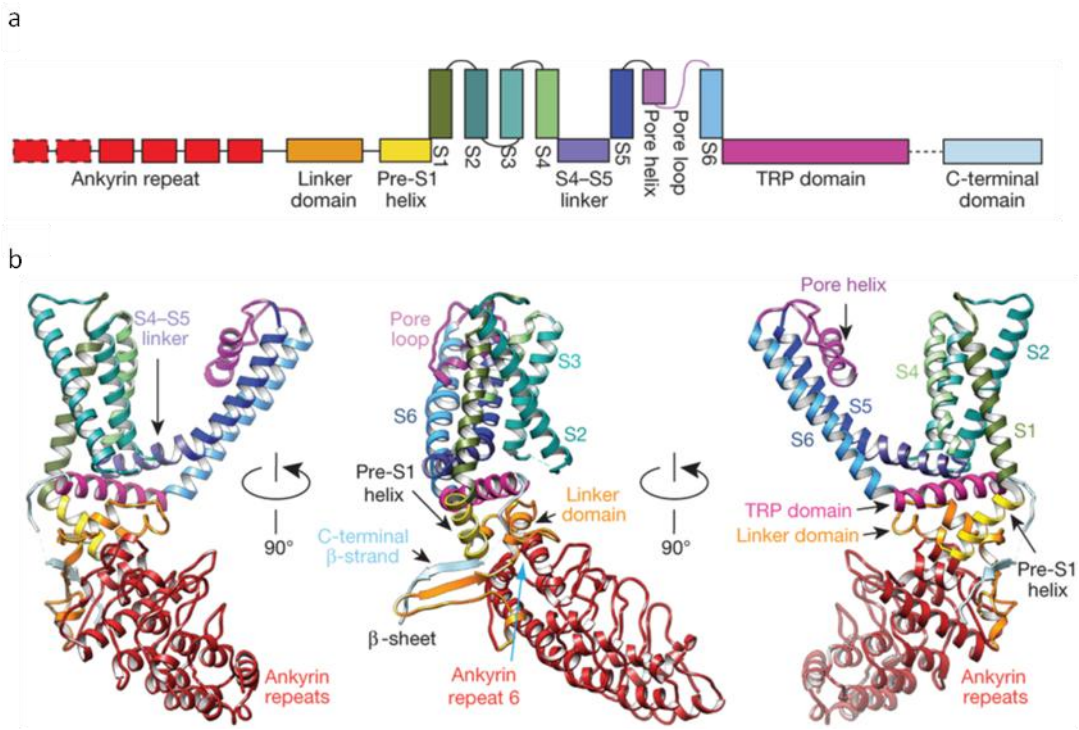

Figure 3. TRPV1 structure by Liao et al. (**a**) Schematic and (**b**) ribbon diagrams of one TRPV1 subunit, color code of the linear diagram matches to the ribbon diagram (S = TMD) (Liao et al. 2013).

The transmembrane domains 1-4 are connected to the TMD 5-P-6 section of an adjacent subunit, establishing a pinwheel-like structure. In contrast to the pore forming TMD 5-P-6 region is the transmembrane domain 1-4 section a solid anchor which is relative stationary during channel activation, but provides the binding of lipophilic ligands such as capsaicin or Resiniferatoxin (RTX). Connection between the transmembrane domain 1-4 and the TMD 5-P-6 section is provided by the flexible TMD 4-5 linker that facilitates the ion channel gating. The TRPV1 ion channel pore is divided into three compartments, the outer pore region, the central selectivity filter, and the lower gate (Liao et al. 2013). Compared to K_V channels is the outer pore of the TRPV1 relatively wide open and has a broad funnel-like structure. The central selectivity filter has a relative small diameter and consists of the amino acids $_{643}$GMGD$_{646}$, in which side chains or backbone carbonyls point into the central pore and form the permeation pathway. In the non-conducting or closed state the restriction point was found between diagonally opposed carbonyl oxygens at G643 (4.6 Å). Whereas in the activated or open state the diameter of the selectivity filter is increased. Interestingly, no hydrogen bonding was found between the adjacent pore helices of TRPV1 receptors, which results in a flexible architecture that might provide the phenomenon of pore dilatation. A pore dilatation occurs when the TRPV1 is repetitively or prolonged activated and lead to a dilatated pore which is permeable for large organic cations. The lower gate consists of the four I679 amino acid residues that form in the closed state a hydrophobic seal with a distance of 5.3 Å between the specific side-chain atoms. During the opening process several rearrangements occur in the selectivity filter and the inner pore (Liao et al. 2013). To investigate these rearrangements Cao et al. analyzed the TRPV1 structure in distinct conformations the apo TRPV1 structure, the capsaicin-bound, and the RTX/DkTx-bound. In the apo TRPV1 structure the widening of the selectivity filter and the lower gate were at its narrowest point at G643 4.6 Å and I679 5.3 Å, representing the closed TRPV1 ion channel. The capsaicin-bound TRPV1 is in an intermediated state, whereas the selectivity filter is unaffected, but the lower gate is significantly widened to a diameter of 7.6 Å. In the RTX/DkTx-bound TRPV1, representing the open TRPV1 ion channel, the selectivity filter is expanded to 7.7 Å at G643 and the lower gate is widened to a diameter of 9.3 Å.

In conclusion, the three conformations of the TRPV1 revealed that the TRPV1 ion channel pore acts as dual gate(Cao et al. 2013). Just after the pore forming TMD 6 is the TRP domain located, the TRP domain has 23-25 amino acids and can be found in many TRP family members. The TRP domain is a α-helical structure that includes a sharp bend after the TMD 6 and runs parallel to the inner membrane. The first two-thirds of the TRP domain were organized as α-helix, while the rest shifts into a random coil structure. Interestingly, the amino acid W697, which is close to the middle of the TRP domain forms hydrogen bounds with the F559 of the S4-S5 linker (Cao et al. 2013). Additionally, it was shown in a W697 mutagenesis study that the disruption of the hydrogen bound notably affects the voltage and capsaicin evoked TRPV1 channel gating (Gregorio-Teruel et al. 2014). The detailed insights into the TRPV1 3D structure may help to understand the molecular mechanisms that occur during TRPV1 activation and/or modification.

3.5 **Activation and inhibition of TRPV1**

TRPV1 receptors are ligand-gated non-selective cation channels, that conduct Ca^{2+} with a 9x higher preference over Na^{+} (Chung et al. 2008). The TRPV1 is polymodally, activated by several exogenous and endogenous chemical and physical stimuli such as the vanilloid capsaicin, protons, heat or voltage (Cortright & Szallasi 2004). However, capsaicin and its biological analogs as well as protons are sensitizers, since it binding lowers the voltage activation threshold of TRPV1, but due to the direct binding, it is by convention allowed to call them activators. In contrast, compounds that affect the TRPV1 function indirectly without binding were called sensitizers (Vriens J. et al. 2009). Activation of the TRPV1 opens the pore and cations flow through the permeation pathway. Under physiological conditions, the electrochemical gradient drives cations from the extracellular into the intracellular compartment, but TRPV1 is also conductive in the opposite direction. Furthermore, the TRPV1 ion channel is outwardly-rectifying and has a reversal potential of 0 mV (Voets et al. 2004; Caterina et al. 1997). One of the first known TRPV1 activators is Capsaicin. It is a specific TRPV1 agonist and the active ingredient in chili peppers that induces in mammals a burning hot sensation (Caterina et al. 1997). The identification of the capsaicin-binding site in the mammalian TRPV1 is interesting.

Since birds does not perceive burning hot sensation induced by capsaicin, Jordt and Julius compared the TRPV1 protein sequences and located the capsaicin binding site between TMD 3 and TMD 4 involving the amino acid residues Y511, T512, M547, and T550 (Jordt & Julius 2002). The most effective naturally stimuli that activates the TRPV1 is the diterpene Resiniferatoxin (RTX); which is a chemical compound of *Euphorbia resinifera* (Szallasi & Blumberg 1989), RTX activates the TRPV1 almost 20x more potent than capsaicin (Caterina et al. 1997). But the TRPV1 ion channel is also activated by molecules with similar structures such as quinazoline (Culshaw et al. 2006), evodiamine (Pearce et al. 2004) and 17-β-estradiol (Xu et al. 2008), as well as molecules with long acyl and amid chains, such as anandamide (Ross 2003), olvaniol, and omega-3 polyunsuturated fatty acids (Jara-Oseguera et al. 2008). Further TRPV1 agonists are 12-HPETE (Hwang et al. 2000), anandamide (Ross 2003), NADA (Premkumar et al. 2004), AEA (Price et al. 2004), piperine (McNamara et al. 2005), eugenol (Yang et al. 2003), zingerone (Liu & Simon 1996) and gingerols (Dedov et al. 2002). Apart from the activation by chemical compounds the TRPV1 is activated by low pH, via interaction of protons with amino acid residues in the outer pore domain E600, E648, F660. To activate the TRPV1 properly, a pH below 6 is required, but even small pH changes (pH 6-7) sensitize the receptor sensitivity to capsaicin or heat (Aneiros et al. 2011; Caterina et al. 1997; Jordt et al. 2000). In contrast to the wide variety of TRPV1 agonists, competitive TRPV1 antagonists are rare. Capsazepine was identified as first competitive antagonist for TRPV1, capsazepine competes with capsaicin for the capsaicin-binding site and can also displace RTX from its binding site. However, the potency of capsazepine is species-specific, while it is relative potent at human TRPV1, it is much less potent ats rat TRPV1 (Liu & Simon 1997; Docherty et al. 1997). Other TRPV1 antagonists are Thapsigargin which is also a potent ATPase inhibitor (Tóth et al. 2002) as well as Yohibine an indole alkaloid that inhibits the TRPV1-induced firing activity of DRG neurons (Dessaint et al. 2004). Endogenous TRPV1 antagonists are dynorphins, a natural arginine-rich peptide, adenosine, fatty acids such as eicosapentaenoic or linolenic acids, and also polyamines have been reported to block TRPV1 (Matta et al. 2007; Puntambekar 2004). Additionally, some noncompetitive antagonists were known, for example Ruthenium Red (RR), which not interacts with the ligand binding site of TRP ion channels but blocks the pore.

Interestingly, the RR induced pore block is voltage-dependent, *i.e.* inward currents were blocked but outward currents were unaffected (Caterina et al. 1997). The classic K^+ blocker tetrabutylammonium (TBA) also blocks the TRPV1 in a voltage-dependent manner, but it blocks the TRPV1 in the open state by interfering with the closing of the lower gate (Oseguera et al. 2007). In summary, the polymodal activation and inhibition of the TRPV1 ion channels by exogenous and endogenous stimuli facilitates the development of new tools for pain treatment.

3.6 **Regulation of TRPV1 receptors**

As already mentioned TRPV1 activation involved in pathophysiological conditions such as allodynia and hyperalgesia, therefore it is necessary to investigate the molecular mechanisms of TRPV1 ion channel regulation in more detail (Caterina et al. 2000; Bölcskei et al. 2005; Christoph et al. 2006). For instance damaged tissue releases several inflammatory mediators such as growth factors, neurotransmitters, peptides or small proteins, lipids, chemokines and cytokines, which results in the sensitization of nociceptors (Ma & Quirion 2007). Via different pathways including receptor tyrosine kinases or G-protein-coupled receptors, inflammatory mediators affect TRPV1 function by kinase-mediated phosphorylation. Phosphorylation in general affects the steric and electric properties of amino acids and lead to conformational changes in the adjacent structures (Johnson & Barford 1993). It is known that phosphorylation of TRPV1 receptors increases their sensitivity to endogenous and exogenous stimuli such as capsaicin, protons, or heat and formerly non-activating concentrations or stimuli become activating (Fig. 4). TRPV1 is phosphorylated by several kinases: protein kinase A (PKA) (Lopshire & Nicol 1998; De Petrocellis et al. 2001; Varga et al. 2006), protein kinase C (PKC) (Cesare et al. 1999; Premkumar & Ahern 2000; Vellani et al. 2001), Ca^{2+}/CaM-dependent kinase II (CaMKII) (Jung et al. 2004) and Src kinase (Jin et al. 2004) (Fig. 5). While, the kinase-mediated phosphorylation sensitizes TRPV1 receptors, the dephosphorylation desensitizes the TRPV1 receptors. Cytosolic Ca^{2+} and calmodulin form a Ca^{2+}/calmodulin-complex, which activate the protein phosphatase calcineurine (CaN) dependent dephosphorylation of TRPV1 receptors. The desensitization of TRPV1 decreases the spontaneous activity of TRPV1 and reduces the stimuli-mediated activity (Lishko et al. 2007; Koplas et al. 1997).

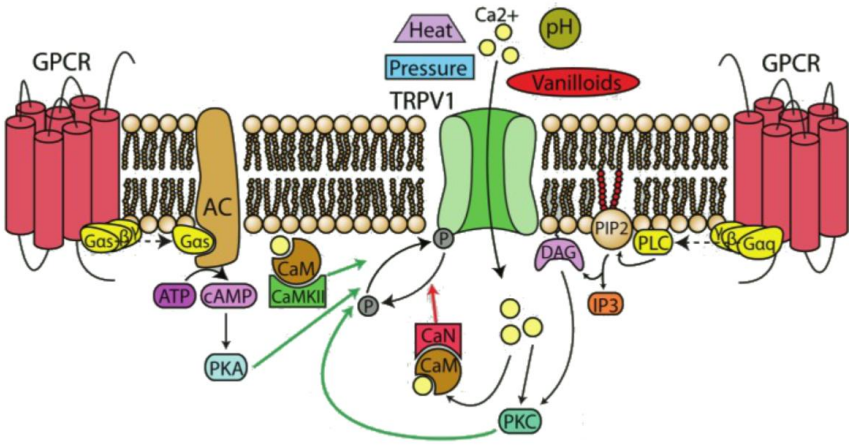

Figure 4. TRPV1 activation and regulation by Ho et al. (**left side**) GPCR-induced activation of the adenylate cyclase pathway facilitates the PKA-mediated phosphorylation of the TRPV1. Ca^{2+}/Calmodulin (CaM)-complex activates CaMKII, which phosphorylates TRPV1. (**right side**) GPCR-mediated activation of PLC cleaves PIP_2 into IP3 and DAG, latter induces the PKC-mediated phosphorylation of TRPV1 receptors. (**center**) Polymodal activation of TRPV1 induces cation influx, Ca^{2+} binds to calmodulin (CaM) and activates the phosphatase Calcineurin (CaN) which dephosphorylates the TRPV1 (Ho et al. 2012).

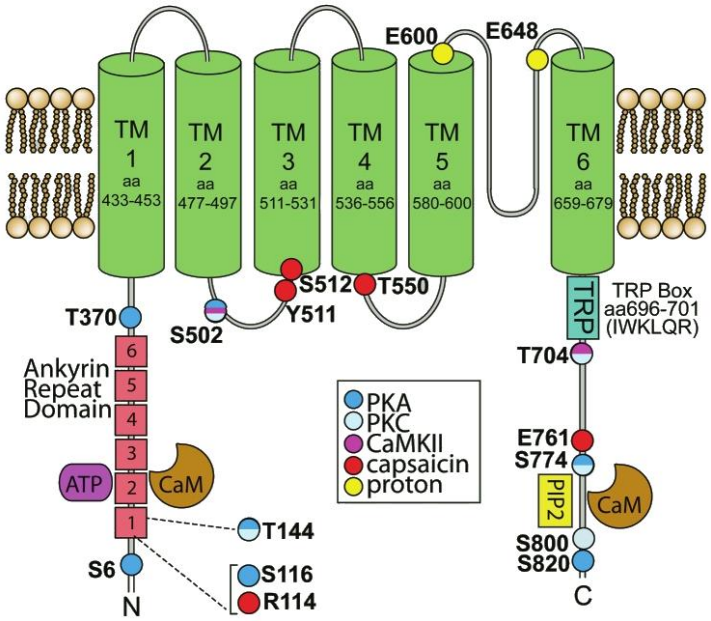

Figure 5. Functionally important amino acids and segments of the TRPV1 receptor by Ho et al. Color coded phosphorylation sites of PKA, PKC, and CaMKII as well as capsaicin and proton binding sites. Structural important domains of TRPV1 such as ankyrin repeat domains, transmembrane domains, pore region, and the TRP domain including the TRP-box. ATP and calmodulin binding side of at intracellular located N- or C- termini (Ho et al. 2012).

Furthermore is the TRPV1 modulated by PIP_2 in the first instance it was shown that PIP_2 binds to TRPV1 and inhibits TRPV1 activity, which was demonstrated by PLC-mediated hydrolysis and antibody-mediated block of PIP_2 (Prescott & Julius 2003; Chuang et al. 2001). But in recent studies it was shown that the decrease of PIP_2 correlates with reduced activity of TRPV1, *e.g.* PIP_2 binding increases the TRPV1 ion channel activity (Lukacs et al. 2007; Yao & Qin 2009; Ufret-Vincenty et al. 2011; Stein et al. 2006). Therefore, it is necessary to study the modification of the TRPV1 function in order to develop new analgesic drugs. In particular, the phosphorylation and dephosphorylation of TRPV1 receptors is an important target.

3.7 **TRPV1 and Cyclin-dependent kinase 5**

In 2006 Pareek et al. showed that Cdk5 and the neuron-specific activator p35 were expressed and active in nociceptors such as DRG or TG neurons. They also revealed that the Cdk5 protein level and activity were increased during carrageenan-induced inflammation. Moreover, they found in genetically engineered mice that the overexpression of p35 (Tgp35) increased the Cdk5 activity and led to hyperalgesia, whereas the knockout of p35 provoke a decreased Cdk5 activity and induced hypoalgesia (Pareek et al. 2006). Therefore, they assume that during inflammatory processes the Ca^{2+} influx into nociceptors increases, which catalyzes the Ca^{2+}-dependent protease calpain. Calpain dependent hydrolysis of p35 in p25 and p10, p25 in turn increases Cdk5 activity. That was supported by a study of Yang et al., which showed that primary sensory neurons express Cdk5 and p35 and that the injection of Freud's complete adjuvant (CFA) increases the Cdk5 activity. Additionally, they could associate the increased Cdk5 activity to hyperalgesia (Yang et al. 2007). Thus, Kulkarni et al. investigated the signal transduction mechanism that is responsible for the modulation of nociceptive transmission in sensory neurons. They associated the Cdk5 activity to the MAPK signaling pathway by proposing that Cdk5/p35 regulates the MEK1/2 activity via a negative feedback loop (Pareek et al. 2006). Simultaneously, they investigated the downstream target of the signal cascade and could show in 2007 that the Cdk5 directly phosphorylates TRPV1 receptors. Subsequently, they analyzed the TRPV1 sequence for putative Cdk5 consensus sites (S/T)PX(K/H/R) and found three putative consensus sites: threonine-108 (TPPR), threonine-407 (TPNR) and serine-612 (SPPH).

Alignment of different mammalian TRPV1 protein sequences revealed that threonine-407 is highly conserved among different species. To demonstrate that the endogenous TRPV1 was phosphorylated by Cdk5, the TRPV1 of genetically engineered $Cdk^{+/+}$ and $Cdk^{-/-}$ mice was tested in kinase assays by using a specific P-TRPV1 antibody. Furthermore, they investigated the effect of the Cdk5-dependent phosphorylation on TRPV1 function. Therefore, a Ca^{2+} influx assay with DRG neurons was performed revealing that the inhibition of Cdk5 activity reduces TRPV1-mediated Ca^{2+} influx. Finally, it was shown that the lack of Cdk5 in DRG neurons prevents the phosphorylation of TRPV1 at position T407 and induced hypoalgesia (Pareek et al. 2007). In 2011 Uteras at al., identified the signal transduction pathway in odontoblast-like MDPC-23 cells. They found that during a bacterial inflammation, TGF-β1 was released into the extracellular matrix and the associated TGF-β1 receptor 1 activates Smad-dependent and independent pathways. These pathways increase the Egr-1 and p35 expression, which in turn activates Cdk5 kinase that phosphorylates TRPV1 receptors (Fig. 6). The TRPV1 phosphorylation results in enhanced Ca^{2+} influx into odontoblast cells, which may induce more action potentials and an increased transmitter release (Utreras et al. 2013). To further investigate the impact of Cdk5 activity on TRPV1 function in detail, our cooperation partners Kulkarni et al. performed several behavioral experiments (Jendryke et al. 2016). They tested the pain tolerance of mice with either increased or decreased Cdk5 activity by treating the animals with stimuli that are known to activate TRPV1. Therefore, the sensitivity to capsaicin was tested in the different genotypes. The oral administration of capsaicin induces a burning sensation and reduces the drinking behavior of mice. Training sessions (water only) allowed the animals to habituate to the lickometer and the basal licking behavior of each genotype was determined. The training sessions revealed no difference in the licking behavior of different mice strains. To investigate the TRPV1-mediated aversive behavior, 15 µM capsaicin were adjusted in the drinking water. Compared to the basal licking behavior, capsaicin reduced the licking behavior of $C57BL6_{WT}$ mice to 16.2%, whereas the licking behavior of p35 KO mice decreased to 35.5% and in Cdk5 CoKo mice to 29.5% (Fig. 7).

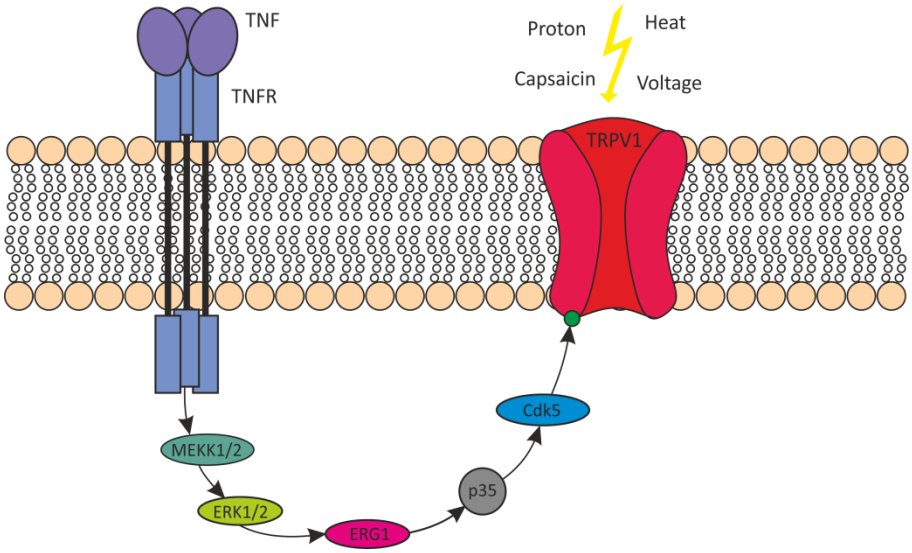

Figure 6. Putative TNFα-induced pathway based on the findings of Pareek at al., TNF binds to TNF-receptors and activates the MEKK1/2-ERK1/2 signaling cascade, which induces the Cdk5-mediated phosphorylation of TRPV1.

The statistical analysis revealed that in the presence of capsaicin the licking behavior of Cdk5 or p35 knockout mice is less affected than the licking behavior of wild-type mice, whereas the licking behavior of TRPV1 KO mice was unaffected (94.7%). These data revealed that the reduced activity or the lack of Cdk5 increases the pain tolerance to TRPV1 specific stimuli. Challenging FVBN WT mice with 15 µM capsaicin reduced the licking behavior to 51.8%, whereas the licking behavior of FVBN Tgp35 mice was reduced to 36.2%. Comparison of the licking behavior of FVBN wild-type and Tgp35 mice revealed that Tgp35 mice were significantly more sensitive to 15 µM capsaicin than the WT mice (unpaired *t-test* $p < 0.05$) (**Fig. 7**). These data indicate that an increased p35 activity sensitizes the nociceptors to capsaicin, probably by promoting Cdk5-mediated phosphorylation of TRPV1.

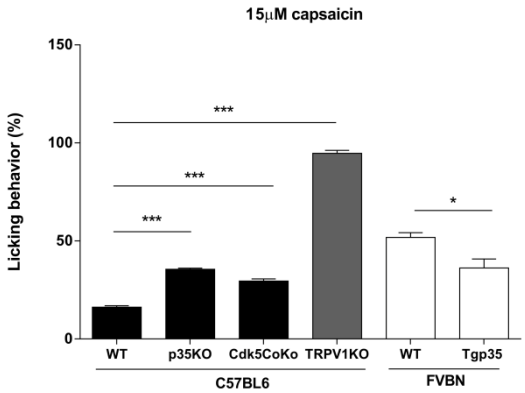

Figure 7. Effect of capsaicin on drinking behavior of wild-type, p35 KO, Cdk5 CoKo, TRPV1 KO and Tgp35 mice. Water deprived mice were tested in the lickometer device with a free access initially to plain water (for training), then to water containing different concentrations of capsaicin. The licking behavior at 15 µM capsaicin, is presented as % of the basal licking behavior (plain water). Compared to wild-type, the licking behavior of p35 KO or Cdk5 CoKo was significantly less reduced, while the Tgp35 mice showed a significantly increased sensitivity to 15 µM capsaicin leading to reduced drinking behavior. Data were presented as mean ± SEM from four animals during five different measurements (One-way Anova ***$p < 0.001$, unpaired *t-test* *$p < 0.05$) (Jendryke et al. 2016).

Since the TRPV1 receptor is activated by hot temperatures Kulkarni et al. set out to investigate the thermal nociception of the genetically engineered mice (Jendryke et al. 2016). Therefore, the OPAD system (Orofacial Pain Assessment Device, Stoelting) was used to measure the licking behavior of mice in the presence of noxious heat. At 37 °C, the consumption of 30% sucrose was equal in all genotypes (Fig. 8a), but increasing the temperature to 45 °C induced an altered licking behavior (Fig. 8b). The licking behavior of C56BL6WT mice was significantly reduced, whereas the licking behavior of p35 KO and Cdk5 CoKo mice was nearly unchanged (unpaired t-test $p < 0.05$). In FVBN mice the licking behavior was reduced by 45 °C, but mice overexpressing p35 were significantly more sensitive than wild-type mice. The unaffected licking behavior of p35KO and Cdk5 CoKo mice as well as the decreased licking behavior of mice overexpressing p35 indicates that Cdk5 activity strongly affects the heat tolerance of mice. In conclusion, the in vivo results reveal that an increased or decreased Cdk5 activity has severe consequences on the TRPV1-mediated nociception. Increased Cdk5 activity induces hyperalgesia and allodynia, whereas the lack of Cdk5 or a reduced Cdk5 activity induces hypoalgesia. The increased TRPV1 sensitivity is probably a result of direct phosphorylation of TRPV1 by Cdk5, but until today hardly any functional characterization of the Cdk5-mediated phosphorylation of the TRPV1 is published. Therefore, we set out to investigate the effect of Cdk5-dependent phosphorylation of TRPV1 *in vitro*.

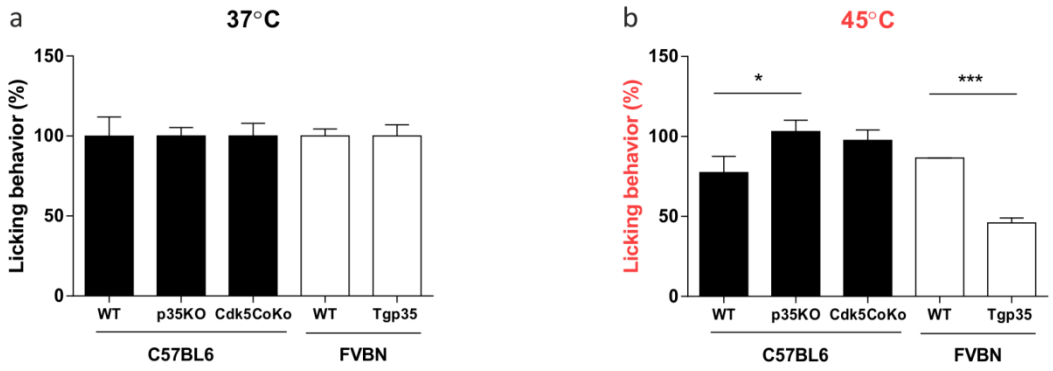

Figure 8. Impact of heat on the licking behavior of wild-type, p35 KO, Cdk5 CoKo and Tgp35 mice. (**a**) At 37 °C, all mice showed similar consumption rates of the sucrose reward. (**b**) At 45 °C, the Tgp35 mice revealed an aversive licking behavior, while the p35 KO mice showed a significantly increased number of licks compared to wild-type controls. Data are presented as mean ± SEM from four animals measured five times using 37 °C and three times at 45 °C (unpaired *t-test* $*p < 0.05$, $***p < 0.001$) (Jendryke et al. 2016).

4 Aims

In order to investigate the effect of Cdk5-mediated phosphorylation on the TRPV1 ion channel function, we set out to analyze

the impact of Cdk5-mediated phosphorylation of TRPV1 *in vitro*.

- The Ca^{2+}-dependent desensitization and capsaicin sensitivity of TRPV1 receptors will be characterized by means of electrophysiological experiments using CHO cells co-expressing a combination of TRPV1, Cdk5, and p35.

the effect of $TRPV1_{T406}$ mutagenesis on the ion channel function.

- The activation and desensitization kinetics, the sensitivity to capsaicin or protons as well as the voltage-dependence of $TRPV1_{T406}$ mutants will be characterized by means of electrophysiological whole-cell recordings of transfected CHO cells.
- The heat sensitivity of $TRPV1_{T406}$ mutants, generated to mimic or inhibit the Cdk5-mediated phosphorylation of TRPV1, will be analyzed by means of Ca^{2+}-imaging experiments in transfected HEK293 cells.
- The plasma membrane expression of GFP-tagged $TRPV1_{T406}$ mutants, will be investigated by means of TIRF microscopy.
- The ion channel gating mechanism of $TRPV1_{WT}$ and $TRPV1_{T406D}$ single-channels will be characterized by means of electrophysiological cell-attached recordings of transfected CHO cells.

the transition pathway which connects the Cdk5-mediated phosphorylation of T406 to the TRPV1 gating mechanism.

- The activation and desensitization kinetics, the sensitivity to capsaicin or protons as well as the voltage-dependence of TRPV1 transition pathway will be analyzed by means of electrophysiological whole-cell recordings of CHO cells expressing TRPV1 double mutant receptors.

5 Methods

5.1 Molecular biological methods

The plasmids used in this thesis were provided by Prof. Dr. D. Julius, University of California, USA (pcDNA3-rTRPV1), Prof. Dr. M. Hollmann, Ruhr-Universität Bochum, Germany (pcDNA3-GFP), Prof. Dr. A. Kulkarni, NIH/NIDCR, Bethesda, USA (pcDNA3-Cdk5, pcDNA3-p35), Dr. V. Milenkovic, UKR, Germany (pGEM-T). The pcDNA3 vector is a mammalian expression vector including the CMV promotor, a multiple cloning site (MCS), and the bacterial resistance ampicillin. Reproduction or manipulation of coding DNA (cDNA) requires various molecular methods that were described in the following.

5.1.1 Chemocompetent *E.coli* bacteria

In order to amplify pcDNA3 vectors we utilized chemocompetent *Escherichia coli* bacteria cells (DH5α). Therefore, 50 µl of the E. coli glycerol stock were plated onto a LB-agar plate and incubated overnight at 37 °C. The next day, one colony was picked and transferred into 4 ml of LB-medium and grew overnight in a hot air shaker (120 rpm) at 37 °C. 500 µl of this preparatory culture were diluted into 750 ml of LB medium and incubated in a hot air shaker at 37 °C. The cell growth was stopped at OD_{600} 0.5-0.7 by cooling the bacteria solution on ice for 15 min and centrifugation at 3500 x g and 4 °C. The supernatant was discarded, and the pellet was resuspended in 125 ml ice-cold 0.1 M $MgCl_2$ and incubated for 10 min on ice. In a second centrifugation step at 4 °C and 2500 x g for 10 min the bacteria were pelleted again. After discarding the supernatant, the pellet was resuspended in 60 ml 0.1 M $CaCl_2$ and incubated for 20 min on ice. In a last centrifugation step at 4 °C and 2500 x g for 10 min the bacteria were collected (discard the supernatant) and finally resuspended in 12 ml 85 mM $CaCl_2$ + 15% glycerol. 100 µl aliquots of the chemocompetent *E. coli* DH5 α were shock-frozen and stored in 1.5 ml Eppendorf tubes at -80 °C.

5.1.2 Transformation of vectors into chemocompetent bacteria

In order to introduce coding DNA into chemocompetent *E. coli*, one bacteria aliquot was thawed on ice and 20-50 ng of ligation product or 5-20 ng of vector DNA was added.

After 30 min on ice the transformation mixture was heat shocked at 45 °C for 45 seconds and subsequently incubated on ice for 1 min. 500 µl SOC medium were added and the

mixture was incubated on a thermal shaker at 90 rpm and 37 °C for 60 min. Finally, 100 µl of the bacteria were spread on $LB_{ampicillin}$ plates and incubated overnight at 37 °C. Once the transformation of the pcDNA-TRPV1 vector was successful, only the ampicillin resistant bacteria survived and appeared as colonies on the $LB_{ampicillin}$-agar plate.

5.1.3 **Isolation of plasmid DNA**

In order to isolate plasmid DNA from transformed bacteria, one successfully transformed colony was inoculated into $LB_{ampicillin}$ medium and incubated at 37 °C in a hot air shaker at 150 rpm. 5 to 100 ml of saturated *E. coli* culture were used for Mini-preparation or Midi/Maxi-preparation (Quiaprep Spin Mini, Midi, Maxi-prep Kit, Qiagen, Hilden, Germany), depending on the amount of plasmid DNA needed. The preparation was performed by the manufacturer's protocol, the Plasmid DNA amount and quality was quantified by Nanodrop spectrophotometry (NanoDrop Technologies, Wilmington, USA) as well as agarose gel electrophoresis.

5.1.4 **Restriction digestion of plasmid DNA**

Digestion of Plasmid DNA was performed by restriction enzymes. The restriction mix is an aqueous solution, which contains 0.2-5 µg of DNA, 5 µl of 10x restriction enzyme buffer, and 1 µl of restriction enzyme (final volume = 50 µl). Depending on the optimal working temperature of the restriction enzyme the mixture was incubated for 1-2 hours at the appropriate temperature (usually 37 °C). In order to verify the digestion and to separate the DNA by their length we used the agarose gel electrophoresis.

5.1.5 **Agarose gel electrophoresis**

The agarose gel electrophoresis technique separates DNA fragments by their length in base pairs. In the electric field of the gel electrophoresis, large DNA fragments migrate slower than small DNA fragments. To prepare a 1% agarose gel we mixed and boiled 1 g agarose and 100 ml 1 x TAE-buffer, and added 3 µl ethidium bromide to visualize the DNA under UV-light. The hot mixture was transferred into the gel chamber to let the gel polymerize for 30-60 minutes. DNA fragments were separated by applying 120-140 V for about 1 h and visualized by means of a UV-camera. Finally, the size of the DNA fragments was determined by comparison to 1 kb Plus DNA Ladder (Invitrogen, Karlsruhe, Germany).

5.1.6 **Gel extraction**

In order to extract DNA fragments from agarose gels we used the NucleoSpin Extract kit (Macherey Nagel, Düren, Germany). The gel slice including the target DNA was cut out and dissolved in NTI buffer at 50 °C for 5-10 min. Then the DNA was washed twice with NT3 buffer utilizing a clean-up column and centrifugation for 30 s at 11000 x g. Finally, the clean DNA fragments were eluted in 20 µl dH_2O and collected in a fresh 0.5 ml Eppendorf tube.

5.1.7 **Ligation of digested DNA fragments**

In order to ligate the purified DNA fragments the T4 DNA ligase (Promega) was used. The 10 µl reaction volume contained digested and purified vector DNA and insert DNA as well as 1 µl 10x ligase buffer, and 1 µl of T4 DNA ligase. Depending on the relative size of the insert and the vector DNA the amount of vector and insert DNA ranges between equimolar ratios to ratios of 1:10 (vector:insert). The ligation reaction was incubated overnight at 14 °C.

5.1.8 **Polymerase chain reaction (PCR)**

In order to amplify DNA we used the polymerase chain reaction (PCR) adapted from Saiki (Saiki et al. 1988). The PCR mix is an aqueous solution that contains a polymerase specific reaction buffer, which provides the optimal chemical environment for the DNA polymerase, and the four triphosphate nucleotides: adenine, guanine, cytosine, and thymine. Additionally, the PCR mix contains the DNA template (50-100 ng) a complementary primer pair that binds to the sense and anti-sense strand of the DNA as well as the DNA-polymerase, which amplifies the DNA. To generate error free DNA replicates the proofreading PfuUltra HF DNA Polymerase (Aglient) was used. The reaction tubes containing the PCR mix were placed in a thermocycler, which heats and cools the PCR mix. The thermocycler performs three discrete temperature changes in 25-35 cycles. Initially, the PCR mix was heated up to a temperature of 94 °C for 10 min to activate the DNA polymerase (i). In the first step of the PCR cycle this temperature of 94°C was held for 1 min (ii). At that time, the double-stranded DNA was separated into two single-stranded DNA molecules, by disrupting the hydrogen bonds between the complementary bases. In the annealing step, the temperature was lowered to 50-65 °C to allow the oligonucleotide to anneal to the complementary sequence of the target DNA.

The annealing temperature is very critical, since low temperatures lead to insufficient primer bindings and high temperatures lead to unspecific primer bindings. The last step of the PCR cycle is the elongation step, its temperature depends on the optimum activity temperature of the used DNA polymerase. For the PfuUltra HF DNA Polymerase we set the temperature to 72 °C (iv). The synthesis velocity of the DNA polymerase was about 1000 bases/min, therefore the elongation time depends on the length of the DNA fragment to amplify. A final elongation step at 72 °C for 10 min was performed after the last PCR cycle to make sure that all remaining single-stranded DNA were fully amplified (**v**). Finally the temperature was set to 15 °C for infinity time (vi) (Fig. 9).

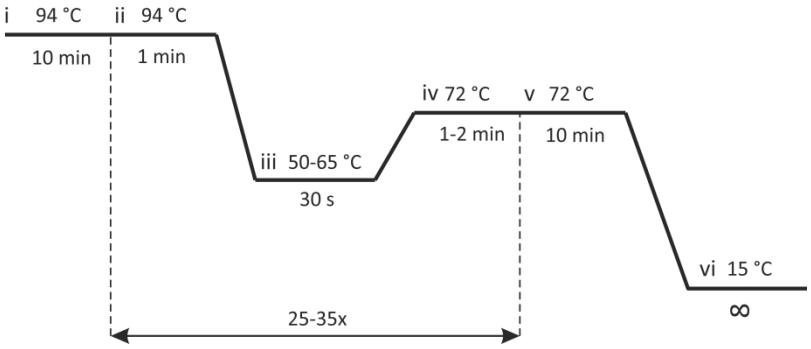

Figure 9. PCR temperature steps: (**i**) initial, (**ii**) denaturation, (**iii**) annealing, (**iv**) elongation, (**v**) final elongation, and (**vi**) final holding temperature.

5.1.9 **Cloning of Cdk5-mCherry, p35-CFP, and TRPV1-GFP fusion proteins**

In order to identify TRPV1 transfected CHO cells we co-transfected the cells with TRPV1 and green fluorescent protein (GFP) coding DNA. To identify cells co-expressing TRPV1, Cdk5, and p35, we C-terminally tagged Cdk5 and p35 with either red-fluorescent protein mCherry or cyan-fluorescent protein CFP, respectively. Therefore, we subcloned the cDNA of mCherry or CFP into the pcDNA3-Cdk5 or pcDNA3-p35 vector, respectively. The coding DNA of mCherry was extracted from the pcDNA3-mcherry vector and introduced into the pcDNA3-Cdk5 vector by using the restriction sites NotI-ApaI. The coding DNA of CFP was extracted from the pcDNA3-CFP vector and introduced into the pcDNA3-p35 vector by using the restriction sites XhoI-ApaI (Fig. 10). Finally, we checked the pcDNA3-Cdk5-mcherry and pcDNA3-p35-CFP construct for unwanted mutations by DNA sequencing.

The TRPV1-GFP fusion protein was created by introducing the cDNA of GFP into the pcDNA3-TRPV1 vector. Therefore, we introduced a new restriction site at the 3'-end of the TRPV1 cDNA (Fig. 11). This ApaI and the NotI restriction sites were used to insert the GFP cDNA in frame.

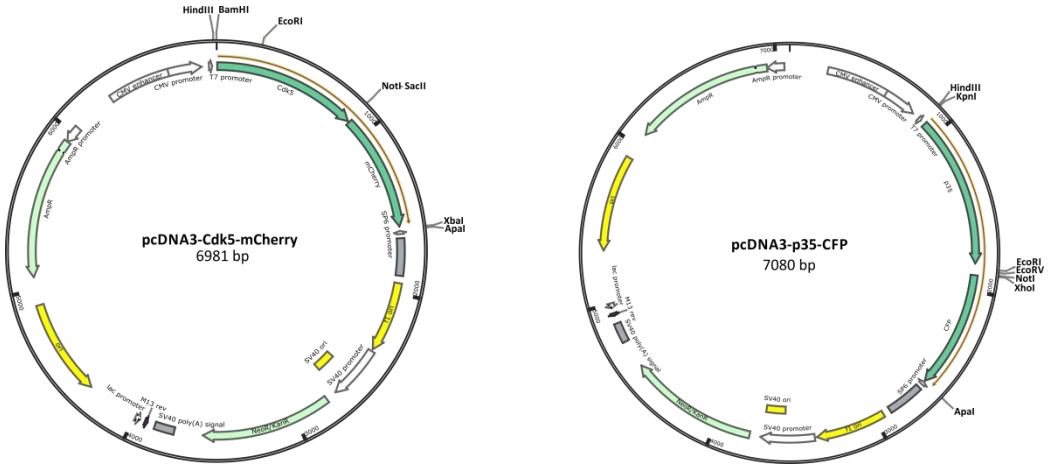

Figure 10. Plasmid maps of pcDNA-Cdk5-mcherry and pcDNA-p35-CFP. pcDNA3 includes the cytomegalovirus (CMV) promoter for transient high-level expression in mammalian cells. The multiple cloning sites (MCS) include various restriction sites, which facilitates cloning. Moreover, the plasmid contains the ampicillin resistance gene for maintenance in bacteria. All remaining restriction sites of the MCS were highlighted.

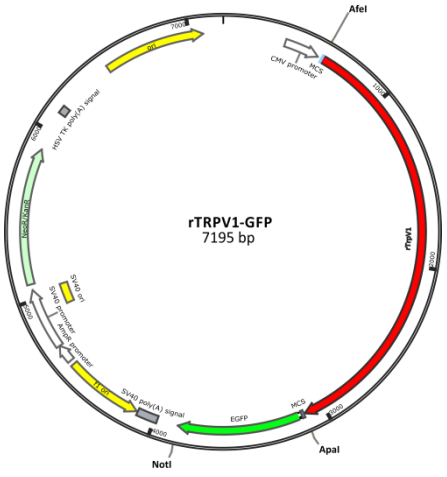

Figure 11. Plasmid map of TRPV1-GFP fusion protein. Plasmid includes the cDNA for TRPV1-GFP fusion proteins, the ampicilin resistance gene, and the multiple cloning site as well as the CMV promoter.

5.1.10 **TRPV1 mutagenesis via Overlap extension PCR**

The overlap extension PCR needs two primer pairs, primer pair A for the cDNA sequence upstream of the targeted amino acid (*e.g.* T406) and primer pair B for the cDNA sequence downstream of the target (Higuchi et al. 1988). The reverse primer A and the forward primer B insert the desired mutation, while forward primer A bound 1440 bp upstream and the reverse primer B bound 1678 bp downstream of the T406 codon. In two independent PCR's, primer pair A or B was used to generate two mutated TRPV1 cDNA sub-fragments: Fragment A (1440 bp) and Fragment B (1678 bp). The generated overlap was used to anneal fragment A and B in a second PCR. The new fragment AB was 3076 bp long and included the intended mutation at position T406. In order to transfer the mutated cDNA into the pCDNA3-TRPV1 vector the purified PCR product and the pCDNA-TRPV1 vector were digested with the restriction enzymes BstEII and SacII. Finally, the 701 bp long BstEII-SacII fragment, including the T406 mutation was ligated into the pCDNA3-TRPV1 vector (Fig. 12). All mutants were confirmed and checked for unwanted mutations by DNA sequencing.

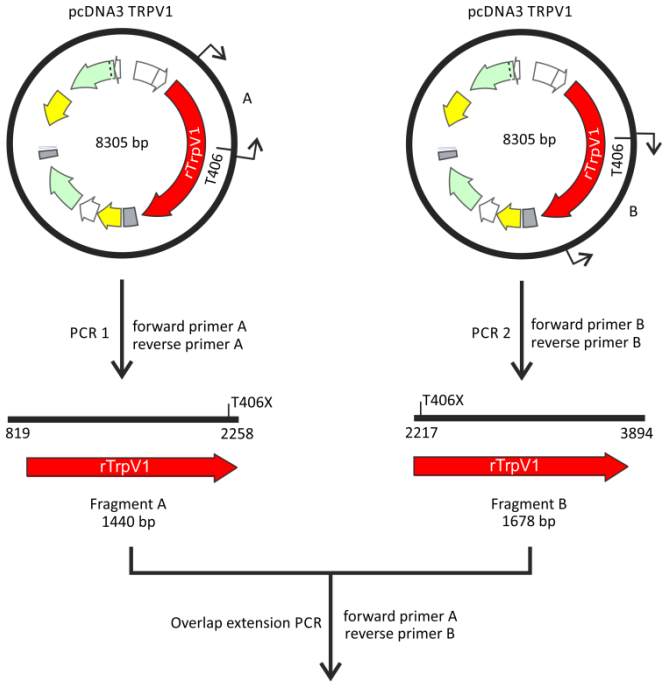

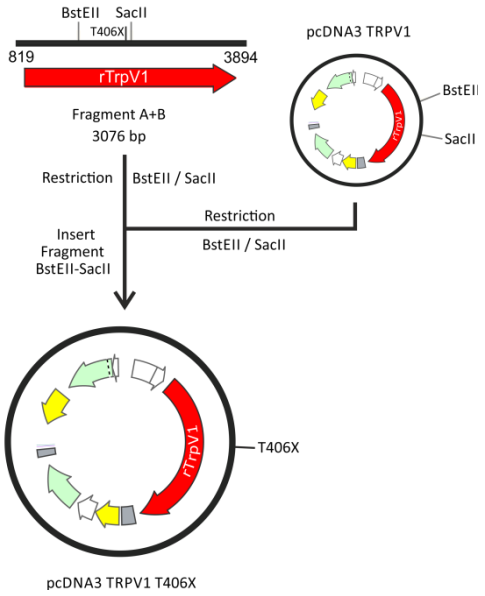

Figure 12. The overlap extension PCR. The mutagenic primers (A_{Rev} and B_{Fov}) and the flanking primers (A_{Fov} and B_{Rev}) were used to generate fragment A and B. Both, fragment A and B were denatured when used as template DNA for the overlap extension PCR. The overlapping strands of each product hybridize and introduce the desired mutation (indicated by T406X). Amplification of fragment AB in the overlap extension PCR was driven by primers A_{Fov} and B_{Rev}. Final product fragment AB was inserted via BstEII and SacII restriction sites into pcDNA3 TRPV1 vector.

5.1.11 **Site-directed TRPV1 mutagenesis via pGEM-T vector cloning**

To insert site-directed mutations into the cDNA of the TRPV1 receptor we also used the T-overhang cloning system. To this end, two different parts of the TRPV1 cDNA were subcloned, the first part included the TRPV1 cDNA sequence between the restriction site BstEII-SacII and the second part includes the TRPV1 cDNA sequence between SacII-XbaI. The targeted sequences were amplified in two independent PCR's, using pcDNA3-TRPV1 as template and BstEII forward and SacII reverse primer or SacII forward and XbaI reverse primer. The purified and linearized PCR products were A-tailed and ligated into the linearized T-tailed pGEM vector. The ligation preparation was transformed into *E. coli* bacteria to amplify and identify via blue/white screening the successfully cloned pGEM-TRPV1 vectors, the pGEM-TRPV1 constructs were checked by colony PCR (Fig. 13). Positive clones were amplified via Mini preparations.

In order to insert the intended mutations mutagenesis PCR's were performed, pGEM-TRPV1 vectors were used as template and forward and reverse mutagenesis primer inserted the mutation. The long elongation time of this mutagenesis PCR led to the full replication of the pGEM-TRPV1 vectors. The amplification of the plasmid DNA in bacteria leads to DNA methylation, whereas the amplification via PCR results in un-methylated DNA. Therefore, the methylation specific restriction enzyme DpnI was used to remove the template pGEM-TRPV1 vectors. The mutated pGEM-TRPV1 and the pCDNA3-TRPV1 vectors were digested with either BstEII-SacII or SacII-XbaI to insert the intended mutation into the pcDNA3-TRPV1 vector (Fig. 14). Finally, pcDNA3-TRPV1 cDNA was checked for unwanted mutation by DNA sequencing.

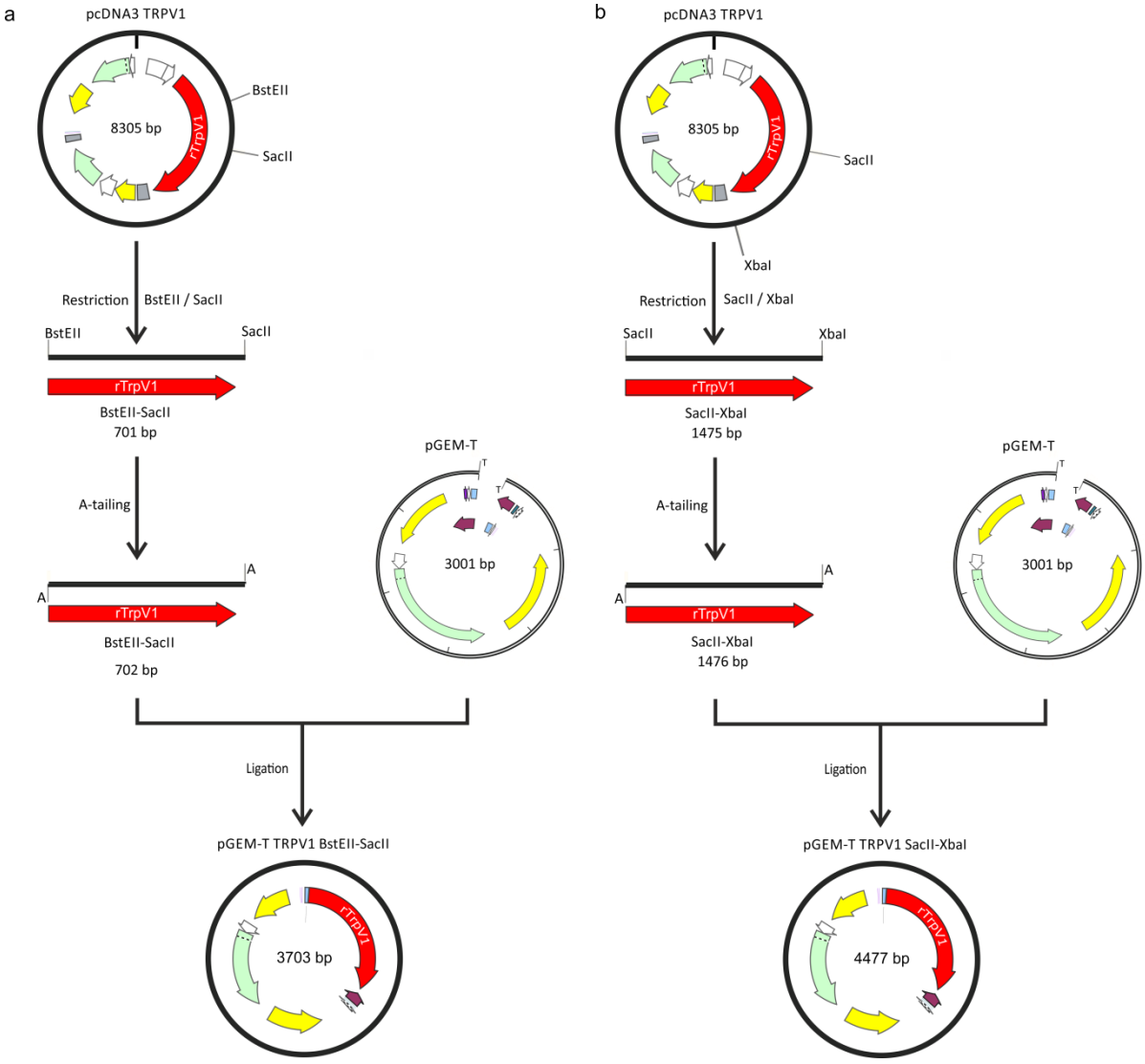

Figure 13. Construction of pGEM-T-TRPV1. TRPV1 fragments (BstEII-SacII and SacII-XbaI) were restricted and subcloned into pGEM-T by TA cloning.

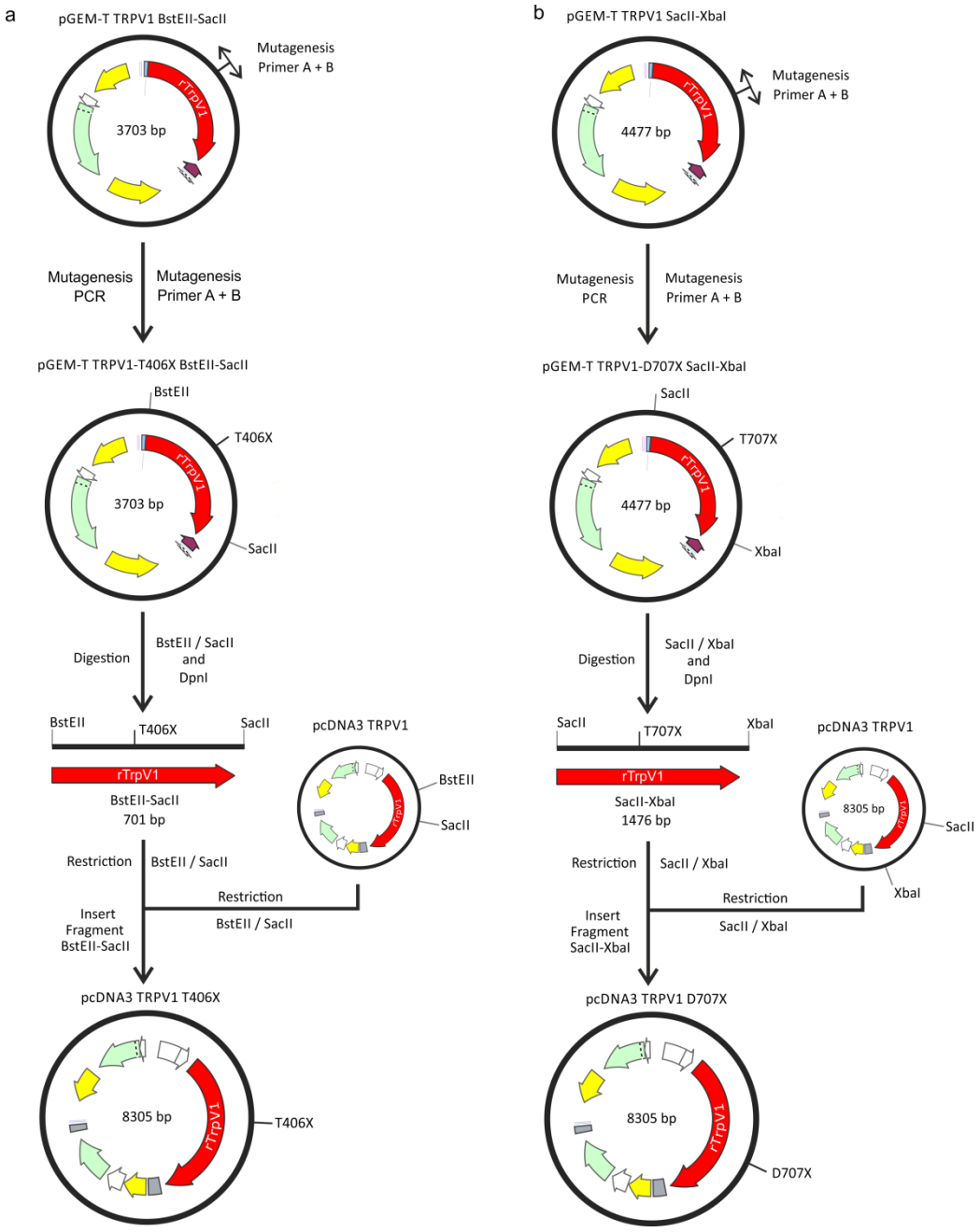

Figure 14. Construction of pCDNA3-TRPV1-mutants. Mutagenesis primer A_{Fov} and B_{Rev} and pGEM-TRPV1-BstEII-SacII or pGEM-TRPV1- SacII-XbaI were used to introduce the desired mutation. DpnI restriction eliminates the template DNA and BstEII-SacII or SacII-XbaI restriction was used to subclone the fragments into the pcDNA3-TRPV1 vector.

5.2 Cell culture

5.2.1 Cultivation of CHO and HEK293 cells

In order to investigate the function of recombinant rat TRPV1 receptors we utilized immortalized Chinese hamster ovary (CHO) and human embryonic kidney (HEK) 293T cells. These cells are characterized by low endogenous expression of ion channels and their simple and reliable cultivation. Chinese hamster ovary (CHO) cells were cultured in MEM (PAN-Biotech, Aidenbach, Germany), whereas HEK293T cells grown in DMEM (Life Technologies, Carlsbad, USA). Both media were supplemented with fetal calf serum 10% (v/v) and anti/anti 1% (v/v) (Sigma-Alderich, St. Louis, USA). Both cells lines were splitted into Ø 10 cm cell culture dishes (TPP, Trasadingen, Switzerland) and incubated at 37 °C and 5% CO_2. After 48 h to 72 h of growth, CHO and HEK293T cells formed adherent monolayers. At a confluency of 80 - 90%, the cells were washed twice with 5 ml $PBS^{-/-}$ (PBS, Sigma Life Science, Sigma Aldrich St. Louis) to remove death cells and Ca^{2+}. In the following, the cells were detached by incubation in 1 ml trypsin/EDTA at 37°C for 2-3 min. The trypsin reaction was stopped by adding 5 ml medium. Then we transferred the cell suspension into 15 ml falcon tubes and centrifuged them for 4 min at 1000 rpm. The supernatant was discarded and the pelletized cells were re-suspended in 2 ml medium, 300 µl of the cell suspension was diluted in 10 ml fresh media and seeded in Ø10 cm culture dishes. For electrophysiological experiments 50k - 100k cells were seeded on Ø 3 cm cell culture dishes (Sarstedt, Nümbrecht, Germany). For Ca^{2+}-imaging or TIRF microscopy about 200k cells were seeded on Ø 2.5 cm glass coverslips (Menzel, Braunschweig, Germany).

5.2.2 Transient transfection of CHO and HEK293 cells

In order to introduce foreign cDNA into eukaryotic host cells, we made use of the Ca^{2+}-phosphate precipitation technique (Gorman et al. 1983). The transfection mix is an aqueous solution containing the target cDNA, Ca^{2+}, and the phosphate buffer HBSS. The cDNA was diluted in distilled water and Ca^{2+} as well as HBSS was added. After an incubation period of 15 min at room temperature, 100 µl of the transfection mix was added to a cell culture dish of CHO or HEK293 cells (Table 1). 12-24 hours after the transfection, we used the cells for electrophysiological experiments, Ca^{2+}-imaging experiments, or TIRF microscopy.

In electrophysiological experiments we used one cell per dish, therefore the transfection efficacy of about 10% was sufficient. To increase the transfection efficiency for Ca^{2+}-imaging and TIRF microscopy experiments we pretreated the cells with chloroqine. 60 minutes before the transfection, we added cloroquine (0.1%), which increased the transfection efficiency to about 30%. The transfection of rTRPV1, CDK5-mCherry, and P35-CFP by means of the Ca^{2+}-phosphate method was inefficient (about 3%), therefore, we made use of the Lipofectamine 2000 reagent. The Lipofectamine reagent is optimized for co-transfection of eukaryotic cells and increased the transfection efficiency to about 10%. The Lipofectamin transfection mix contained 4-6 µg of the target cDNA and the appropriate amount of the Lipofectamine. The cDNA and the Lipofectamin reagent were separately diluted in equal volumes of Optimem and incubated for 10 min. In the following, we mixed the compounds and incubated the solution for 5 min at room temperature (Table 2). Finally, we added the transfection mixture to the cells and after incubation for 12-18 h we used the cells in electrophysiological experiments.

Table 1. Ca^{2+}-phosphate transfection mix.

	Volume per dish	Concentration
Distilled water	36 µl	
cDNA TRPV1	5 µl	1 µg/µl
cDNA GFP	4 µl	1 µg/µl
Ca^{2+}	5 µl	
HBSS	50 µl	

Table 2. Lipofectamin 2000 transfection mix.

	Volume per dish	Concentration
Optimem	100µl	
cDNA TRPV1	4 µl	1 µg/µl
cDNA Cdk5-mCherry	6 µl	1 µg/µl
cDNA p35-CFP	6 µl	1 µg/µl
Lipofectamin 2000	4 µl	

5.3 Electrophysiological experiments

5.3.1 The patch-clamp technique

The patch-clamp technique was developed by Erwin Neher and Bert Sakmann in order to investigate the function of ion channels (Neher & Sakmann 1976). For that purpose two electrodes were either placed in the bath solution (ground electrode) or in a glass micropipette (recording electrode). To close the electric circuit the micropipette is filled with an electrically conductive solution. The tip of the micropipette is characterized by a small opening (1-2 µm), which defines the diameter of the patch and the series resistance (4-6 MΩ). In our experiments, we used two patch configurations, the cell attached or whole-cell configuration. The cell-attached configuration enabled us to characterize single ion channels, whereas the whole-cell configuration allowed us to investigate the function of multiple ion channels in the plasma membrane. In order to establish the cell-attached configuration the tip of the micropipette was placed close to the cell membrane so that tip and membrane form a tight connection (Gigaseal >1 GΩ). We either recorded single-channel events or the whole-cell configuration was established, by disrupting the cell membrane in the micropipette opening. The pre-amplifier or headstage is the key component of the patch-clamp setup. It contains the operating amplifier and the feedback resistor R_f. These electronic components facilitate to inject currents and to measure voltages with the same electrode. The cell itself acts as electronic component: the lipid membrane is an insulator that is surrounded by conductive saline solution, which is the definition for a capacitor. Additionally, the membrane has a defined resistance R_m. Ion channels that conduct ions through the membrane affect the capacitor and resistance characteristics of cell membranes (Fig. 15). The opening of ion channels lowers the membrane resistance and the electrochemical gradient drive the ion flux through the ion channel pore. These currents can be detected and amplified by the patch-clamp technique.

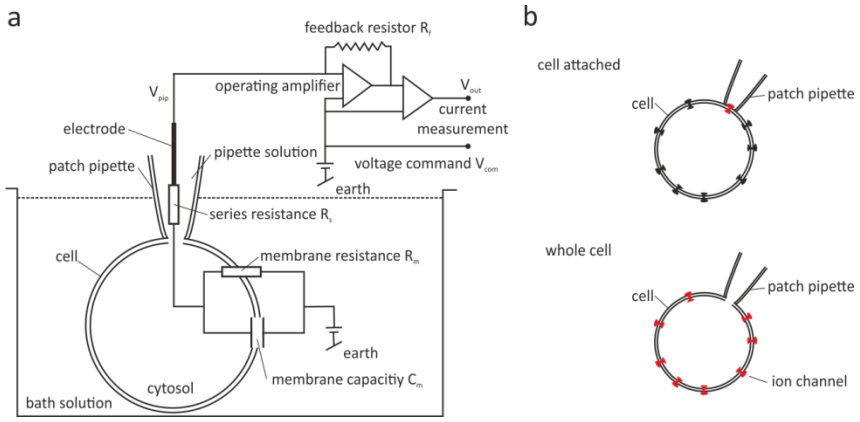

Figure 15. (**a**) Schematic and simplified circuit diagram of the patch-clamp technique, including the electric properties of the plasma membrane, patch pipette, and pre-amplifier. (**b**) Used patch clamp configurations, for single channel characterization the cell attached configuration and for multiple ion channel characterization the whole-cell configuration.

5.3.2 **Experimental design**

Shortly before the patch-clamp experiments start, the cell culture media was replaced by extracellular solution. The recording chamber, including the transfected cells, was placed on the stage of an inverse microscope and the ground electrode was positioned in the bath solution. Fluorescent cells were magnified by means of a 32x objective and 10x oculars and identified by utilizing a xenon short-arc lamp (Osram GmbH, Munich, Germany). The tip of the application system was placed next to the target cell by means of a micro manipulator. In order to adjust and calibrate leak currents, capacity, and series resistance we used the integrated compensation algorithms of the amplifier. Patch-clamp recordings were performed at room temperature (22 °C) using a HEKA EPC10 amplifier (HEKA, Lambrecht, Germany) and HEKA Patchmaster software was used for data acquisition.

5.3.3 **Electrode preparation**

To prevent voltage differences between ground and recording electrode, both were chlorinated. Therefore, the surface of the silver wires were roughened and incubated for 5 to 10 min in $FeCl_3$ solution. Patch pipettes were pulled with a horizontal pipette puller (Zeitz Instruments, Munich, Germany) from borosilicate glass (1.17x 1.50x 100 mm) and had a resistance of 3-5 MΩ for whole cell or 6-8 MΩ for cell-attached configuration.

5.3.4 **Application system**

In order to apply stimuli on the targeted cells, the tip of the application system (ALA Scientific Instruments, Farmigdale, USA) was placed next to the cells. The velocity of the outward flow was air pressure driven and adjusted to about 20 drops/min. 8 reservoirs that contained the different stimuli were connected via silicone tubes to the 8 in 1 mixing chamber and the flow was controlled by squeeze valves.

5.3.5 **Preparation of TRPV1 stimuli**

In order to induce TRPV1-mediated currents the TRPV1 specific agonist capsaicin was used in different concentrations (0.05, 0.1, 0.3, 1, and 3.3 µM). Therefore, capsaicin powder was dissolved in DMSO at a stock concentration of 33.3 mM, this stock solution was diluted in Ringer's solution to the intended concentration. In order to generate the low pH stimulus we reduced the pH of the extracellular solution from 7.35 to 6 by adding HCl.

5.3.6 **Voltage-ramp and voltage-step protocols**

To measure TRPV1-mediated inward and outward currents in whole-cell configuration, cells were held at -60 mV and voltage ramp protocols were applied every second. Voltage ramps started at the holding potential of -60 mV for 100 ms, followed by a voltage step to -100 mV for 100 ms to record inward currents. To obtain outward currents a 500 ms long linear ramp segment from -100 mV to +100 mV was applied and then the ramp was held for 100 ms at +100 mV. The voltage ramp protocol was completed by a last step to -60 mV for 100 ms (Fig. 16a). In order to investigate the current-voltage relationship we made use of voltage-step protocols. The voltage-step protocol began with an initial voltage of 0 mV for 20 ms, followed by 200 ms long steps, which increased from -120 mV to +160 mV in 20 mV intervals. After each voltage-step the cell was held at +60 mV for 20 ms (Fig. 16b). Voltage-ramp and voltage-step protocols were acquired with 2 kHz or 50 kHz, additionally, a low pass Bessel filter at 2.9 kHz was used to reduce noise.

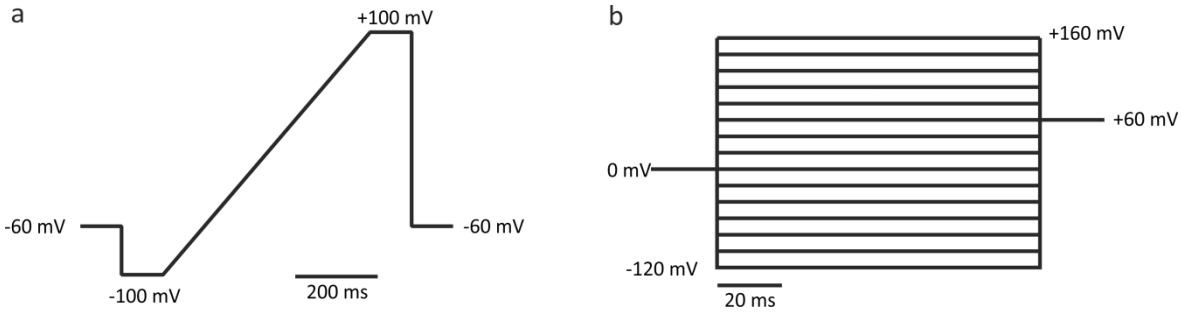

Figure 16. Electrophysiological protocols for measuring whole-cell currents. (**a**) Voltage-ramp protocols (-100 mV to +100 mV) were used to record inward and outward currents. (**b**) Voltage-step protocols (-120 mV to +160 mV) were used to analyze the voltage dependence of TRPV1 receptors.

5.3.7 **Analysis of voltage-ramp and voltage-step protocols**

The average inward and outward current was automatically calculated by the PatchMaster software and plotted as current vs. ramp index graph. Following, the current vs. index graph was transformed into a current vs. time [s] graph and exported as Igor file for further analysis. In order to analyze the current-voltage relationship the PatchMaster software calculated the average current at the end of each voltage step. The current vs. voltage graph was exported as Igor file for further analysis (Fig. 17). The Igor Pro (WaveMetrics, Oregon, USA) was used to collect all necessary data for the statistical analysis e.g. the baseline current, the maximal induced current or the time to the half maximal activation. Moreover, we used the Igor Pro software to calculate the EC_{50} or the conductance G.

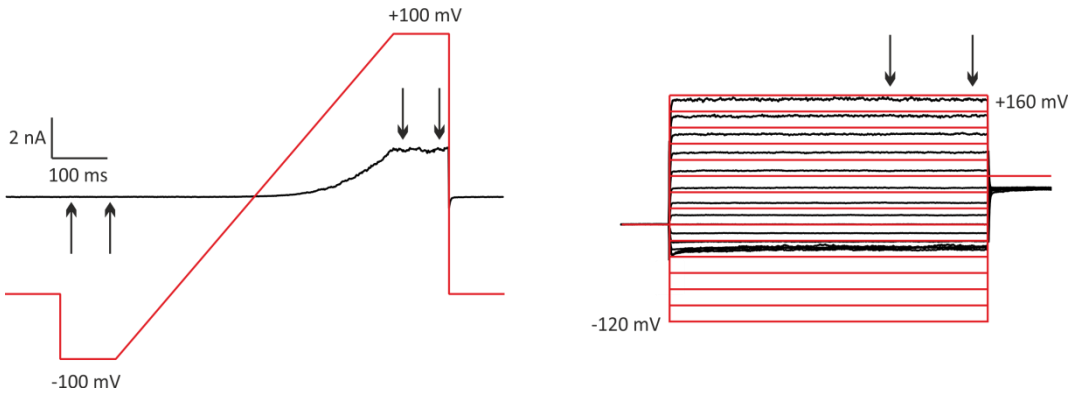

Figure 17. Data acquisition of voltage-ramp and voltage-step protocols. (**a**) The Patchmaster software calculated the average current at -100 mV and +100 mV. (**b**) The current/voltage-relationship of TRPV1 was obtained at the end of each voltage step. The area between the arrows was used to calculate the average current.

5.3.8 **Cell-attached single-channel recordings**

Single TRPV1 channels were recorded in cell-attached configuration, with a series resistance of >1 GΩ (Gigaseal) and leak currents below 50 pA. To equilibrate the membrane potential to about 0 mV the extracellular Na^{2+} ions were replaced by K^{+} ions. Additionally, the pipette solution contained Cs^{2+} and Ba^{2+} to block endogenous K^{+} channels. Depending on the experimental approach 0.3 µM capsaicin was added to the pipette solution and the pipette potential was held at -60 mV. Data were collected for <2 min with a sampling rate of 10 kHz and filtered with a 2.9 low pass Bessel filter.

5.3.9 **Analysis of single-channel recordings**

In order to analyze the single-channel recordings, sweeps were exported from PatchMaster and loaded in the TAC software (Bruxton Corporation). If necessary the sweep was fitted and corrected by integrated algorithms. The open probability (NP_O) and the amplitudes of the opening events were analyzed by means of the sweep histograms (Fig. 18).

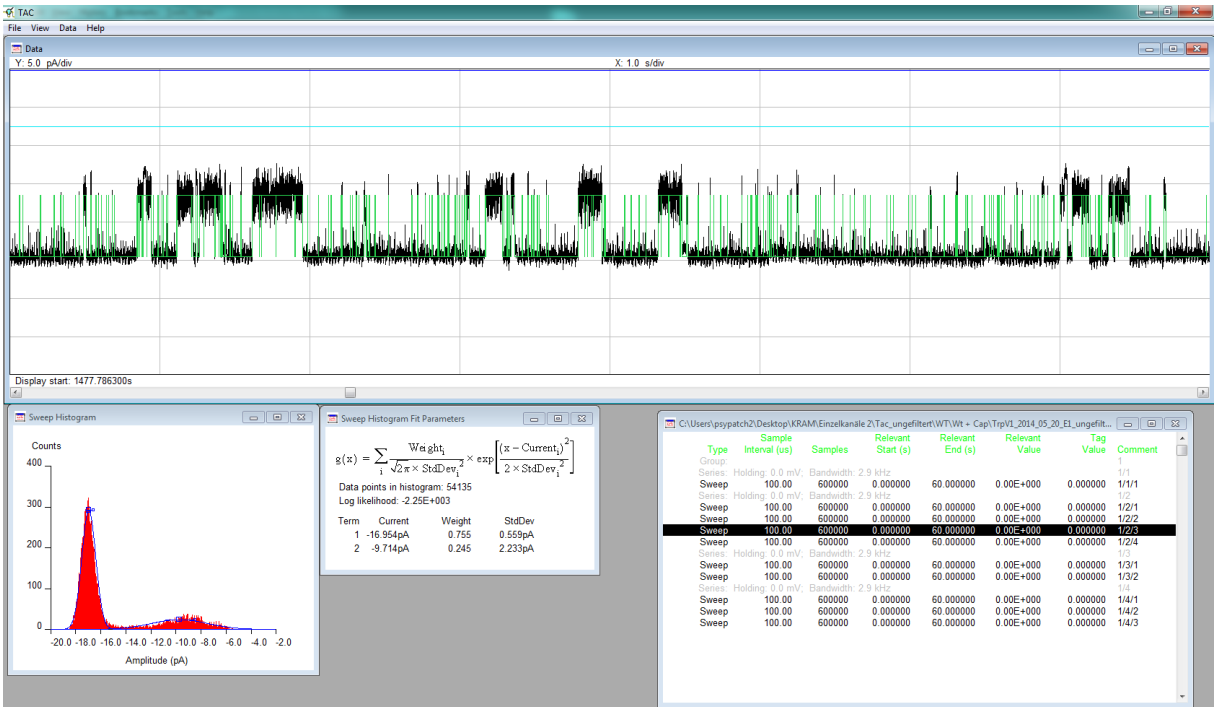

Figure 18. Tac Software for TRPV1 single-channel analysis. (**a**) Exemplary event analysis of TRPV1 single-channel open and closing events. The green line indicates the open or closing of the receptor. (**b**) The sweep histogram (counts vs. amplitude) was used to calculate the open probability NP_O and the amplitude.

Following, the open and close events were collected and exported for further analysis. The dwell time distribution of open and close events was calculated by means of the TacFit software. Finally, we calculated in excel (Microsoft) the average open probability (NP_O). The normalized dwell time distribution and the state time constants of the open and closed states were fitted in Igor Pro with polynomial functions to discriminate between the different open and closed states. For illustration of single channel recordings a 1 kHz low pass filter was added.

5.4 **Fura-2 Ca^{2+} imaging**

The Ca^{2+} imaging technique was designed to investigate the calcium status of cells or tissue by means of fluorescent indicators. We used the ratiometric Ca^{2+} indicator Fura-2-AM, which is based on the Ca^{2+} chelator BAPTA. The Ca^{2+} unbound fura-2 is exited best at wavelength of about 380 nm, whereas the Ca^{2+} bound fura-2 is excited best at wavelength of about 340 nm, while the emission wavelength is at about 510 nm.

5.4.1 **Experimental design**

Ca^{2+} imaging experiments were performed using a ZEISS live cell imaging setup, based on an Observer Z.1. HEK293T cells expressing the TRPV1 or $TRPV1_{T406D}$ were pretreated with the solubilizer Pluronic acid 45-120 min before the measurement and loaded with 2 µl Fura-2-AM (1 mM) that was diluted in 1 ml Opti-MEM. Shortly before the measurement the culture medium of the loaded cells was replaced by Ringer's solution and the cells were placed into the recording chamber. The illumination control system was equipped with a UV-light source and a high speed wavelength switch (Lamda DG4, Sutter instruments, Novato, USA), including optical filters for the wavelengths 340 nm and 380 nm (Carl Zeiss GmbH, Jena, Germany). The excitation light was guided trough a 410 nm dichroic mirror and a 20x Plan-Neofluar or a 40x Fluar objective onto the cells. Before the emitted light was captured by the CCD MRm AxioCam, it was filtered by a BF510 emission band filter. Image recording and control of the microscope and Lambda DG4 was performed with the Zen imaging software (Carl Zeiss GmbH, Jena, Germany). TRPV1-mediated Ca^{2+} influx was induced by application of heated Ringer's solution (about 42°C) or 3.3 µM capsaicin.

The 8 in 1 inline application system with an integrated Peltier-element (Warner Instruments, Hamden, USA) allowed a fast change from cold to hot temperatures.

5.4.2 **Recording settings**

Fura-2 is excited by 340 nm or 380 nm of light and the ratio of the emission at 510 nm is directly related to the amount of intracellular Ca^{2+}. Dependent on the fura-2 loading the exposure time varied between 20 and 200 ms and the binning was set to 5 x 5. The ratio was automatically calculated by the Zen software (Carl Zeiss GmbH, Jena, Germany). Regions of interest (ROI) were defined in order to analyze only the cells, and background correction was used to reduce noise.

$$Ratio = \frac{\mathrm{E}_{\mathrm{Fura-2}}(340\ nm)}{\mathrm{E}_{\mathrm{Fura-2}}(380\ nm)}$$

5.4.3 **Ca^{2+} imaging data analysis**

A detailed description of the Ca^{2+} imaging analysis can be found in the Masterthesis of G. Nordmann (Nordmann 2015). By using a MATLAB algorithm an automated and unbiased response detection system was evolved. Additionally, the MATLAB program was able to evaluate the maximal induced response and the rise time ($t_{10\text{-}90}$) for each cell and each stimulus.

5.5 **TIRF microscopy**

In order to investigate the plasma membrane expression of TRPV1 and $TRPV1_{T406}$ mutants we used the total internal reflection fluorescence (TIRF) microscopy. The TIRF microscopy was developed to investigate a thin region of a specimen. Therefore, CHO cells were seeded on glass cover slips and were transiently transfected with GFP-tagged $TRPV1_{WT}$, $TRPV1_{T406A}$, or $TRPV1_{T406D}$ plasmids. By means of a Leica AF 6000LX system using a HCX PL APO 100x/1.47 oil objective, we monitored 24 h later the GFP fluorescence (488 nm) of the transfected cells. The penetration depth was set to 90 nm to gain the best signal to noise ratio. The GFP fluorescence was imaged in presence of Ca^{2+} Ringer's solution and 5 min after the application of a high concentration of capsaicin resulting in a final concentration 6.6 µM. Cells were selected and used to analyze the time course of the fluorescence by capturing images every 5 s.

5.6 Statistical analysis

The statistical analysis of mouse behavioral tests was performed by Kulkarni et al. with GraphPad Prism software, version 6 (GraphPad, San Diego, CA, USA). Data are expressed as mean ± SEM, with n = number of animals. Statistical differences were assessed by unpaired t-test or by One-way ANOVA followed by Dunnett's multiple comparisons test. Data of electrophysiological, Ca^{2+} imaging, and TRIF microscopy experiments are also expressed as mean ± SEM (n = number of cells). Data were analyzed and visualized by means of Igor Pro 6.37 (WaveMetrics, Oregon, USA), TAC x4.3.3, and TACfit (Bruxton Corporation,Seattle, USA), Microsoft Office (Microsoft Corporation, Redmond, USA), and CorelDraw X6 (Corel Corporation, Ottawa, Canada). Prior to the statistical analysis, we tested the data for normal distribution. The Student's t-test was used for parametric data and the Wilcoxon signed-rank test for non-parametric data. The level of significance was set to $p < 0.05$. In order to calculate the EC_{50} or $V_{1/2}$ of the capsaicin concentration-response relationship or conductance/voltage-relationship, we used the Wavemetrics Igor Pro 6.37 software.

5.7 Equations

Hill's Equation:

$$\frac{I}{I_{max}} = \frac{[x]^n}{EC_{50}{}^n + [x]^n}$$

I = current, I_{max} = maximal current at saturating concentration, x = concentration of tested agonist, EC_{50} = the calculated concentration that elicits 50% of maximal current, and n = Hill coefficient.

Sigmoidal function:

$$G = \frac{[G_{max} - G_{min}]}{1 + \exp\left[\frac{V_{1/2} - V}{V_{slope}}\right]}$$

G = conductance, G_{max} = maximal conductance, G_{min} = minimal conductance, V = applied voltage, $V_{1/2}$ = voltage at half maximal conductance and V_{slope} = slope of the activation curve.

6 Results

6.1 TRPV1 desensitization is modulated by co-expression of Cdk5 and p35

Since Ca^{2+}-dependent desensitization is a characteristic feature of TRPV1 receptor function and may have impact on the sensitivity of TRPV1 expressing nerve fibers, we set out to investigate the effect of Cdk5-mediated phosphorylation of TRPV1 receptors on ion channel function. To this end, CHO cells co-expressing TRPV1, Cdk5-mCherry and p35-CFP or TRPV1 and GFP were patched in whole-cell configuration and voltage-ramp protocols (-100 mV to +100 mV) were consecutively applied to investigate inward and outward currents. The co-expression of fluorescent proteins was required to visually select transfected CHO cells. In untransfected CHO cells the application of voltage-ramps induced only minor voltage-dependent currents (few endogenous voltage-dependent K^+ ion-channels), which were not affected by the application of 3.3 µM capsaicin (Fig. 19). In TRPV1-expressing CHO cells, TRPV1-mediated currents were induced by perfusing the recorded cell with 3.3 µM capsaicin in physiological Ringer's solution for 200 s. The capsaicin-induced inward and outward currents were characterized by fast activation kinetics as well as a strong acute desensitization in the presence of the agonist (Fig. 20a).

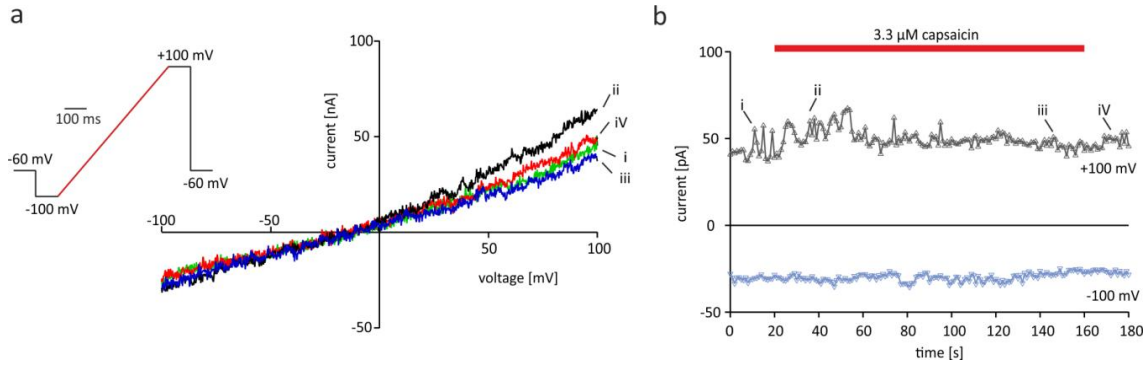

Figure 19. Untransfected CHO cells do not show capsaicin-induced currents. Cells were patched in Ringer's extracellular solution and 3.3 µM capsaicin was applied, but no TRPV1-mediated currents were recorded. (**a**) Voltage ramp-induced currents (-100 mV to +100 mV) in the presence or absence of 3.3 µM capsaicin. (**b**) Temporal course of inward (-100 mV) and outward (+100 mV) currents before, while and after the washout of 3.3 µM capsaicin (n = 5).

In CHO cells co-expressing TRPV1, Cdk5 and p35, the capsaicin-induced currents showed still fast activation kinetics, but did no longer desensitize in the presence of capsaicin (Fig. 20b). The desensitization ratio of TRPV1-mediated outward currents (+100 mV) was 0.54 ± 0.04 and 0.43 ± 0.05 for inward currents (-100 mV), whereas the co-expression of TRPV1, Cdk5, and p35 induced a significant reduction of Ca^{2+}-dependent desensitization, with ratios of 0.78 ± 0.06 at +100 mV and 0.68 ± 0.07 at -100 mV (unpaired *WR-test* $p < 0.05$). Since the desensitization of TRPV1 ion channels is known to depend on extracellular Ca^{2+} (Rosenbaum et al. 2004; Koplas et al. 1997), we set out to analyze the TRPV1 receptor desensitization in the absence of external Ca^{2+}. The data revealed that the lack of external Ca^{2+} prevented the acute desensitization of TRPV1 receptors (Fig. 20c). The maximal currents recorded in TRPV1, Cdk5 and p35 co-expressing cells were analyzed and compared to the currents evoked in cells expressing TRPV1 only, and revealed a slight but significant reduction in the maximal current (unpaired *WR-test* $p < 0.05$) (Fig. 20d). This reduction in amplitude may reflect reduced expression levels of receptor proteins, since the size of the recorded cells was consistent at 25 ± 2.4 pF (n = 91). The acute desensitization of the receptors was analyzed by calculating the ratio of the maximal current and the plateau of the steady state current ($I_{maximal}/I_{steady}$) (Fig. 20f). The desensitization ratio of TRPV1-mediated outward currents (+100 mV) was 0.54 ± 0.04 and 0.43 ± 0.05 for inward currents (-100 mV), whereas the co-expression of TRPV1, Cdk5, and p35 resulted in ratios of 0.78 ± 0.06 at +100 mV and 0.68 ± 0.07 at -100 mV. The activation kinetics represented as time to half-maximal response (t_{50}) of cells co-expressing TRPV1, Cdk5, and p35 was significantly increased (TRPV1: 3.2 ± 0.2 s at +100 mV, and 4.5 ± 0.3 s at -100 mV; TRPV1, Cdk5, p35: 4.8 ± 0.8 s at +100 mV, and 12.6 ± 3.2 s at -100 mV; unpaired *WR-test* $p < 0.05$) (Fig. 20e). These data indicate that Cdk5-mediated phosphorylation of TRPV1 in CHO cells co-expressing TRPV1, Cdk5, and p35 has severe consequences on TRPV1 function. Therefore, we hypothesize that the reduced Ca^{2+}-dependent desensitization in cells co-expressing TRPV1, Cdk5 and p35 induces an increased receptor efficacy and promotes the development of allodynia and hyperalgesia in sensory neurons.

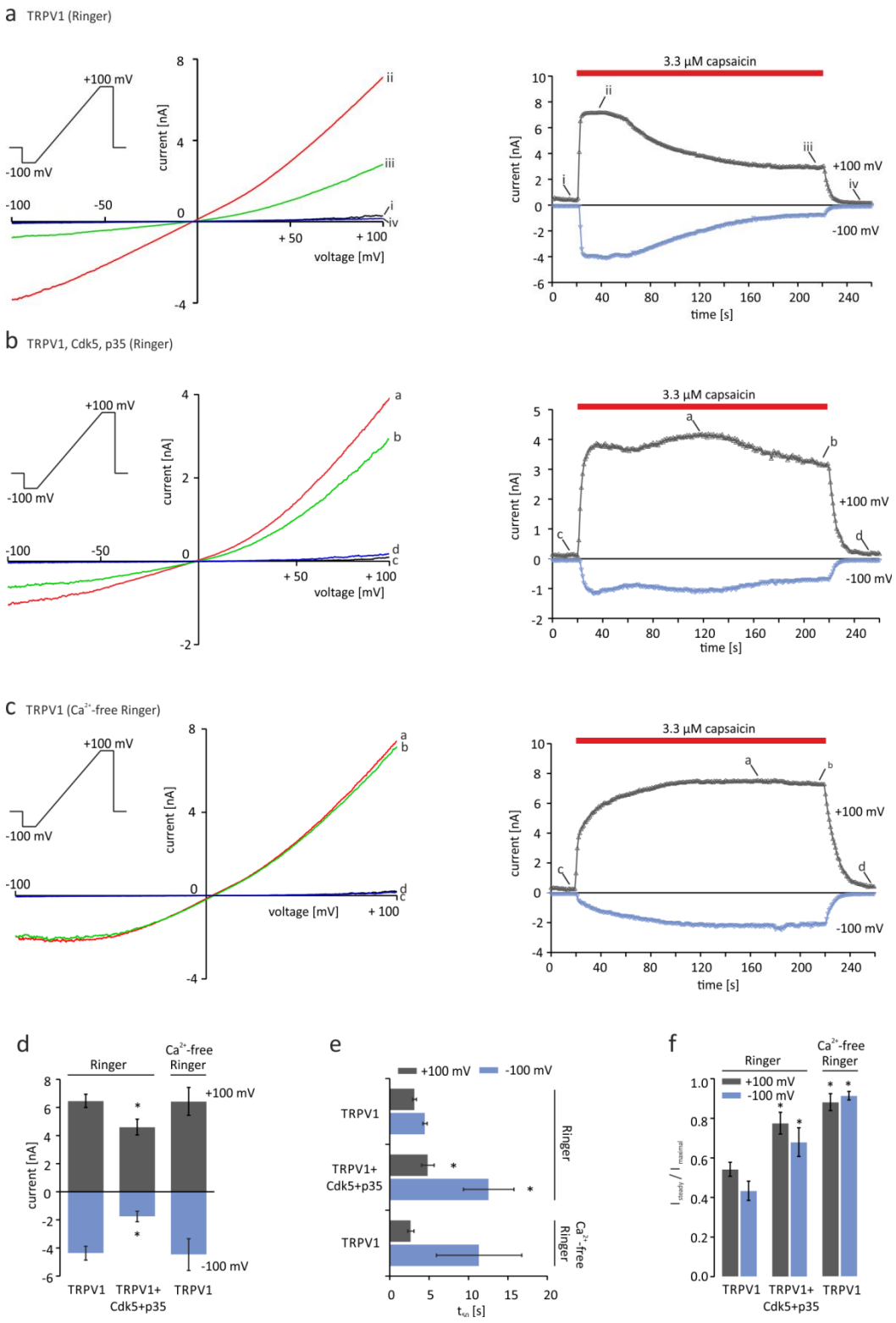

Figure 20. Functional characterization of capsaicin-induced TRPV1-mediated currents. (**a**) Application of 3.3 µM capsaicin in the presence of extracellular Ca^{2+} induced fast activating TRPV1-mediated currents. The Ca^{2+}-dependent desensitization decline the TRPV1 currents to a steady-state. (**b**) Co-expression of TRPV1, Cdk5-mCherry and p35-CFP inhibits the Ca^{2+}-mediated desensitization, similar to (**c**) the capsaicin-induced TRPV1-mediated currents in the absence of extracellular Ca^{2+}.

(**d**) Maximal currents, (**e**) time to half-maximal response represented as t_{50} and (**f**) desensitization as ratio I_{steady} / $I_{maximal}$ of n = 10-36 independent measurements. Asterisk (*) indicates significant differences compared to the corresponding parameter recorded under Ca^{2+}-containing conditions (unpaired *WR-test* $p < 0.05$).

6.2 TRPV1, Cdk5 and p35 co-expression does not affect the capsaicin sensitivity

To investigate the effect of Cdk5-mediated phosphorylation on capsaicin sensitivity of TRPV1, we set out to analyze the concentration/response-relationship of CHO cells expressing TRPV1 or TRPV1, Cdk5 and p35. Again voltage-ramp protocols (-100 mV to +100 mV) were used to drive outward and inward currents and various capsaicin concentrations (0.05, 0.1, 0.3, 1 and 3.3 µM) were successively applied in the absence of extracellular Ca^{2+}. Representative recordings of CHO cells expressing (a) TRPV1 or (b) TRPV1, Cdk5, and p35 are shown in Figure 21 and reveal that increasing concentrations of capsaicin induce increasing TRPV1-mediated responses (Fig. 21). For analysis, the TRPV1-mediated responses were normalized to the maximal response induced by 3.3 µM capsaicin and the Hill equation was used to calculate EC_{50} values. Due to the voltage-dependence of TRPV1 receptors, the outward currents were increased compared to the inward currents, leading to different EC_{50} values for outward and inward signals. EC_{50} values were calculated to be 0.25 ± 0.05 µM at +100 mV and 0.63 ± 0.13 µM at -100 mV, whereas co-expression of TRPV1, Cdk5, and p35 resulted in EC_{50} values of 0.28 ± 0.04 µM at +100 mV and 0.55 ± 0.08 µM at -100 mV. The statistical analysis of EC_{50} values revealed no significant sensitization of TRPV1 ion channels due to the co-expression of Cdk5 in CHO cells (unpaired *t-test:* +100 mV: $p = 0.34$, -100 mV: $p = 0.51$). In conclusion the concentration-response relationship of TRPV1, Cdk5, and p35 indicates that the sensitivity of TRPV1 to capsaicin is unaffected by Cdk5-mediated phosphorylation.

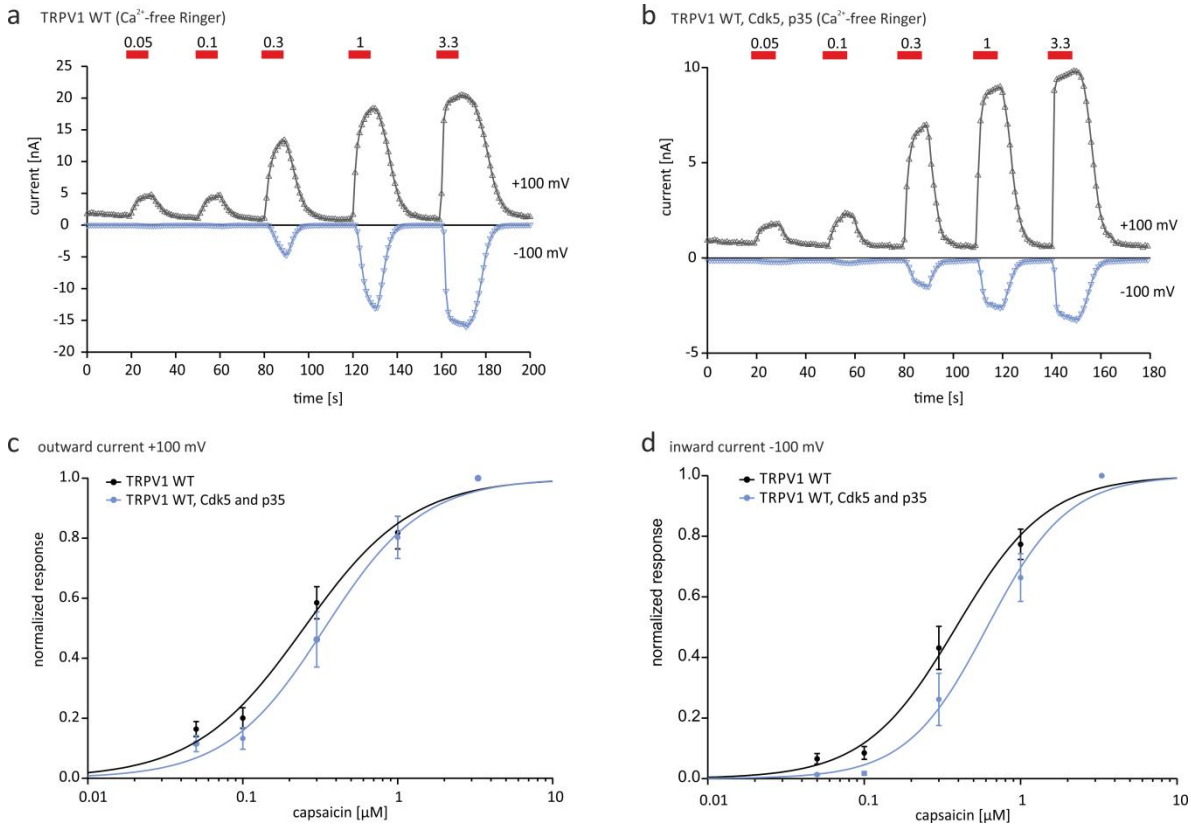

Figure 21. Capsaicin concentration/response-relationship of CHO cells co-expressing TRPV1 or TRPV1, Cdk5 and p35. Voltage-ramp protocols (-100 mV to +100 mV) were used to record TRPV1-mediated outward and inward currents in absence of extracellular Ca^{2+}. (**a, b**) Increasing capsaicin concentrations induced increasing responses in CHO cells expressing TRPV1 or TRPV1, Cdk5, and p35. (**c, d**) Normalization to the maximal response and calculation of EC_{50} values by means of the Hill equation of inward and outward responses revealed that Cdk5 co-expression does not affect the TRPV1 sensitivity. EC_{50} values: TRPV1 (+100 mV): 0.25 ± 0.05, (-100 mV): 0.63 ± 0.13; TRPV1, Cdk5, p35 (+100 mV): 0.28 ± 0.04, (-100 mV): 0.55 ± 0.08; unpaired *t-test* (+100 mV): $p = 0.34$, (-100 mV): $p = 0.51$; (n = 8-10).

6.3 TRPV1 T406 is located close to the TRP domain

The *in vivo* and *in vitro* findings revealed that the co-expression of Cdk5 modulates the TRPV1 ion channel function and has severe physiological consequences. Furthermore, Pareek et al. could show that the TRPV1 is phosphorylated by Cdk5 at threonine-407 in mice, which correspond to threonine-406 in rat (Pareek et al. 2007). In order to investigate the functional impact of Cdk5-mediated phosphorylation on rTRPV1 at position T406 in detail, we made use of the high resolution cryo-microscopy structures of rTRPV1, which were published by Cao et al. and Liao et al. in 2013 (Liao et al. 2013; Cao et

al. 2013). Three different conformations of the TRPV1 are available: The apoprotein (3j5p) representing the closed state, the capsaicin bound (3j5r) showing an intermediated state, and the RTX/DkTx bound (3j5q) representing the open state (Fig. 22). The structure of the apoprotein reveals that the amino acid T406 is located in a flexible loop. Considering the conformational change in the capsaicin bound state, T406 moves to the end of an alpha-helix and resides in the open state near to the alpha-helix. Due to the relative proximity of this flexible loop to the TRP-domian, which is connected to the pore-forming transmembrane domain (TMD) 6, we assume that the structural changes could be part of the gating mechanism. Thus, we aim to characterize the functional consequences of steric and electric alterations at position T406. To this end T406 was replaced by the negatively charged amino acids Asp or Glu, the positively charged amino acids His, Lys, and Arg and the neutral amino acids Ile, Ala, Met, Phe, Tyr, and Pro. Since, the introduction of a negatively charged phosphate group at T406 led to significant functional changes, we were especially interested in the effect of negatively charged residues. Due to the steric properties of proline (helix breaking) we also replaced proline-407 by alanine to evaluate its functional effect. To replace the amino acids we made use of site-directed mutagenesis and verified each TRPV1 mutant via sequencing. By this approach we force the TRPV1 structure in non-native conformations, but we were able to characterize the effect of this specific amino acid on TRPV1 function in detail. In particular, we were interested in TRPV1 ion channel desensitization, sensitization, voltage-dependence, polymodal activation as well as single channel properties.

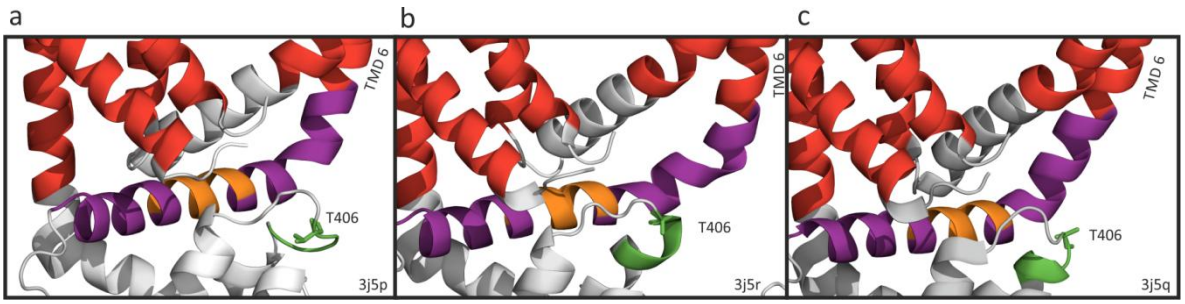

Figure 22. TRPV1 structure in distinct conformations revealed structural changes at position T406. Analysis of the TRPV1 (**a**) apoprotein, (**b**) capsaicin bound and (**c**) RTX/DkTx bound revealed that T406 is located in a flexible linker close to the TRP domain including the TRP box. Relevant TRPV1 structures were color coded: **Red** transmembrane domain (TMD) 1-6, **Purple** TRP domain, **Orange** TRP box, and **Green** Cdk5 consensus site.

6.4 **TRPV1 T406 mutagenesis modulates receptor function**

In order to investigate the effect of $TRPV1_{T406}$ mutagenesis on receptor function, CHO cells expressing mutant receptors were challenged with 3.3 µM capsaicin for 200 s in the presence of extracellular Ca^{2+}. Figure 23 shows representative capsaicin-induced outward and inward currents of (a) $TRPV1_{WT}$, (b) $TRPV1_{T406D}$, (c) $TRPV1_{406E}$, (d) $TRPV1_{T406H}$, (e) $TRPV1_{T406K}$, (f) $TRPV1_{T406R}$, (g) $TRPV1T_{406I}$, (h) $TRPV1_{P407A}$, (i) $TRPV1_{T406A}$, (j) $TRPV1T_{406M}$, (k) $TRPV1_{T406F}$, (l) $TRPV1_{T406Y}$, and (m) $TRPV1_{T406P}$ (Fig. 23). 3.3 µM capsaicin induced robust inward and outward currents in all TRPV1 mutants, but major differences were found in the activation kinetics and desensitization. The amplitudes of the TRPV1-mediated currents were highly variable, which is probably due to different expression rates (Fig. 24a). The most conspicuous effects were related to the activation kinetics of $TRPV1_{T406D}$ and $TRPV1_{T406E}$, with t_{50} values of > 30 s demonstrating significantly slowed receptor kinetics (t_{50} at +100 mV: WT 3 ± 0.2 s, T406D 36 ± 6 s, T406E 16 ± 3 s, at -100 mV: WT 4 ± 0.2 s, T406D 57 ± 12 s, T406E 31 ± 5 s) (*Tukey's-test* $p < 0.05$) (Fig. 24b). Moreover, the Ca^{2+}-dependent desensitization of $TRPV1_{WT}$ (I_{steady} / $I_{maximal}$ at +100 mV: 0.47 ± 0.04, at -100 mV: 0.39 ± 0.04) was affected by introducing at position T406 the negatively charged Asp or Glu, the positively charged His or Lys, as well as the bulky Pro. Analyzing the acute desensitization of the $TRPV1_{T406}$ mutants revealed a significant reduction of Ca^{2+}-dependent desensitization of CHO cells expressing $TRPV1_{T406D}$ (+100 mV: 0.85 ± 0.04, -100 mV: 0.86 ± 0.03), $TRPV1_{T406E}$ (+100 mV: 0.80 ± 0.04, -100 mV: 0.81 ± 0.04), $TRPV1_{T406H}$ (+100 mV: 0.76 ± 0.06), $TRPV1_{406K}$ (+100 mV: 0.87 ± 0.06, -100 mV: 0.86 ± 0.04), or $TRPV1_{T406P}$ (+100 mV: 0.90 ± 0.02, -100 mV: 0.86 ± 0.04) (*Tukey's-test:* $p < 0.05$) (Fig. 24c). In contrast, no differences were found in the other T406 mutants compared to $TRPV1_{WT}$. Neither the activation kinetics with t_{50} values of 3 to 7 s nor the acute desensitization with I_{steady} / $I_{maximal}$ ratios of 0.2 to 0.6 were significantly different from the $TRPV1_{WT}$. In conclusion, these data show that position T406 is crucial for TRPV1 function. In particular, negatively charged amino acid residues affect the activation kinetics and acute desensitization, but also the positively charged amino acids His and Lys, as well as the bulky Pro prevent the Ca^{2+}-dependent desensitization. Interestingly, the exchange of P407 to alanine at the directly adjacent position had no effect on the TRPV1 ion channel gating.

In summary, the reduced desensitization in T406D and T406E mutants is in line with our previous findings. Introduction of a negative charge at T406 (by Cdk5-mediated phosphorylation) inhibits the Ca^{2+}-induced desensitization. However, the slow activation kinetics of $TRPV1_{T406D}$ and $TRPV1_{T406E}$ are an exclusive hallmark of the mutations, not found in the wild-type TRPV1 channels. Thus, we set out to investigate this aspect of TRPV1 activation in detail.

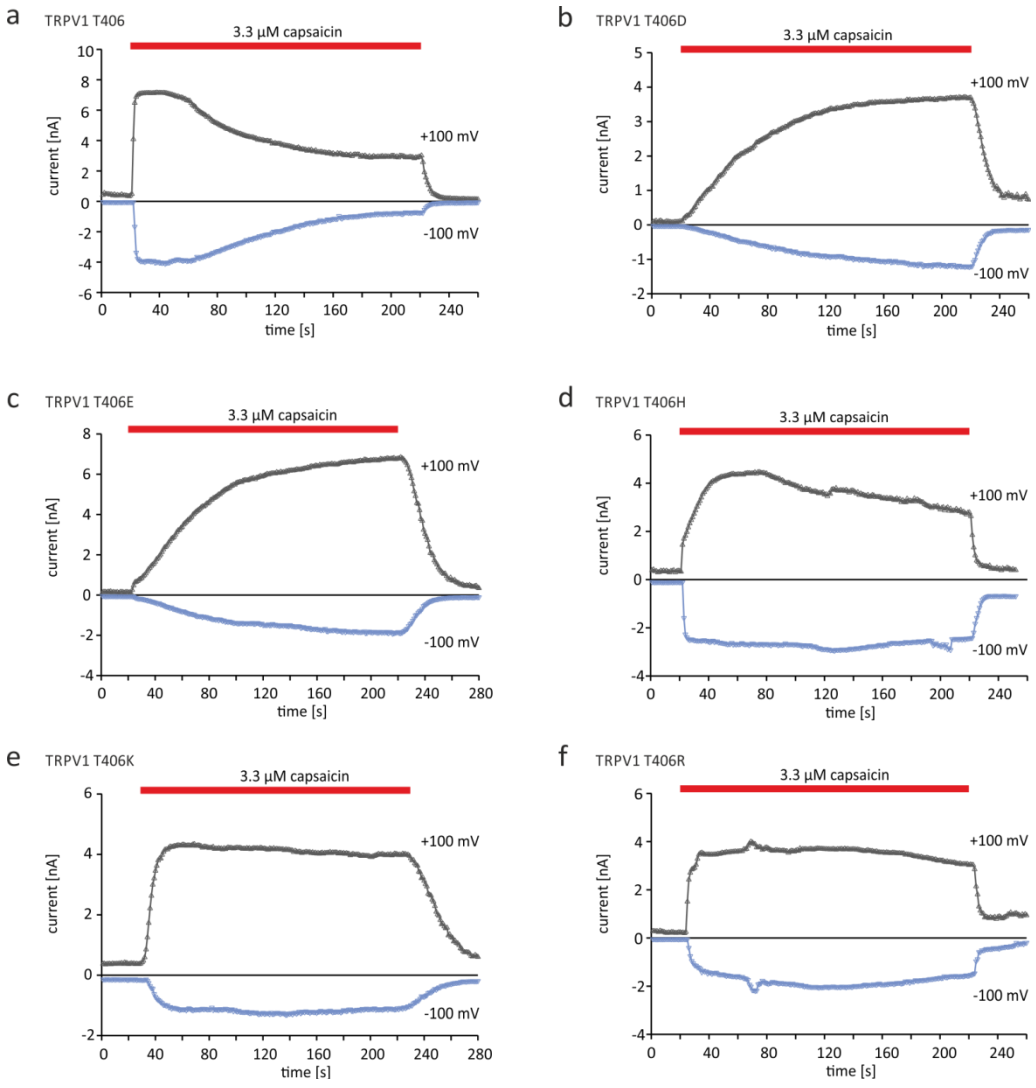

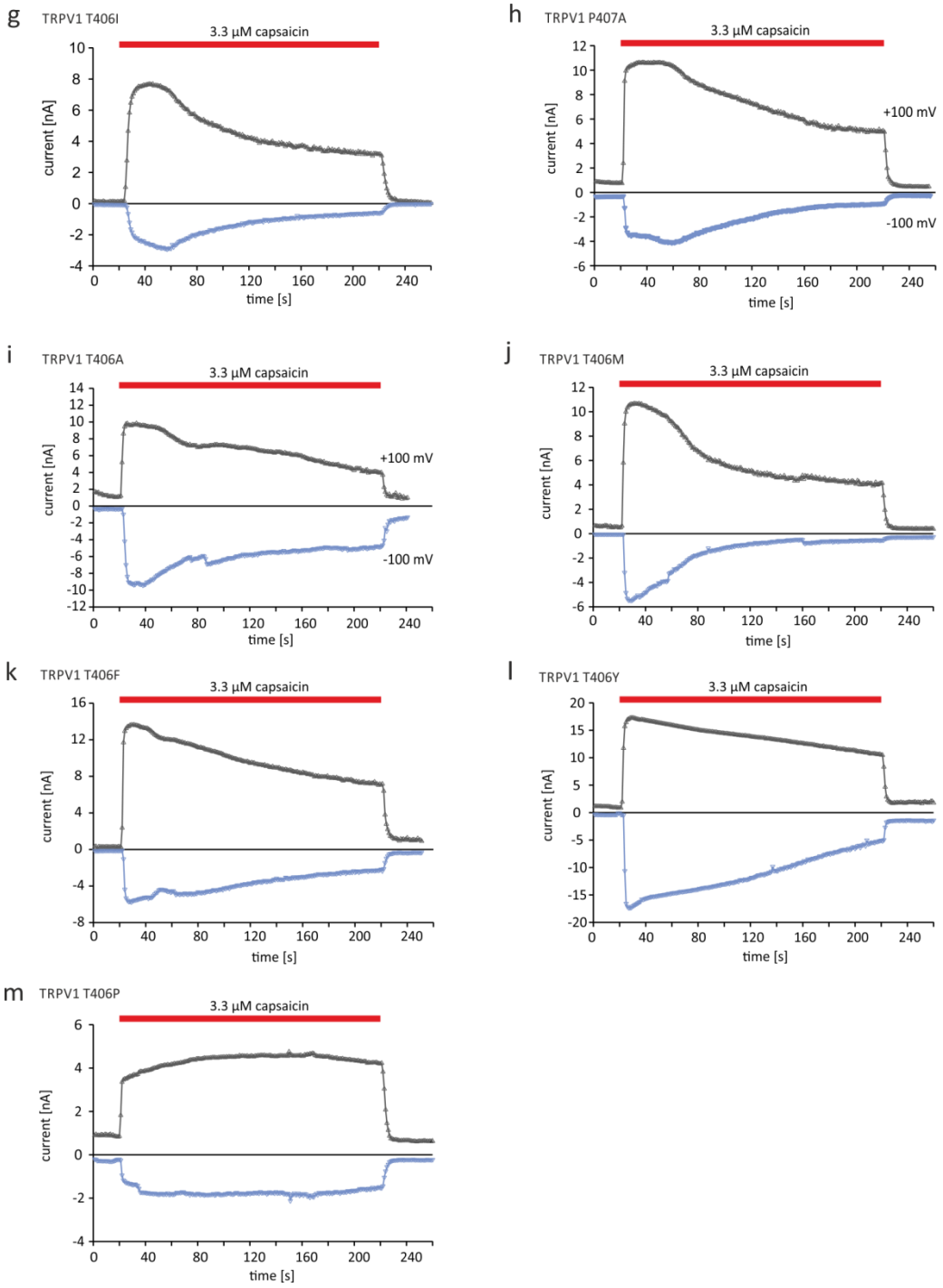

Figure 23. Representative inward and outward currents of CHO cells expressing $TRPV1_{WT}$ or $TRPV1_{T406}$ mutants. Application of 3.3 µM capsaicin for 200 s induced TRPV1-mediated currents in Ca^{2+} containing extracellular Ringer's solution to allow for ion channel desensitization. Inward (-100 mV) and outward (+100 mV) currents of (**a**) $TRPV1_{WT}$, (**b**) $TRPV1_{T406D}$, (**c**) $TRPV1_{406E}$, (**d**) $TRPV1_{T406H}$, (**e**) $TRPV1_{T406K}$, and (**f**) $TRPV1_{T406R}$, (**g**) $TRPV1_{P406I}$, (**h**) $TRPV1_{P407A}$, (**i**) $TRPV1_{P406A}$, (**j**) $TRPV1_{P406M}$, (**k**) $TRPV1_{P406F}$, (**l**) $TRPV1_{P406Y}$, and (**m**) $TRPV1_{T406P}$.

The activation kinetics (t_{50}) of $TRPV1_{T406D}$ and $TRPV1_{T406E}$ were remarkably slowed down and the introduction of negatively (Asp,Glu) or positively (His,Lys) charged amino acid residues, as well as Pro at position T406, prevented the Ca^{2+}-induced desensitization (n = 7-14).

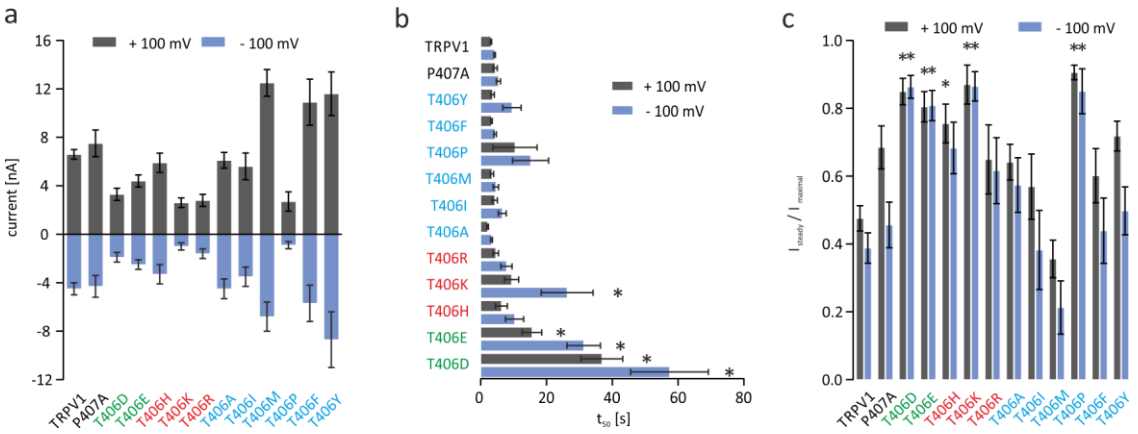

Figure 24. Statistical analysis of data obtained from $TRPV1_{T406}$ mutants. Data are presented as mean ± sem. (**a**) Maximal TRPV1-mediated response induced by 3.3 µM capsaicin. (**b**) Activation kinetics presented as t_{50} revealed that $TRPV1_{T406D}$, $TRPV1_{T406E}$ and the inward current of $TRPV1_{T406K}$ were significantly reduced (*Tukey's-test* $p < 0.05$). (**c**) Acute desensitization presented as ratio (I_{steady} / $I_{maximal}$) indicates that in $TRPV1_{T406D}$, $TRPV1_{T406E}$, $TRPV1_{T406H}$, $TRPV1_{406K}$ or $TRPV1_{T406P}$ the Ca^{2+}-dependent desensitization was significantly reduced (*Tukey's-test:* $p < 0.05$) *(*n = 7 - 14).

6.5 Use-dependent activation of $TRPV1_{T406D}$

The next step was to investigate the activation kinetics of $TRPV1_{T406D}$ in detail. In particular, we were interested in the characteristics of the first and second series of responses induced by consecutive applications of capsaicin. Therefore, CHO cells expressing $TRPV1_{WT}$ $TRPV1_{T406A}$ or $TRPV1_{T407D}$ were recorded in the whole-cell configuration using Ringer's bath solution and held for > 2 min at +100 mV. Voltage-ramp protocols (-100 mV to +100 mV) were used to drive inward and outward currents through activated TRPV1 receptors. The initial TRPV1-mediated response was evoked by the application of 0.3 µM or 3.3 µM capsaicin for 220 s, the second response was induced by the same capsaicin concentration 1 min after the capsaicin washout (Fig. 25). In CHO cells expressing $TRPV1_{WT}$ and $TRPV1_{T406A}$, the first application of 0.3 µM capsaicin induced fast responses (WT t_{50}, at +100 mV: 4 ± 0.4 s, at -100 mV: 6 ± 0.8 s) with maximal currents of WT at +100 mV: 3.5 ± 0.8 nA, at -100 mV: 1.8 ± 0.8 nA.

These TRPV1-mediated responses were characterized by a strong acute desensitization with I_{steady} / $I_{maximal}$ ratios about 0.6 (WT, at +100 mV: 0.59 ± 0.04; at -100 mV: 0.50 ± 0.05). CHO cells expressing $TRPV1_{WT}$ or $TRPV1_{T406A}$ were also challenged with 3.3 µM capsaicin. The TRPV1-mediated currents had similar activation kinetics and desensitization ratios as the responses evoked by 0.3 µM capsaicin, but 3.3 µM capsaicin evoked significantly increased maximal responses (unpaired *WR-test* $p < 0.05$). CHO cells expressing $TRPV1_{T406D}$ were also held at +100 mV for > 2 min and challenged with 0.3 µM capsaicin, but the TRPV1-mediated currents were characterized by significantly slowed activation kinetics (T406D t_{50}, at +100 mV: 63 ± 4.4 s, at -100 mV: 66 ± 6.4 s) (*Tukey's-test* $p < 0.05$) and maximal amplitudes of 2.0 ± 0.6 nA at +100 mV and 0.4 ± 0.1 nA at -100 mV. Furthermore, the I_{steady} / $I_{maximal}$ ratios 0.94 ± 0.02 at +100 mV and 0.94 ± 0.01 at -100 mV revealed that $TRPV1_{T406D}$ did not desensitize. Interestingly, the second application of the same stimulus (0.3 µM capsaicin) induced a fast $TRPV1_{T406D}$-mediated response (T406D t_{50}, at +100 mV: 2 ± 0.2 s, at -100 mV: 3 ± 0.4 s) with maximal amplitudes of 1.4 ± 0.5 nA at +100 mV, and 0.3 ± 0.2 nA at -100 mV. Comparing the 1st and 2nd maximal currents of $TRPV1_{WT}$ and $TRPV1_{T406A}$ revealed that the 2nd response was significantly reduced (unpaired *WR-test:* $p < 0.05$). However, in $TRPV1_{T406D}$ we did not found a reduction of 2nd maximal current, supporting the hypothesis that the T406D mutation prevents the Ca^{2+}-dependent desensitization. Moreover, challenging $TRPV1_{T406D}$ with 3.3 µM capsaicin evoked currents with activation kinetics and desensitization rates which were similar to the currents evoked by 0.3 µM capsaicin, but with increased maximal responses. Additionally, we analyzed the TRPV1-mediated currents of CHO cells co-expressing $TRPV1_{T406D}$, Cdk5, and p35. Interestingly, we found no difference in activation and desensitization kinetics compared to cells only expressing $TRPV1_{T406D}$ (Fig. 26). The 1st $TRPV1_{T406D}$-mediated response in cells co-expressing $TRPV1_{T406D}$, Cdk5, and p35 showed slowed activation kinetics of about 40 s at +100 mV and about 60 s at -100 mV (Fig. 26c). The analysis of the I_{steady} / $I_{maximal}$ ratios revealed that the co-expression of $TRPV1_{T406D}$, Cdk5, and p35 prevents the ion channel desensitization (Fig. 26d). These data demonstrate that a preceding voltage stimulus of +100 mV or the co-expression of $TRV1_{T406D}$, Cdk5, and p35 does not affect the initial slow activation kinetics of $TRPV1_{T406D}$. However, the priming of $TRPV1_{T406D}$ with capsaicin accelerates the activation kinetics of

TRPV1$_{T406D}$ receptors. In conclusion the use-dependent activation of TRPV1$_{T406D}$ revealed that a negative charge at position T406 had severe consequences on TRPV1 the activation and desensitization kinetics. Since we found these altered activation kinetics, we were interested in the molecular mechanism, which lead to this use-dependent behavior. Two mechanisms could play a role, the expression of TRPV1 ion channels in the plasma membrane or the ion channel gating mechanism.

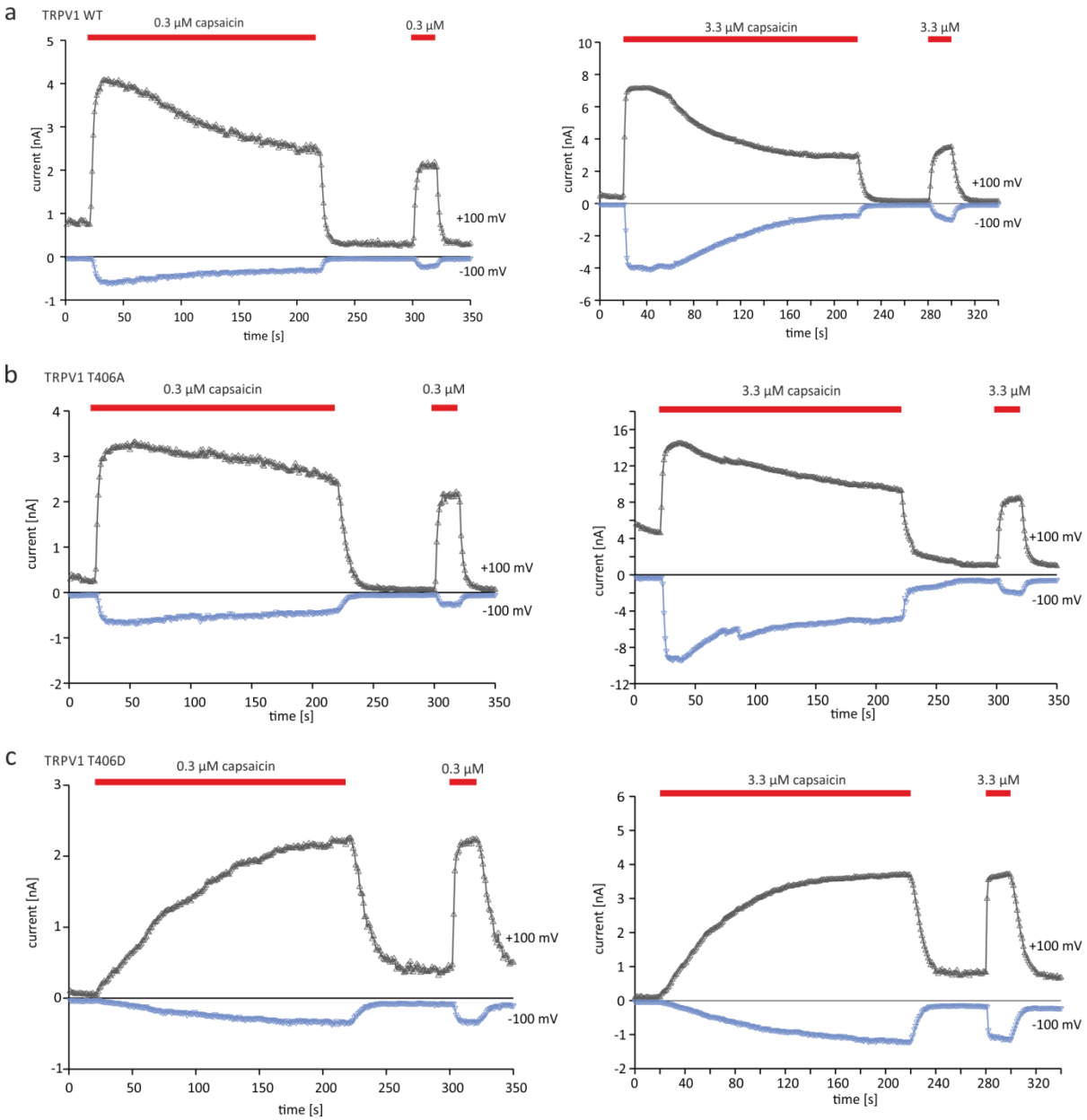

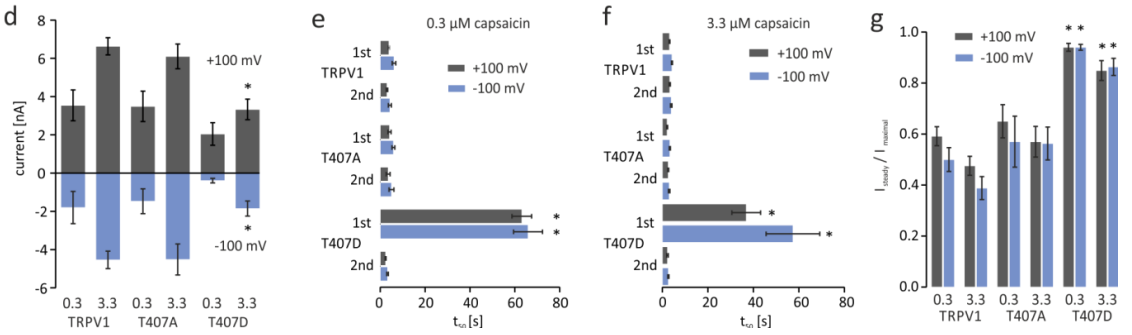

Figure 25. Capsaicin-induced currents of $TRPV1_{WT}$, $TRPV1_{T406A}$, and $TRPV1_{T406D}$ in presence of extracellular Ca^{2+}. CHO cells expressing $TRPV1_{WT}$, $TRPV1_{T406A}$ or $TRPV1_{T406D}$ were challenged with 0.3 µM or 3.3 µM capsaicin after a continuous voltage stimulus of +100 mV for 2 min. (**a, b**) TRPV1-mediated currents of $TRPV1_{WT}$ or $TRPV1_{T406A}$ induced by 0.3 µM or 3.3 µM capsaicin. The activation kinetics of the 1st and 2nd responses were fast (t_{50} < 6 s) and the responses underlie a strong Ca^{2+}-dependent desensitization. (**c**) In $TRPV1_{T406D}$, the activation kinetics of the 1st responses was slowed (t_{50} > 60 s), but the second response to the same stimulus was fast activating (t_{50} < 3 s). (**d**) Maximal responses of $TRPV1_{WT}$, $TRPV1_{T406A}$, and $TRPV1_{T406D}$ to 0.3 µM or 3.3 µM capsaicin. (**e, f**) Activation kinetics presented as time to half maximal activation (t_{50}), reveal that the activation kinetics of the 1st $TRPV1_{T406D}$ responses were significantly slowed ($p < 0.05$). (**g**) Normalized desensitization of $TRPV1_{WT}$, $TRPV1_{T406A}$, and $TRPV1_{T406D}$ indicate a significant reduction in Ca^{2+}-dependent desensitization of $TRPV1_{T406D}$ (*unpaired Wilcoxon rank test:* $p < 0.05$) (mean ± sem n = 4-11).

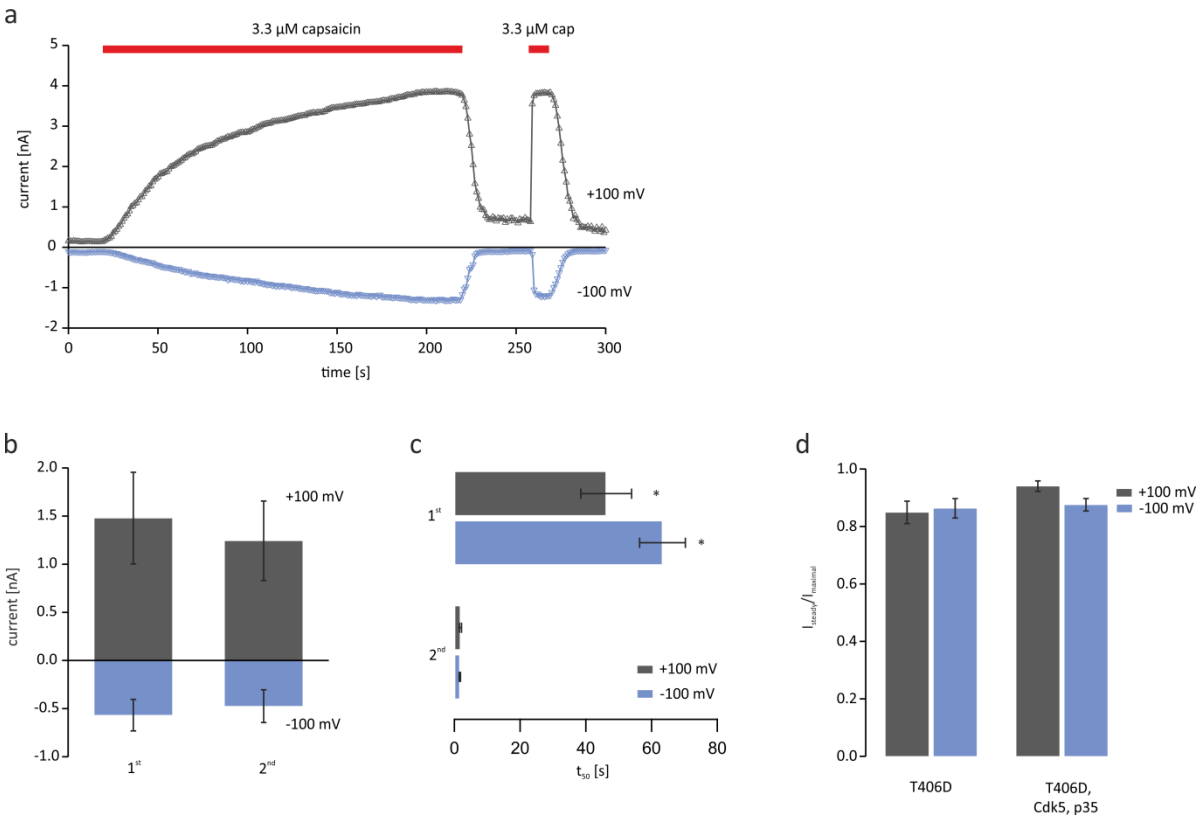

Figure 26. TRPV1-mediated currents of CHO cells co-expressing $TRPV1_{T406D}$, Cdk5, and p35. (**a**) Representative $TRPV1_{T406D}$-mediated inward (-100 mV) and outward (+100 mV) currents, induced by 3.3 µM capsaicin in the presence of Ca^{2+}-containing Ringer's solution. (**b**) maximal induced response, (**c**) time to half maximal activation (t_{50}), and (**d**) normalized desensitization. Asterisk (*) indicates significant differences (*paired or unpaired WR test* respectively; $p<0.05$), mean ± SEM of n = 6 independent measurements (Jendryke et al. 2016).

6.6 Membrane trafficking of TRPV1 and $TRPV1_{T406}$ mutants

In order to analyze the molecular mechanisms that lead to the altered activation kinetics of $TRPV1_{T406D}$, and to address the question of whether changes in response kinetics might be dependent on dynamic receptor trafficking, we monitored the dynamics of membrane localization of directly C-terminally GFP-tagged $TRPV1_{T406}$ receptor variants. Electrophysiological recordings of the GFP-tagged receptor variants ($TRPV1_{WT}$-GFP, $TRPV1_{T406D}$-GFP, and $TRPV1_{T406A}$-GFP) proved that they were functional and showed the characteristic behavior of the respective untagged receptor.

$TRPV1_{WT}$-GFP and $TRPV1_{T406A}$-GFP mutants showed fast activating capsaicin-induced currents, and Ca^{2+}-dependent desensitization, whereas $TRPV1_{T406D}$-GFP receptors exhibited slow activation kinetics paralleled by reduced Ca^{2+}-dependent desensitization (Fig. 27). The membrane expression of the fluorescent TRPV1 receptors was visualized by means of TIRF microscopy before, during and after application of a supra-maximum concentration of capsaicin (6.6 µM) (Fig. 28a). Fluorescence analysis of $TRPV1_{T406}$-GFP receptors revealed that treating the cells with capsaicin does not change the fluorescence of TRPV1-GFP receptors in the membrane (Fig. 28b, c), indicating that the density/expression of TRPV1 receptors in the membrane is not altered during capsaicin treatment.

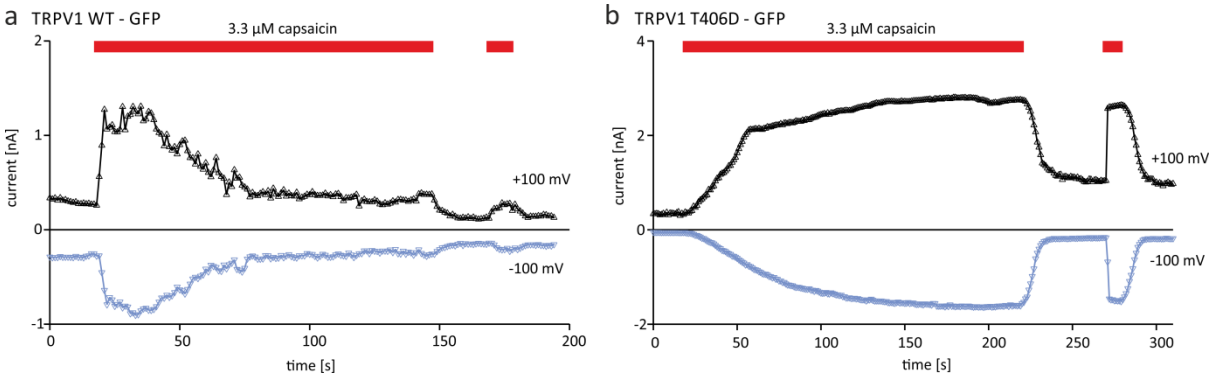

Figure 27. TRPV1-mediated currents of TRPV1-GFP fusion proteins. Representative capsaicin-induced inward (-100 mV) and outward (+100 mV) currents of (**a**) TRPV1-GFP and (**b**) $TRPV1_{T406D}$-GFP in presence of Ca^{2+} Ringer's solution (n = 3).

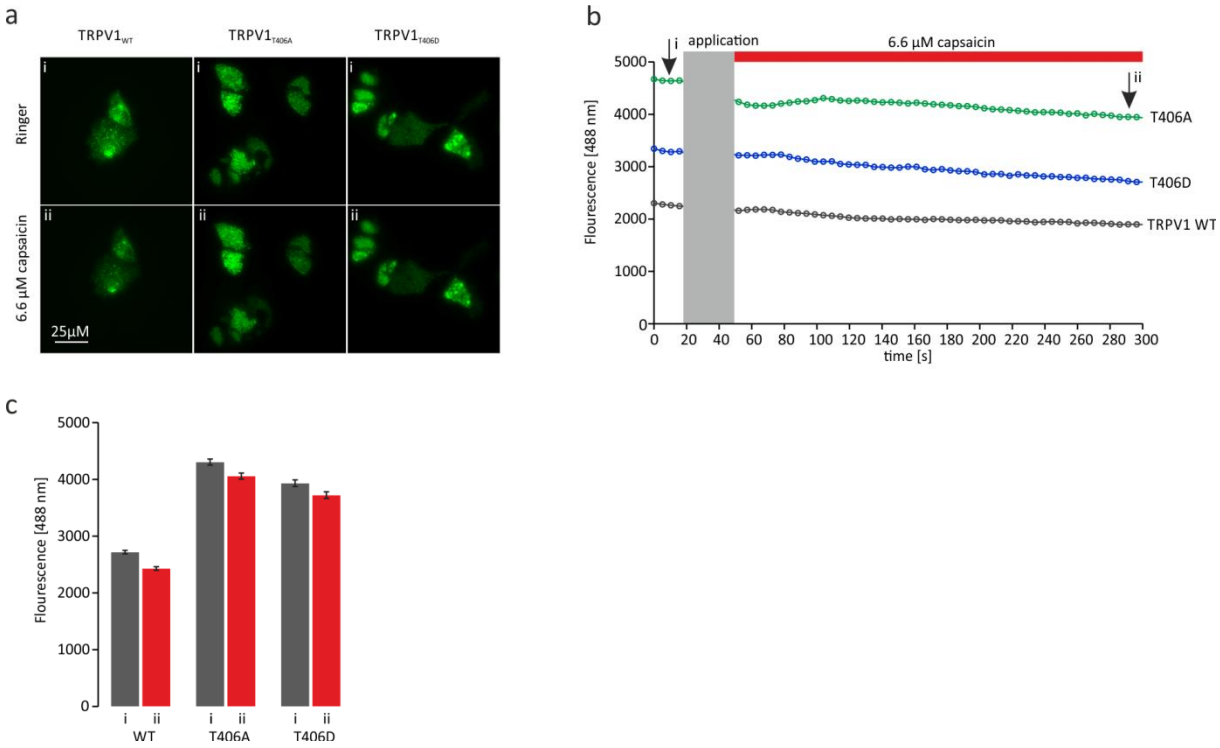

Figure 28. Trafficking of GFP-tagged TRPV1 receptors in the plasma membrane of CHO cells expressing GFP-tagged TRPV1 receptor variants. (**a**) Representative GFP fluorescence of CHO cells expressing $TRPV1_{WT}$-GFP, $TRPV1_{T406A}$-GFP or $TRPV1_{T406D}$-GFP fusion proteins in Ringer's solution and after 5 min treatment with 6.6 µM capsaicin. (**b**) Time course of the GFP fluorescence of selected regions of interests (ROI)/cells $TRPV1_{WT}$-GFP, $TRPV1_{T406A}$-GFP or $TRPV1_{T406D}$-GFP, image capturing was stopped during the capsaicin application (grey bar). (**c**) Mean GFP-fluorescence in Ringer's solution (i) and 5 min after the application of capsaicin (ii). Mean ± SEM of n = 31-59 cells.

6.7 T406D mutagenesis affects the voltage-dependence of TRPV1

Interestingly, in addition to the markedly altered channel activation and desensitization kinetics, we observed that the $TRPV1_{T406D}$-mediated outward currents (at +100 mV) after maximal stimulation did not reach baseline, but stayed at a higher activation level, which is suggestive of an altered voltage-dependence. In order to investigate the voltage-dependence of $TRPV1_{T407D}$, voltage-induced currents were measured before, during the application of 3.3 µM capsaicin, and after the capsaicin washout. To avoid Ca^{2+}-dependent desensitization, a Ca^{2+}-free extracellular solution was used. $TRPV1_{WT}$, $TRPV1_{T407A}$, and $TRPV1_{T407D}$ cells were patched in whole-cell configuration and defined voltage steps (-120 mV to +160 mV) were applied.

$TRPV1_{WT}$ and $TRPV1_{T407A}$ recordings revealed the TRPV1 characteristic outward rectifying voltage-dependent currents, but hardly any currents were found in the $TRPV1_{T407D}$ recordings (Fig. 29a). However, application of 3.3 µM capsaicin induced in $TRPV1_{WT}$, $TRPV1_{T407A}$, and $TRPV1_{T407D}$ (after priming for 200 s) robust inward and outward currents with maximum currents of about 0.5 to 0.7 pA/pF at +160 mV (Fig. 29b). Finally, voltage-dependent currents were recorded 1 min after the washout of capsaicin (Fig. 29c). The currents mediated by $TRPV1_{WT}$ and $TRPV1_{T407A}$ showed neither sensitization nor desensitization (Fig. 29d, e), while the voltage-induced currents of $TRPV1_{T407D}$ mutants were significantly increased (paired *t-test* $p < 0.05$) (Fig. 29f). Additionally, voltage-induced currents of $TRPV1_{T406D}$ were measured 2, 3, and 5 min after the capsaicin washout (Fig. 30). To further evaluate the voltage-dependence, the conductance G was calculated and the ratio of G/G_{max} (G_{max} = maximal conductance) was plotted against the voltage (Fig. 31). In this conductance/voltage relationship, the data revealed changes in the voltage-dependence of TRPV1 channels. Therefore, the data were fitted by means of a sigmoidal fit and the $V_{1/2}$ ($V_{1/2}$ = voltage at half maximal activation) was calculated (Fig. 31a, b, c). Analyzing the conductance of $TRPV1_{WT}$, $TRPV1_{T406A}$, and $TRPV1_{T406D}$ receptors revealed that the application of 3.3 µM capsaicin led not only to an increase in conductance, but also to a marked reduction in $V_{1/2}$ from about 120 mV to about -20 mV. However, in contrast to $TRPV1_{WT}$ and $TRPV1_{T406A}$, where the conductance recovered after washout, $TRPV1_{T406D}$ persisted in a high conducting state with a significantly reduced (left shifted) $V_{1/2}$ from about +110 to about +69 mV after the washout of 3.3 µM capsaicin (paired *WR-test* $p<0.05$) (Fig. 31d). This significant reduction of $V_{1/2}$ was also persistent 2, 3, and 5 min after the capsaicin-induced activation (Fig. 31e, f), which indicates that the priming of $TRPV1_{T406D}$ with capsaicin has severe consequences on the voltage-dependence of the ion channel. In conclusion, these data demonstrate that the mutation of T406 to a negatively charged aspartic acid (T406D) strongly affects the voltage-dependence of TRPV1 receptors, which also indicates that the use-dependent behavior is related to an altered ion channel gating.

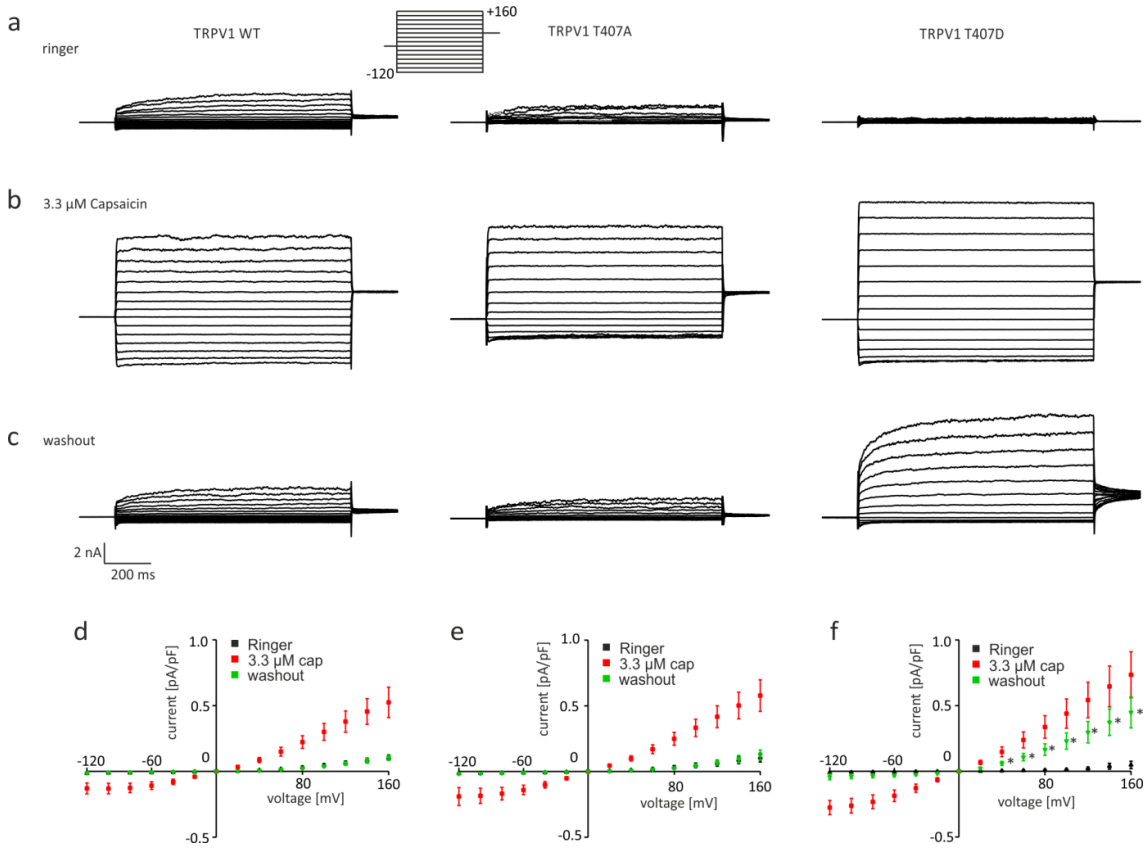

Figure 29. T406 mutagenesis affects the voltage-dependence of TRPV1 receptors. Transiently transfected CHO cells were measured by voltage step protocols with depolarizing pulses from -120 mV to +160 mV. (**a**) In Ca^{2+}-free Ringer's solution, voltage-dependent currents were recorded in $TRPV1_{WT}$ and $TRPV1_{T406A}$, but not in $TRPV1_{T406D}$. (**b**) Application of 3.3 µM capsaicin induced robust voltage-dependent currents in CHO cells expressing $TRPV1_{WT}$, $TRPV1_{T406A}$ or $TRPV1_{T406D}$. (**c**) Voltage-dependent currents evoked one minute after washout of capsaicin, revealed an increased voltage-dependence of $TRPV1_{T406D}$, whereas the voltage-induced currents of $TRPV1_{WT,}$ $TRPV1_{T406A}$ recover to the same level as under Ringer conditions. Normalized voltage-dependence of (**d**) $TRPV1_{WT}$, (**e**) $TRPV1_{T406A}$, and (**f**) $TRPV1_{T406D}$. Asterisk (*) indicates significantly increased outward currents of $TRPV1_{T406D}$ after priming with 3.3 µM capsaicin (paired *WR-test* $p < 0.05$) (n = 6-7).

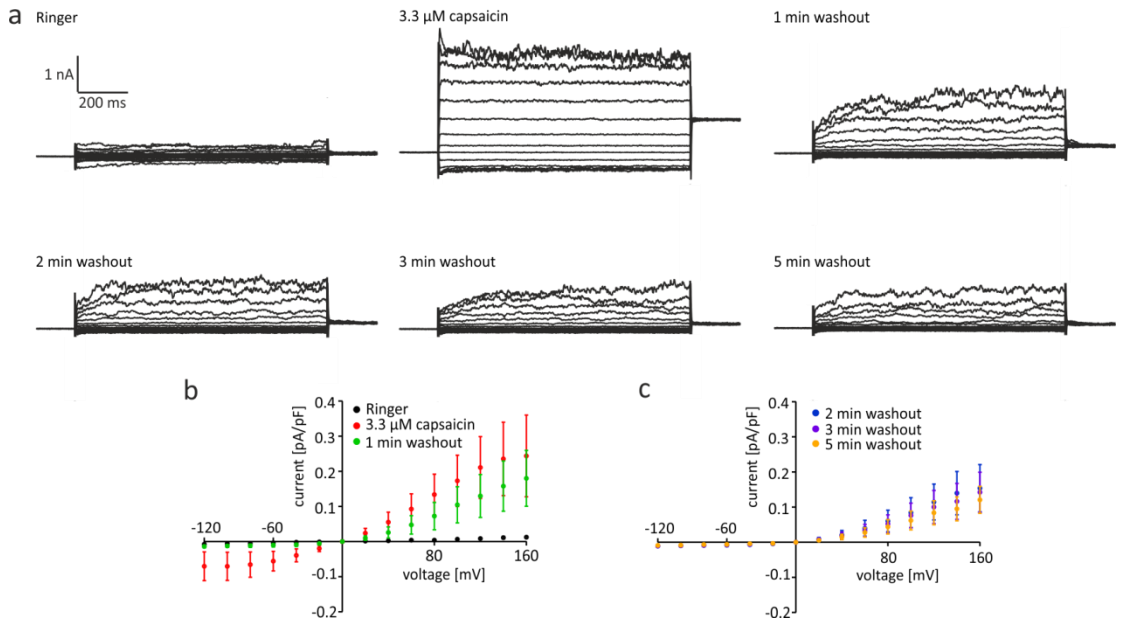

Figure 30. Voltage-dependence of $TRPV1_{T406D}$-mediated currents 2, 3, and 5 min after the capsaicin washout. Same experimental setup as in the previous step protocol measurements n = 4.

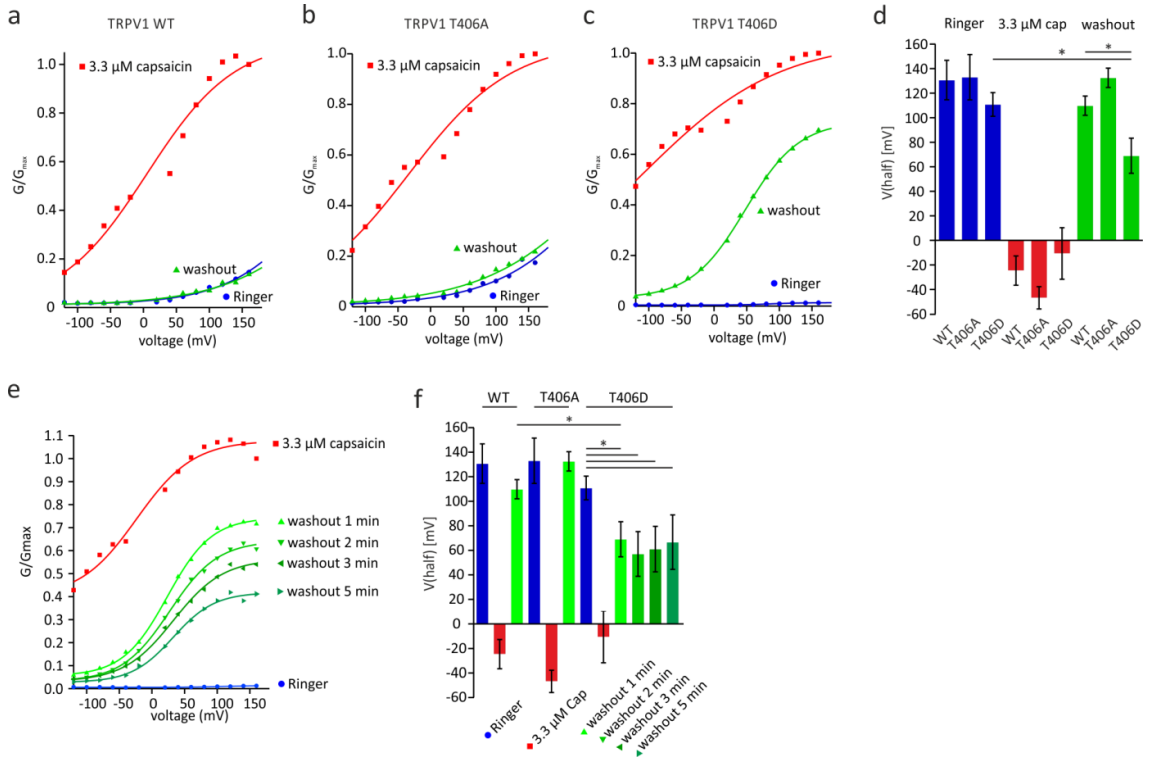

Figure 31. Conductance/voltage analysis of $TRPV1_{WT}$, $TRPV1_{T406A}$, and $TRPV1_{T406D}$. The normalized conductance (G/G_{max}) was fitted with a sigmoidal equation to analyze $V_{1/2}$.

Representative conductance/voltage-relationships of (**a**) $TRPV1_{WT}$, (**b**) $TRPV1_{T406A}$ and (**c**) $TRPV1_{T406D}$ under Ringer's solution, 3.3 µM capsaicin and 1 min after the capsaicin washout. (**d**) Statistical analysis of $V_{1/2}$ of $TRPV1_{T406D}$ revealed a significant decrease after the priming with 3.3 µM capsaicin (unpaired *t-test* $p < 0.05$). (**e,f**) Analysis of voltage-induced currents 1, 2, 3 and 5 min after the capsaicin washout revealed that $V_{1/2}$ of $TRPV1_{T406D}$ was significantly reduced even 5 min after the washout of capsaicin (paired *t-test* $p < 0.05$).

6.8 $TRPV1_{T406}$ mutation alters the capsaicin sensitivity

In order to investigate the capsaicin sensitivity of the different TRPV1 receptor mutants, we analyzed the concentration/response-relationship. Therefore, various capsaicin concentrations (0.05, 0.1, 0.3, 1, and 3.3 µM) were applied to stimulate TRPV1 receptors. TRPV1 receptor desensitization was prevented by using a Ca^{2+}-free extracellular solution. Due to the use-dependent activation of $TRPV1_{T407D}$ the capsaicin concentration/response-relationship was analyzed in two consecutive sets of application (before and after priming with 3.3 µM capsaicin). To analyze the EC_{50} values the responses were normalized to the maximal induced response and the concentration-response curves were approximated by the Hill-equation. In $TRPV1_{WT}$, $TRPV1_{T406R}$, and most of the neutral $TRPV1_{T406}$ mutants (expect T406P), we found no changes between the EC_{50} values of the 1st and 2nd capsaicin series (Fig. 32) (Table 3). Introduction of proline or the positively charged residues histidine or lysine induced a left shift of the 2nd concentration-response curves, with decreased EC_{50} values (Fig. 32d, e, m) (Table 3). The low responsiveness of $TRPV1_{T406D}$ and $TRPV1_{T406E}$ in the first set of capsaicin application prevented an accurate approximation to the Hill-curves. The second set of capsaicin application after priming with 3.3 µM capsaicin induced robust responses (Fig. 32b, c). The sensitivity of $TRPV1_{T406D}$ or $TRPV1_{T406E}$ was significantly increased after priming the receptors with 3.3 µM capsaicin, compared to $TRPV1_{WT}$ (*Tukey's-test* $p < 0.05$). EC_{50} values at -100 mV were for $TRPV1_{WT}$: 1st 0.63 ± 0.13 µM, 2nd 0.66 ± 0.14 µM; $TRPV1_{T406D}$: 2nd 0.26 ± 0.03 µM and at +100 mM: $TRPV1_{WT}$: 1st 0.25 ± 0.05 µM, 2nd 0.28 ± 0.06 µM; $TRPV1_{T406D}$: 2nd 0.11 ± 0.01 µM (Table 3). Different EC_{50} values for inward and outward currents were based on the voltage-dependence of TRPV1 ion channels, demonstrating that positive potentials (+100 mV) increased the TRPV1 receptor sensitivity to capsaicin (Gunthorpe et al. 2000).

The altered capsaicin sensitivity of $TRPV1_{T406}$ mutants, especially the sensitization of $TRPV1_{T406D}$ and $TRPV1_{T406E}$ during the second application series supports the hypothesis that amino acid properties such as charge or bulkiness had severe consequences on TRPV1 ion channel function.

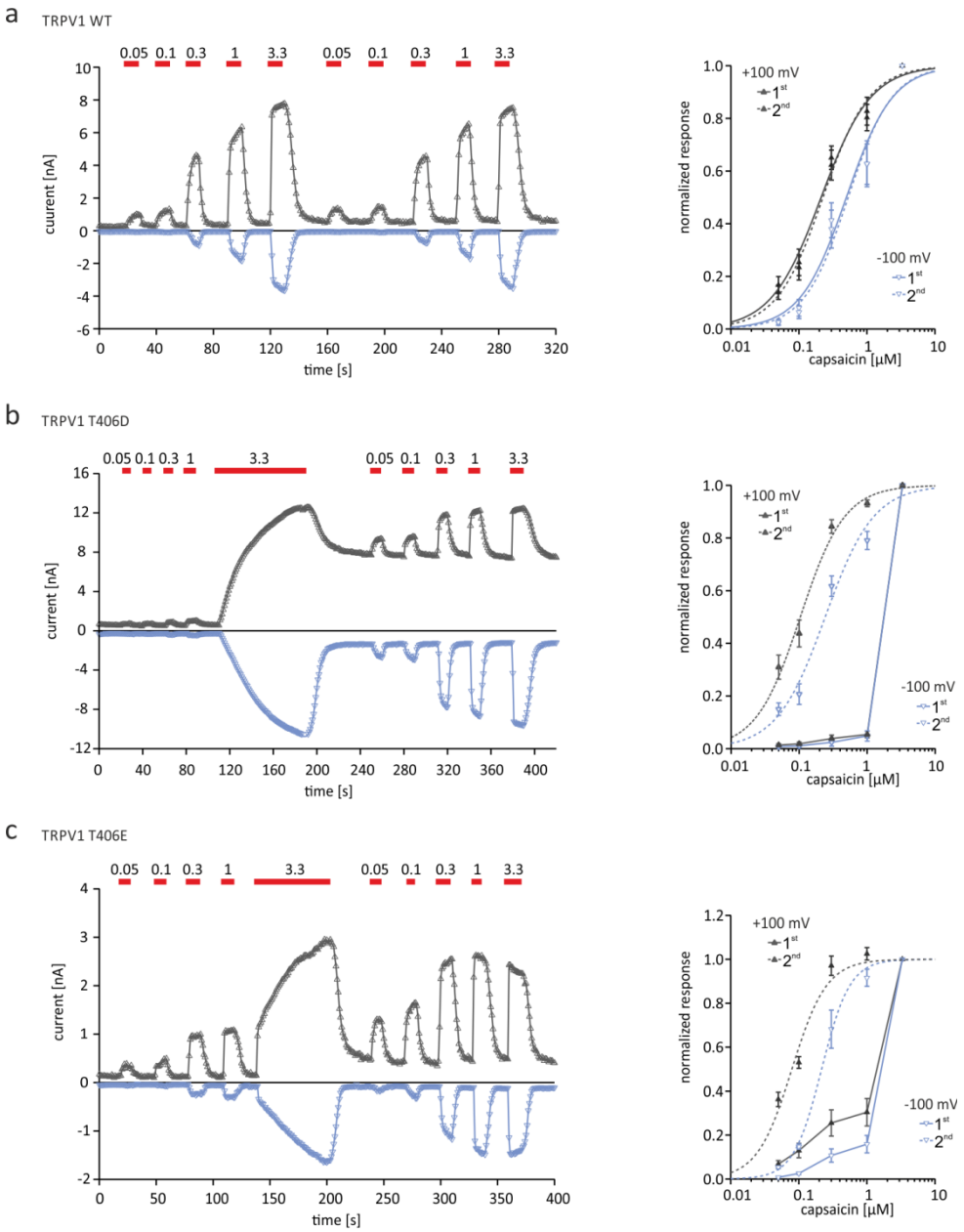

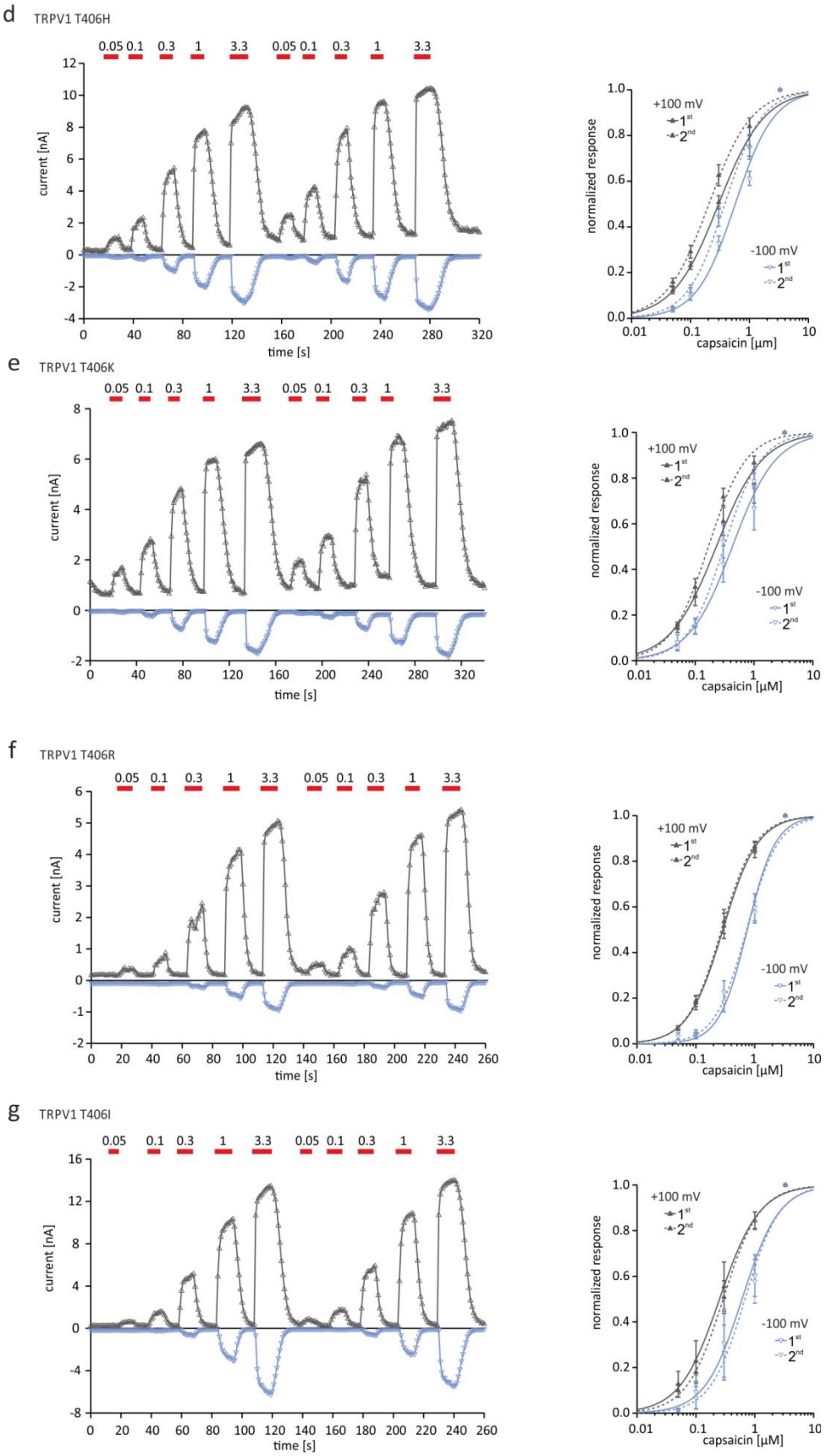
d
TRPV1 T406H
0.05 0.1 0.3 1 3.3 0.05 0.1 0.3 1 3.3
current [nA]
time [s]
+100 mV
1st
2nd
-100 mV
1st
2nd
normalized response
capsaicin [µm]
e
TRPV1 T406K
0.05 0.1 0.3 1 3.3 0.05 0.1 0.3 1 3.3
current [nA]
time [s]
+100 mV
1st
2nd
-100 mV
1st
2nd
normalized response
capsaicin [µM]
f
TRPV1 T406R
0.05 0.1 0.3 1 3.3 0.05 0.1 0.3 1 3.3
current [nA]
time [s]
+100 mV
1st
2nd
-100 mV
1st
2nd
normalized response
capsaicin [µM]
g
TRPV1 T406I
0.05 0.1 0.3 1 3.3 0.05 0.1 0.3 1 3.3
current [nA]
time [s]
+100 mV
1st
2nd
-100 mV
1st
2nd
normalized response
capsaicin [µM]

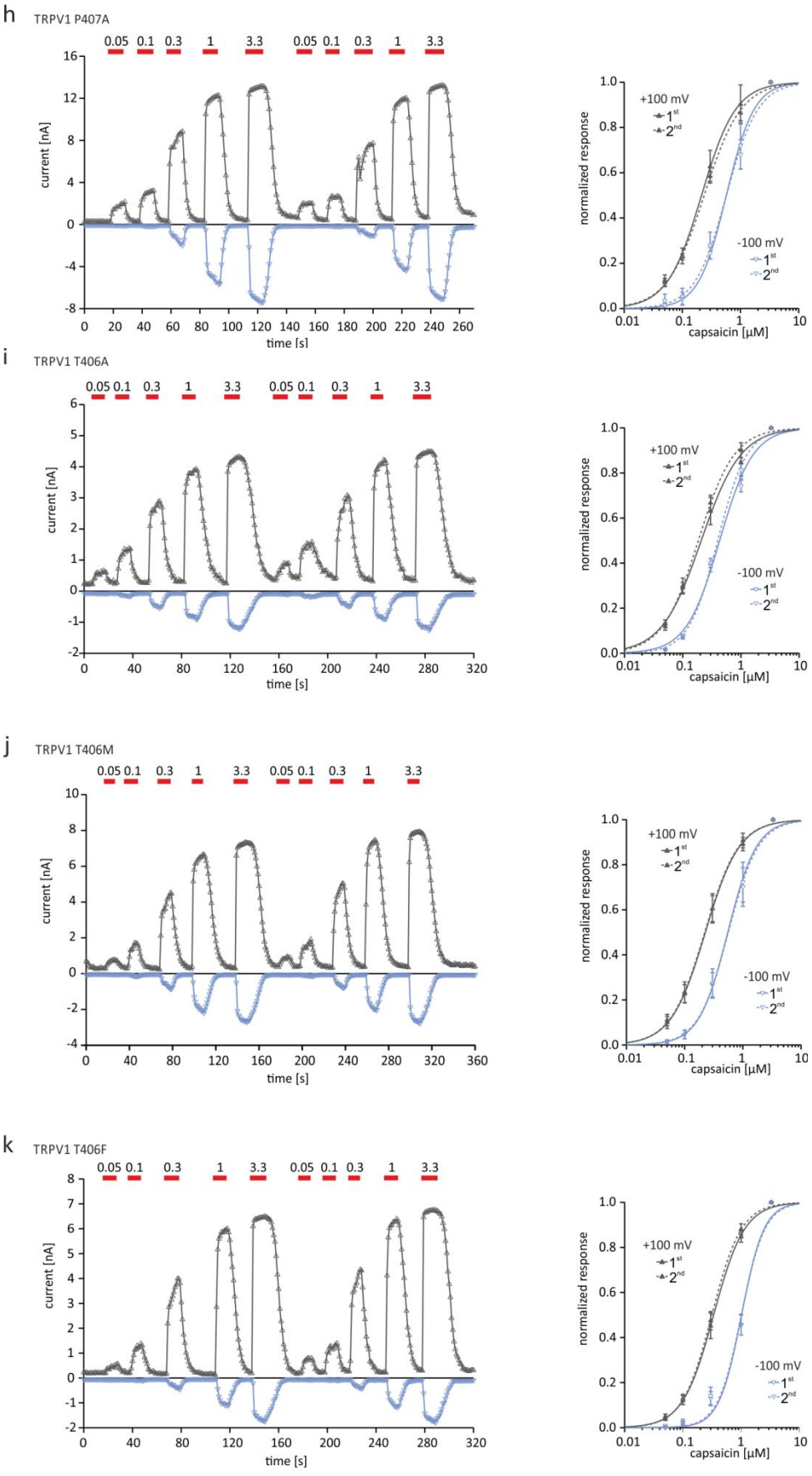
h
TRPV1 P407A
0.05 0.1 0.3 1 3.3 0.05 0.1 0.3 1 3.3
current [nA]
time [s]
+100 mV
1st
2nd
-100 mV
1st
2nd
normalized response
capsaicin [µM]
i
TRPV1 T406A
0.05 0.1 0.3 1 3.3 0.05 0.1 0.3 1 3.3
current [nA]
time [s]
+100 mV
1st
2nd
-100 mV
1st
2nd
normalized response
capsaicin [µM]
j
TRPV1 T406M
0.05 0.1 0.3 1 3.3 0.05 0.1 0.3 1 3.3
current [nA]
time [s]
+100 mV
1st
2nd
-100 mV
1st
2nd
normalized response
capsaicin [µM]
k
TRPV1 T406F
0.05 0.1 0.3 1 3.3 0.05 0.1 0.3 1 3.3
current [nA]
time [s]
+100 mV
1st
2nd
-100 mV
1st
2nd
normalized response
capsaicin [µM]

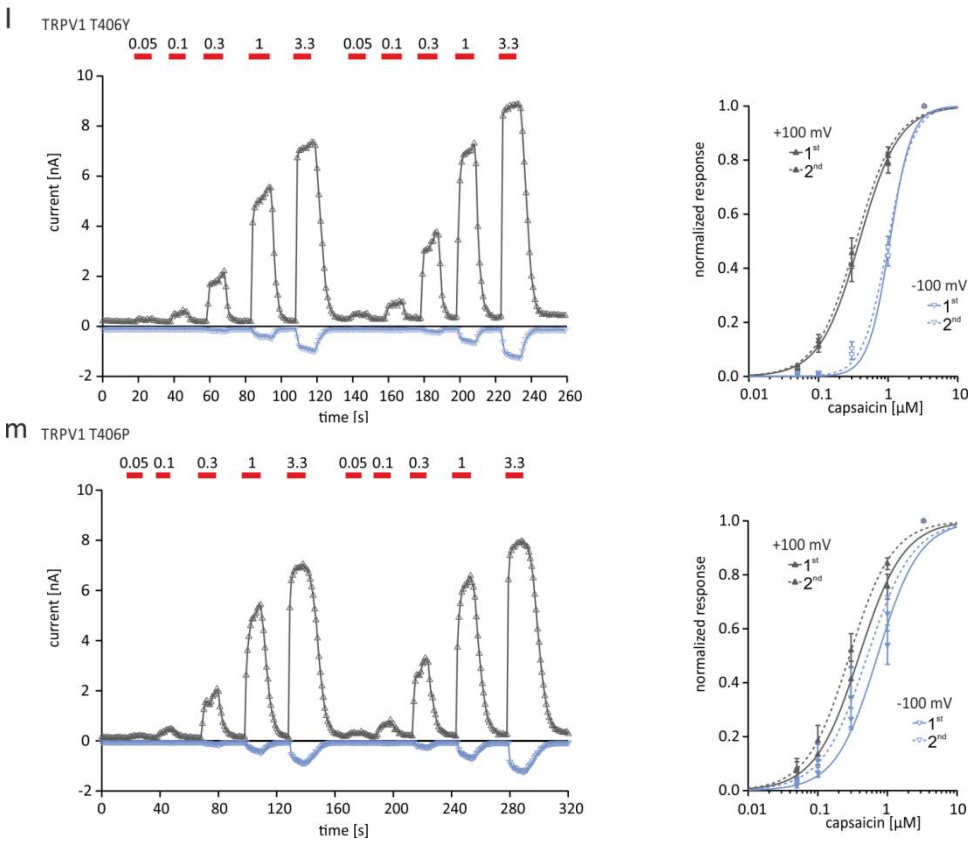

Figure 32. Capsaicin concentration/response-relationship of $TRPV1_{WT}$ and TRPV1 mutants. Based on the use-dependent activation of $TRPV1_{T406D}$ and $TRPV1_{T406E}$ the TRPV1 expressing cells were challenged twice with increasing capsaicin concentrations (0.05 to 3.3 µM). Ca^{2+}-free extracellular solution was used to avoid ion channel desensitization. The first and second application series of capsaicin induced in (**a**) $TRPV1_{WT}$, (**f**) $TRPV1_{T406R}$, (**g**) $TRPV1_{T406I}$, (**h**) $TRPV1_{P407A}$, (**i**) $TRPV1_{T406A}$, (**j**) $TRPV1_{T406M}$, (**k**) $TRPV1_{T406F,}$ and (**l**) $TRPV1_{T406Y}$ similar responses. The low responsiveness of (**b**) $TRPV1_{T406D}$ and (**c**) $TRPV1_{T406E}$ in the first series of applications did not allow for an accurate estimation of the EC_{50}. Priming the receptors with 3.3 µM capsaicin increased the sensitivity. Analysis of the positively charged mutants (**d**) $TRPV1_{T406H}$, (**e**) $TRPV1_{T406K}$, as well as (**m**) $TRPV1_{T406P}$ revealed a left-shift in the second concentration/response-relationship. Data were collected form n = 5 - 10 independent measurements.

	Inward current (-100 mV)		Outward current (+100 mV)	
	1st	2nd	1st	2nd
TRPV1	EC_{50} ± SEM	EC_{50} ± SEM	EC_{50} ± SEM	EC_{50} ± SEM
WT	0.63 ± 0.13	0.66 ± 0.14	0.25 ± 0.05	0.28 ± 0.06
P407A	0.61 ± 0.11	0.58 ± 0.08	0.25 ± 0.06	0.24 ± 0.02
T406D	–	*0.26 ± 0.03	–	*0.11 ± 0.01
T406E	–	*0.23 ± 0.03	–	*0.08 ± 0.01
T406H	0.58 ± 0.06	0.40 ± 0.07	0.31 ± 0.03	0.22 ± 0.03
T406K	0.50 ± 0.16	0.33 ± 0.06	0.29 ± 0.11	0.18 ± 0.02
T406R	0.77 ± 0.09	0.76 ± 0.09	0.31 ± 0.04	0.29 ± 0.04
T406A	0.43 ± 0.02	0.40 ± 0.02	0.24 ± 0.06	0.19 ± 0.02
T406I	0.75 ± 0.16	0.80 ± 0.16	0.30 ± 0.07	0.32 ± 0.05
T406M	0.58 ± 0.12	0.60 ± 0.13	0.24 ± 0.05	0.24 ± 0.05
T406P	0.80 ± 0.13	0.60 ± 0.11	0.43 ± 0.08	0.30 ± 0.05
T406Y	1.03 ± 0.06	0.98 ± 0.07	0.41 ± 0.07	0.37 ± 0.06
T406F	1.00 ± 0.08	0.97 ± 0.08	0.35 ± 0.05	0.32 ± 0.03

Table 3. EC_{50} values of $TRPV1_{WT}$ and TRPV1 mutants. Left panel: 1st and 2nd EC_{50} ± SEM at -100 mV, right panel: 1st and 2nd EC_{50} ± SEM at +100 mV. Due to the weak responses of $TRPV1_{T406D}$ and $TRPV1_{T406E}$ in the first set of applications, EC_{50} values could not be calculated. Asterisk (*) indicates significantly reduced EC_{50} values of $TRPV1_{T406D}$ and $TRPV1_{T406E}$ after priming with 3.3 µM capsaicin compared to the 2nd EC_{50} value of $TRPV1_{WT}$ (*Tukey*-test $p < 0.05$) (n = 5-10).

6.9 TRPV1 T407 mutagenesis affects the proton activation

The TRPV1 receptor can be activated by various stimuli such as voltage, capsaicin, heat or protons. In contrast to the intracellularly located capsaicin binding site, the proton binding site is located at the extracellular part of the pore-loop and may trigger a different gating mechanism. Thus, we wanted to investigate the sensitivity of $TRPV1_{WT}$ and TRPV1 mutants to low pH. For this purpose, CHO cells expressing the respective receptors were challenged with two consecutive sets of applications of pH 6, followed by 0.3 µM and 3.3 µM capsaicin in the absence of extracellular Ca^{2+}. $TRPV1_{WT}$ and $TRPV1_{T406}$ mutants with positively charged residues as well as most of the neutral T406 mutants responded similar to pH 6, 0.3 µM and 3.3 µM capsaicin in the first and second series of application (Fig. 33a, d-l). In contrast, the negatively charged $TRPV1_{T406D}$ or $TRPV1_{T406E}$, as well as $TRPV1_{T406P}$ did not respond (or only weakly) to the first application of pH 6 and 0.3 µM capsaicin. However, after priming with 3.3 µM capsaicin, they gained full responsiveness to low pH and 0.3 µM capsaicin (Fig. 33b, c, m). To describe the response characteristics, ratios were calculated between the amplitudes of 1st and 2nd responses. Ratios of >1 represent ion channel desensitization, whereas ratios of <1 indicates ion channel sensitization.

In $TRPV1_{WT}$, and $TRPV1_{T406}$ mutants with positively charged as well as neutral residues (expect proline) we found ratios of 0.8 - 1.2 for pH 6, 0.3 µM and 3.3 µM capsaicin. These data indicate that the receptors do not sensitize or desensitize after maximal stimulation with 3.3 µM capsaicin. The ratios of $TRPV1_{T406P}$ (0.49 - 0.64), revealed a slight but significant sensitization to pH 6 and 0.3 µM capsaicin (*Tukey's test* $p < 0.05$). $TRPV1_{T406D}$ and $TRPV1_{T406E}$ revealed ratios of <0.2 for pH 6 and 0.3 µM capsaicin, indicating a strong sensitization after priming with 3.3 µM capsaicin (*Tukey's test* $p < 0.05$) (Fig. 34a, b). Furthermore, we found increased ratios of the 3.3 µM capsaicin-induced response indicating an increased voltage-dependence of $TRPV1_{T406D/E}$ mutants (Fig. 34c). In summary, these data reveal that $TRPV1_{T406}$ mutagenesis not only affects the capsaicin, but also the pH 6-mediated activation of TRPV1, supporting the hypothesis that the mutation of T406 modulates the TRPV1 ion channel gating mechanism.

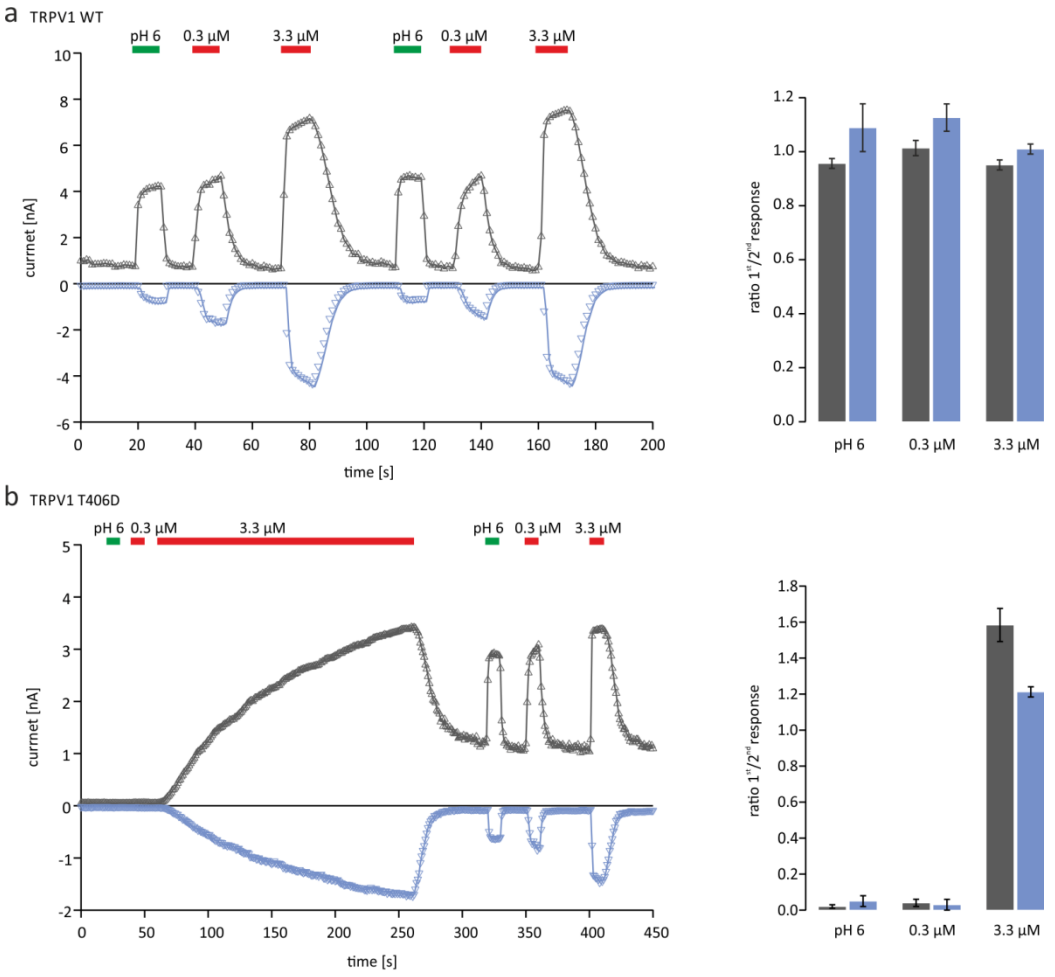

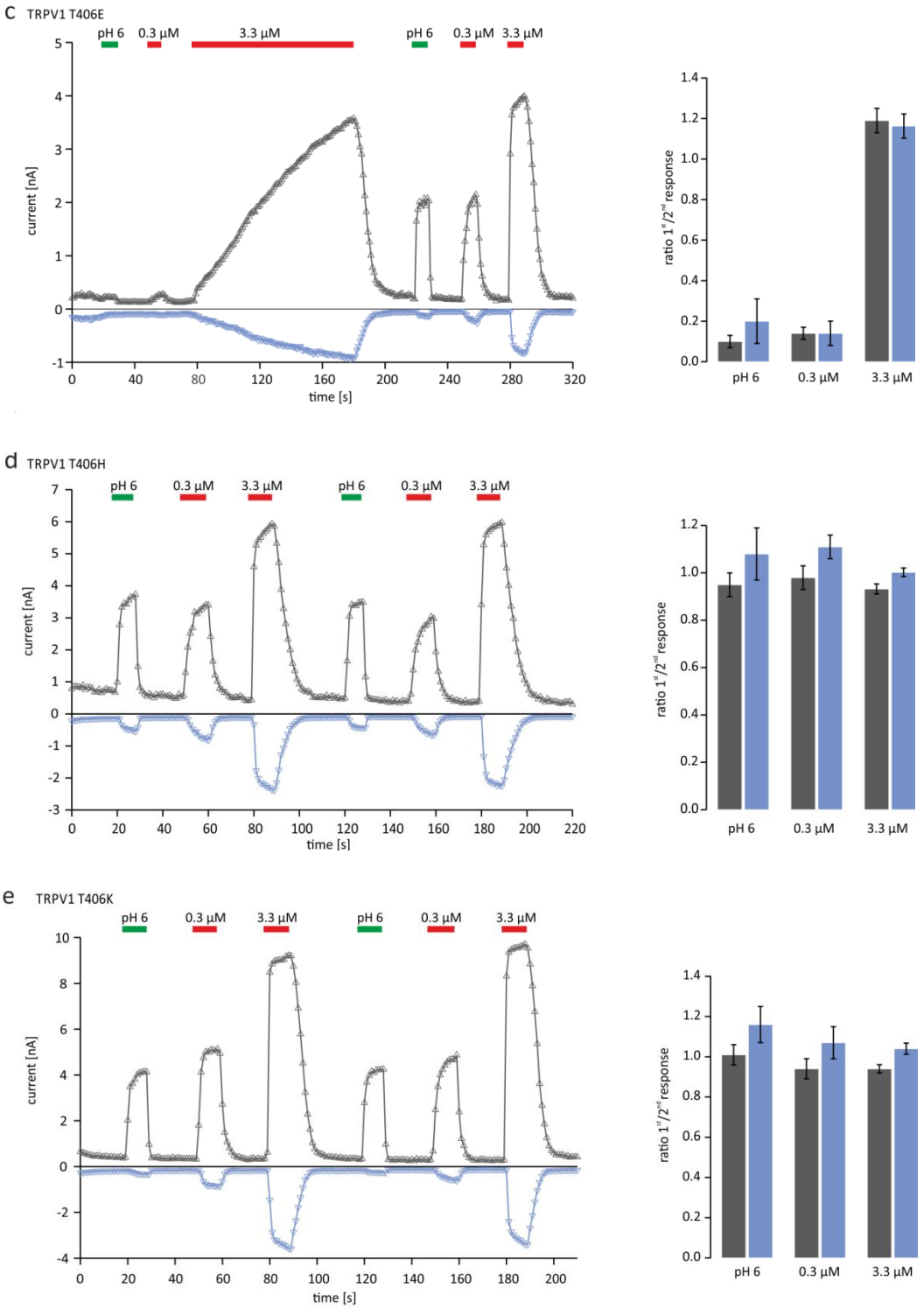
c
TRPV1 T406E
pH 6
0.3 µM
3.3 µM
pH 6
0.3 µM
3.3 µM
current [nA]
time [s]
ratio 1st/2nd response
pH 6
0.3 µM
3.3 µM
d
TRPV1 T406H
pH 6
0.3 µM
3.3 µM
pH 6
0.3 µM
3.3 µM
current [nA]
time [s]
ratio 1st/2nd response
pH 6
0.3 µM
3.3 µM
e
TRPV1 T406K
pH 6
0.3 µM
3.3 µM
pH 6
0.3 µM
3.3 µM
current [nA]
time [s]
ratio 1st/2nd response
pH 6
0.3 µM
3.3 µM

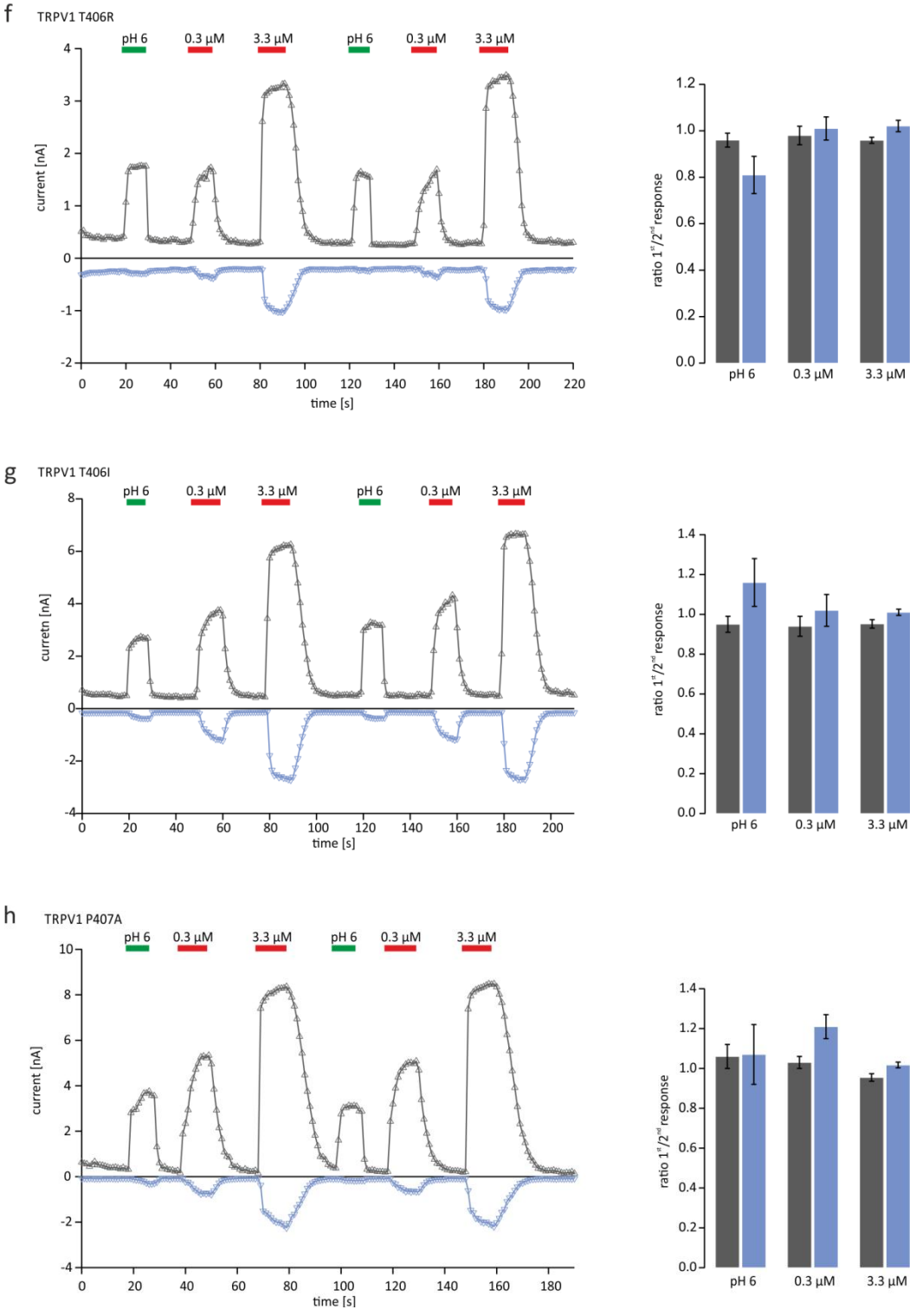
f
TRPV1 T406R
pH 6
0.3 µM
3.3 µM
pH 6
0.3 µM
3.3 µM
current [nA]
time [s]
ratio 1st/2nd response
pH 6
0.3 µM
3.3 µM
g
TRPV1 T406I
pH 6
0.3 µM
3.3 µM
pH 6
0.3 µM
3.3 µM
curretn [nA]
time [s]
ratio 1st/2nd response
pH 6
0.3 µM
3.3 µM
h
TRPV1 P407A
pH 6
0.3 µM
3.3 µM
pH 6
0.3 µM
3.3 µM
current [nA]
time [s]
ratio 1st/2nd response
pH 6
0.3 µM
3.3 µM

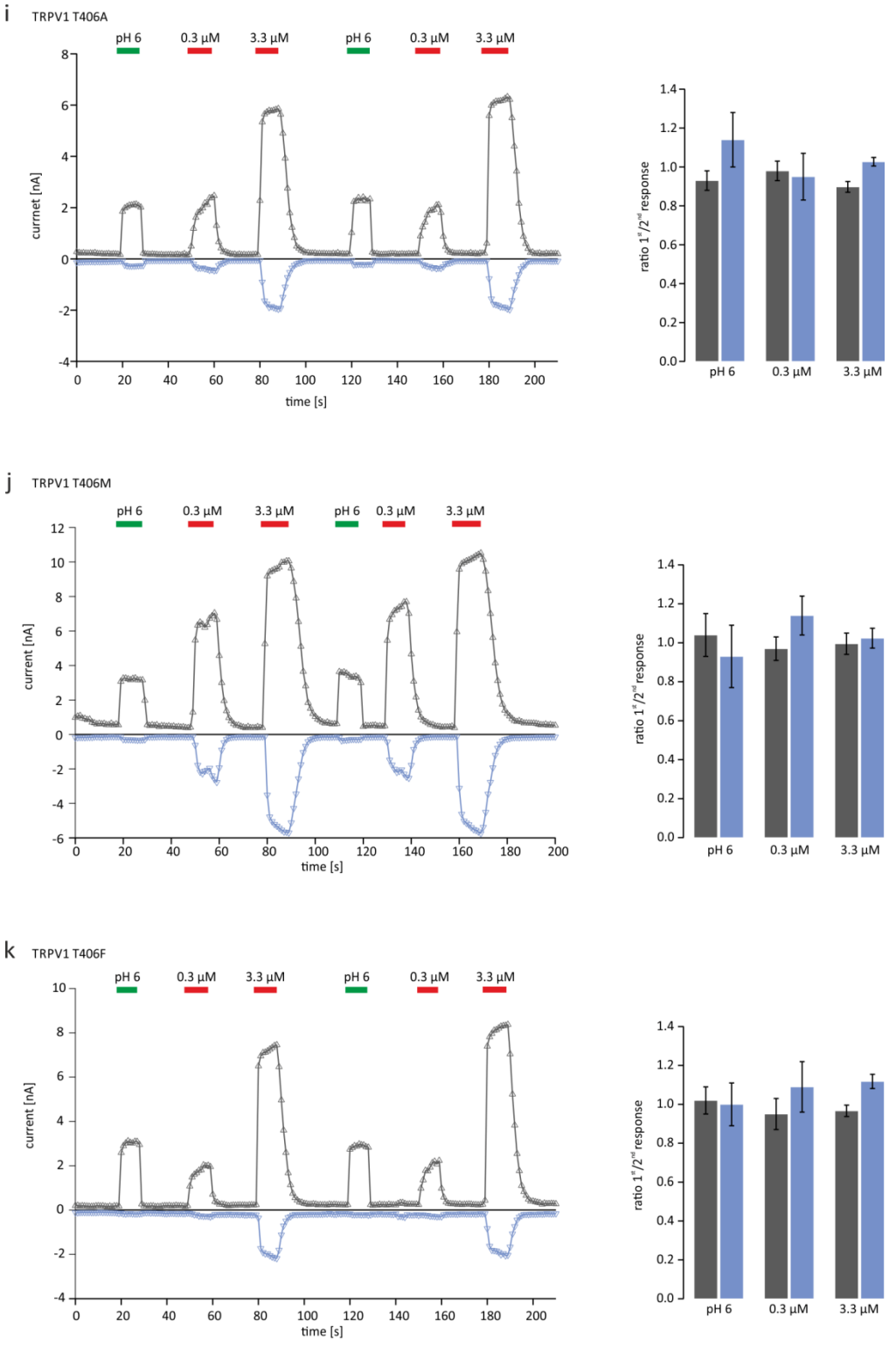
i
TRPV1 T406A
pH 6
0.3 µM
3.3 µM
pH 6
0.3 µM
3.3 µM
curmet [nA]
time [s]
ratio 1st/2nd response
pH 6
0.3 µM
3.3 µM
j
TRPV1 T406M
pH 6
0.3 µM
3.3 µM
pH 6
0.3 µM
3.3 µM
current [nA]
time [s]
ratio 1st/2nd response
pH 6
0.3 µM
3.3 µM
k
TRPV1 T406F
pH 6
0.3 µM
3.3 µM
pH 6
0.3 µM
3.3 µM
current [nA]
time [s]
ratio 1st/2nd response
pH 6
0.3 µM
3.3 µM

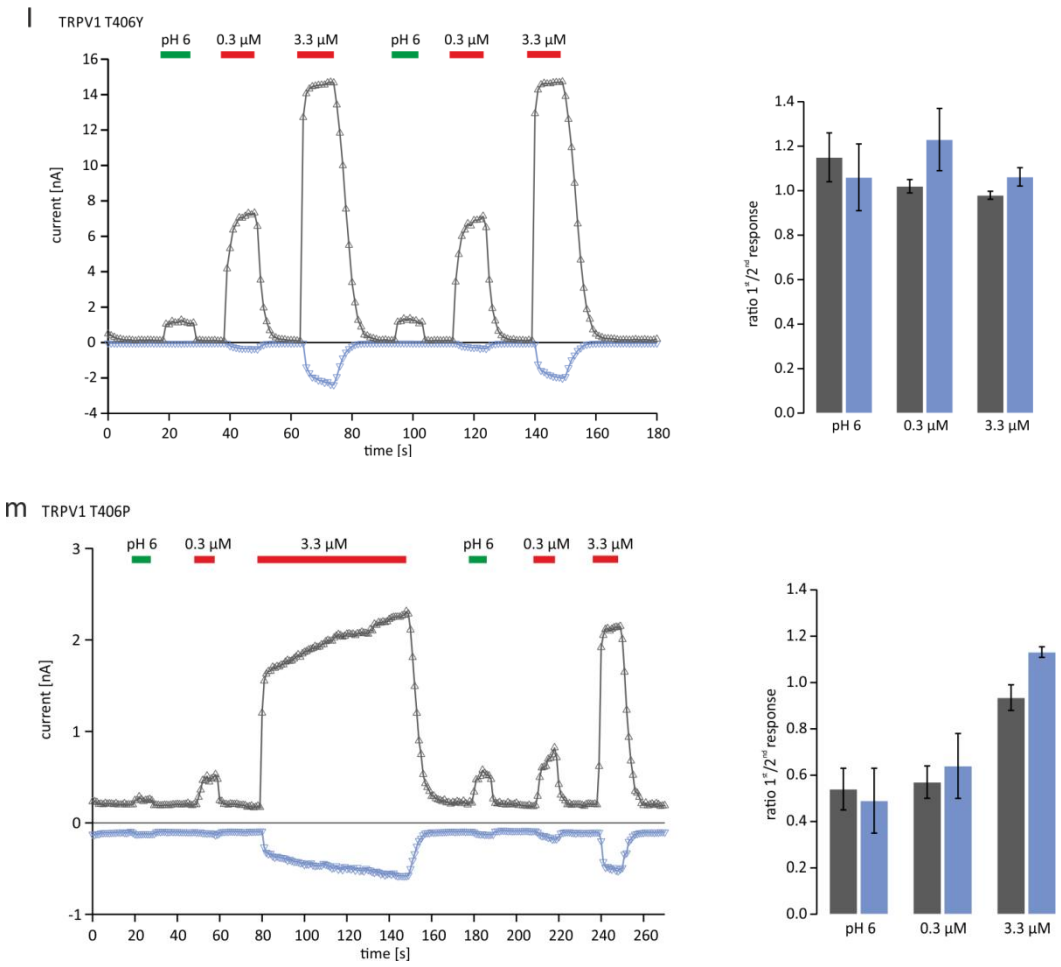

Figure 33. Proton and capsaicin mediated activation of $TRPV1_{WT}$ and TRPV1 mutants. TRPV1-mediated currents were evoked by application of Ca^{2+}-free extracellular solution at pH 6, followed by the application of 0.3 µM and 3.3 µM capsaicin. Left panel: representative recordings of voltage-ramp induced inward and outward currents. Right panel: Ratios of 1st and 2nd response to the same stimuli, values >1 indicates desensitization and values <1 indicates sensitization after priming (n = 5-15).

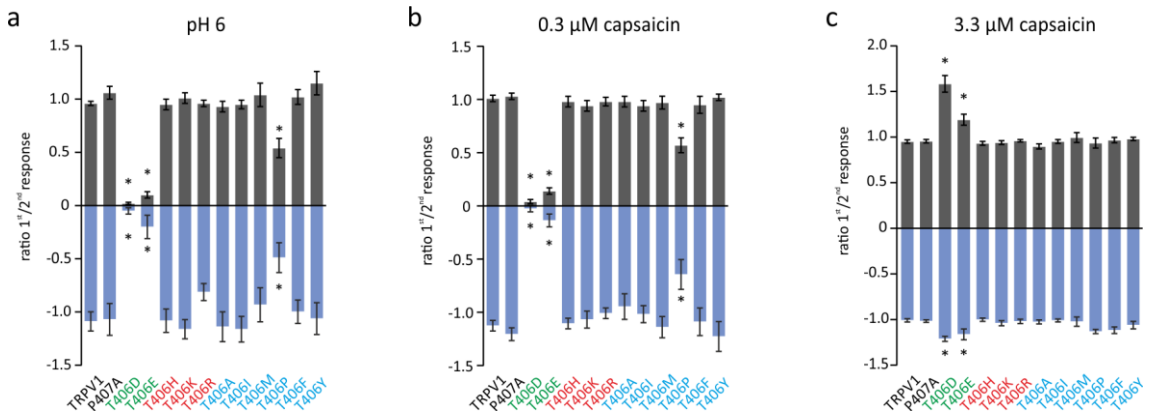

Figure 34. Statistical analysis of pH 6, 0.3 µM or 3.3 µM capsaicin evoked responses. After priming with 3.3 µM capsaicin $TRPV1_{T406D}$, $TRPV1_{T406E}$, and $TRPV1_{T406P}$ were significantly sensitized to (**a**) pH 6 and (**b**) 0.3 µM capsaicin (*Tukey's test* $p < 0.05$). (**c**) The ratios of the outward current of $TRPV1_{T406D}$ and $TRPV1_{T406E,}$ induced by 3.3 µM capsaicin, were significantly increased, indicating an increased voltage-dependence after priming. Ratios of peak amplitudes of n = 5-15 independent measurements were presented as mean ± sem (*Tukey's test:* $p < 0.05$).

6.10 Heat activation of $TRPV1_{T406D}$ in Ca^{2+} imaging experiments

To further investigate the polymodal activation of TRPV1 receptor mutants, we set out for another experimental approach. Together with G. Nordmann we performed the following Fura-2 Ca^{2+} imaging experiments (Nordmann 2015). The aim was to investigate the heat sensitivity of TRPV1 receptor mutants by utilizing HEK293T cells expressing $TRPV1_{WT}$ or $TRPV1_{T407D}$. The TRPV1 ion channel is highly permeable to Ca^{2+}, therefore we induce TRPV1-mediated Ca^{2+} influxes by challenging cells with capsaicin (3.3 µM), or by perfusing the recording chamber with physiological Ringer's solution heated up to 42 °C. Representative Ca^{2+} imaging measurements of HEK293T cells expressing $TRPV1_{WT}$ or $TRPV1_{T406D}$ are presented in Figure 35. Cells were challenged by heating up the bath solution to 42 °C for at least 2 min. After a recovery phase of about 5 min, the maximal TRPV1-mediated Ca^{2+} influx was induced by the application of 3.3 µM capsaicin at room temperature (24 °C). A second heat activation was performed 15 min after the washout of 3.3 µM capsaicin (Fig. 35). In order to quantify the sensitization of TRPV1 receptors, the first and second heat responses were normalized to the peak amplitude of the capsaicin-induced responses. The analysis revealed no differences between the first and second heat-induced responses of $TRPV1_{WT}$, but we found significantly increased amplitudes of the second heat-induced responses in $TRPV1_{T406D}$ receptors (paired *t-test* $p < 0.05$) (Fig. 35e). Furthermore, recordings of $TRPV1_{WT}$ receptors revealed similar activation kinetics (t_{10-90}) of first and second responses (about 40 s), whereas the responses of $TRPV1_{T406D}$ expressing cells showed accelerated activation kinetics in the second series of applications (paired *t-test* $p < 0.05$) (Fig. 35f). The Ca^{2+} imaging data revealed that $TRPV1_{T406D}$ mutants were less sensitive to the first heat stimuli, but gained full responsiveness after priming with 3.3 µM capsaicin. These observations are in line with

our previous patch-clamp recordings and support the hypothesis that $TRPV1_{T406D}$ affects the gating mechanism of TRPV1.

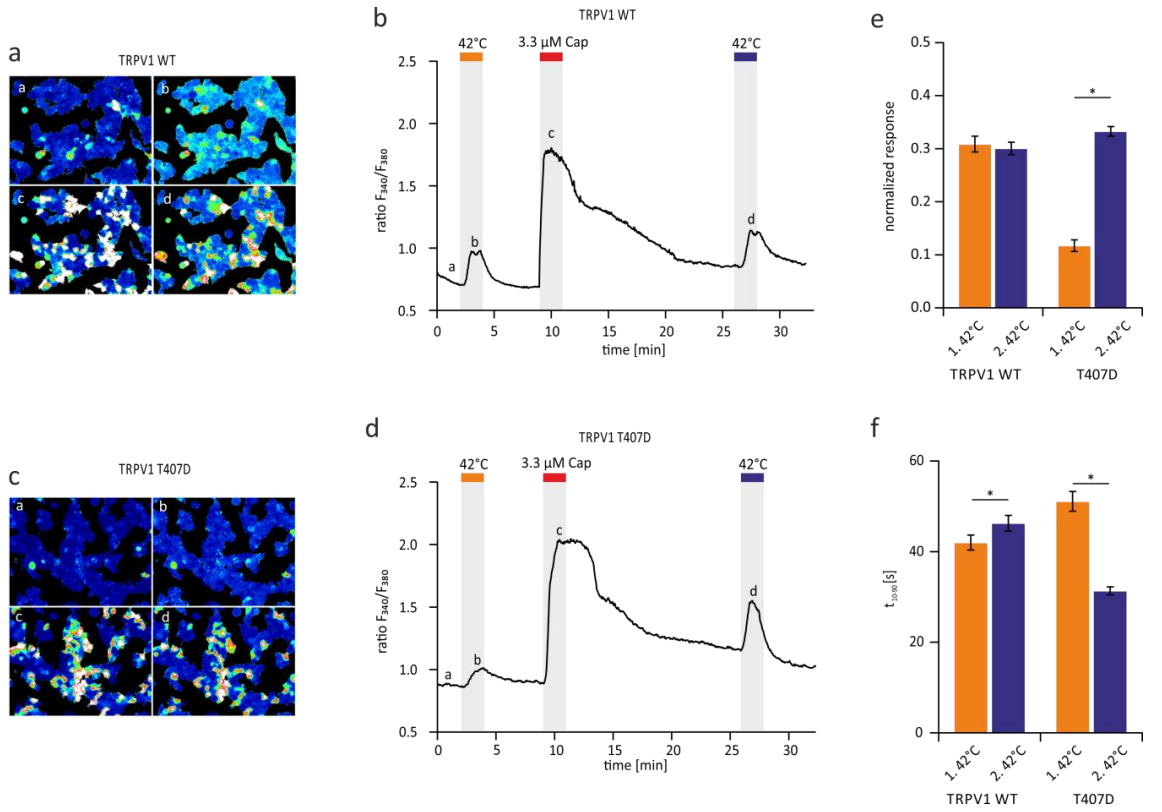

Figure 35. Fura-2 Ca^{2+} imaging of HEK293T cells expressing $TRPV1_{WT}$ or $TRPV1_{T406D}$. Representative ratio images and time courses of (**a**, **b**) $TRPV1_{WT}$ and (**c**, **d**) $TRPV1_{T406D}$ measurements. The TRPV1-mediated influx of Ca^{2+} was induced by challenging cells with 42 °C, 3.3 µM Capsaicin and a 2nd heat application. (**e**) First and second responses to heat were normalized to the responses induced by 3.3 µM capsaicin. Statistical analysis revealed that the first responses of $TRPV1_{T406D}$ were significantly smaller, but gained full responsiveness after priming with 3.3 µM capsaicin (paired *t-test,* $p < 0.05$). (**f**) The activation kinetics ($t_{10\text{-}90}$) of $TRPV1_{WT}$ were similar in first and second heat induced responses (1st 42 ± 1.6 s, 2nd 46 ± 1.7 s), but after the maximum activation the rise time of the second responses of $TRPV1_{T406D}$ were significantly accelerated (1st 51 ± 2.2 s, 2nd 31 ± 0.8 s) (paired *t-test* $p < 0.05$) (n = 131-135) (Nordmann 2015).

6.11 **TRPV1 single-channel characteristics are altered in T406D mutants**

In order to investigate the function of the $TRPV1_{T407D}$ mutant on the single-channel level, we set out to analyze several biophysical single-channel properties such as amplitude, open probability and dwell-time distribution. Therefore, the opening and closing events of $TRPV1_{WT}$ and $TRPV1_{T407D}$ channels were recorded for periods of 2 min in the cell-attached configuration. A high [K^+] (140 mM) extracellular solution was used to equalize the cell membrane potential to 0 mV and 10 mM $BaCl_2$ was added to the patch pipette solution to block endogenous K^+ ion channels. Figure 36 shows representative single-channel recordings and event distribution histograms of $TRPV1_{WT}$ and $TRPV1_{T406D}$. In general, the single-channel amplitudes depend on the driving force (electrochemical gradient) and the ion channel pore characteristics. Based on an approximated membrane potential of 0 mV and a pipette potential of -60 mV, the TRPV1 single-channel amplitudes were measured to be 5 to 8 pA. Interestingly, the open events of $TRPV1_{T406D}$ before priming did not show constant amplitudes, but tend to decrease from an initial high to a lower plateau conductance state (Fig. 36). This behavior indicates a dynamic process within the pore, leading to alteration of conductance/permeability during gating of $TRPV1_{T406D}$. However, the mechanism behind this observation is not clear at the moment. In order to analyze the open probability (NP_O) of $TRPV1_{WT}$ and $TRPV1_{T406D}$, ion channel event distribution histograms were extracted from the data. The average NP_O was found to be 16.5 ± 5.1% in $TRPV1_{WT}$ and 1.5± 1.2% in $TRPV1_{T407D}$ recordings. Adding 0.3 µM capsaicin to the pipette solution increased the average open probability of $TRPV1_{WT}$ ion channels to 60.6 ± 8.2%, whereas in $TRPV1_{T407D}$ recordings the NP_O increased only to 4.9 ± 2%, demonstrating the low activity of $TRPV1_{T406D}$ under these conditions. Pre-treating $TRPV1_{T407D}$ expressing cells for two minutes with 3.3 µM capsaicin led to priming of the receptor and increased the open probability to 88.8 ± 5% when 0.3 µM capsaicin was added to the pipette solution (after washout of the external capsaicin), again reflecting the use-dependent activation of $TRPV1_{T406D}$.

The statistical analysis of the open and closed states of $TRPV1_{WT}$ and $TRPV1_{T406D}$ receptors (at +60 mV and in the presence of 0.3 µM capsaicin) revealed that $TRPV1_{T406D}$ receptors spent significantly less time in the open state (unpaired *WR-test* $p < 0.05$), but priming $TRPV1_{T406D}$ receptors with 3.3 µM capsaicin shifted the open probability to about 90%, similar to what is obtained in $TRPV1_{WT}$ (Fig. 37). These findings were in line with the previous whole-cell recordings, indicating that the use-dependent activation of $TRPV1_{T406D}$ might be based on the engagement of different confirmations.

In order to determine the state time constants of the open and closed states, the recorded single-channel events were further analyzed by calculating the open and close dwell-time distribution. Thus the root square of the frequency was plotted against the natural logarithm of time and fitted with polynomial functions. That enabled us to discriminate between the different open and closed states of the receptor and to analyze the gating mechanisms of the TRPV1 ion channel protein. Figure 38 shows representative dwell-time histograms for the activity of $TRPV1_{WT}$ and $TRPV1_{T406D}$. Similar to Studer and McNaughton we were able to identify three open states (O1-O3) and four closed states (C1-C4) (Studer & McNaughton 2010). The time constants of the open states as well as the relative contribution of the O1-O3 states seem to slightly vary with different experimental conditions (0.3 µM, with/without priming with 3.3 µM capsaicin), the open states were not significantly different between $TRPV1_{T406D}$ mutant and $TRPV1_{WT}$. However, the detailed analysis of the closed states C1-C4 revealed an (compared to $TRPV1_{WT}$) increasing long time constants C4 in the $TRPV1_{T406D}$ mutant, which is markedly reduced in both, time and relative contribution in the presence of 0.3 µM capsaicin after priming. However, closed states of $TRPV1_{WT}$ are only slightly modulated by capsaicin. Therefore, the analysis of the gating properties point to the involvement of closed states modulation of $TRPV1_{T406D}$, resulting in the observed use-dependent behavior.

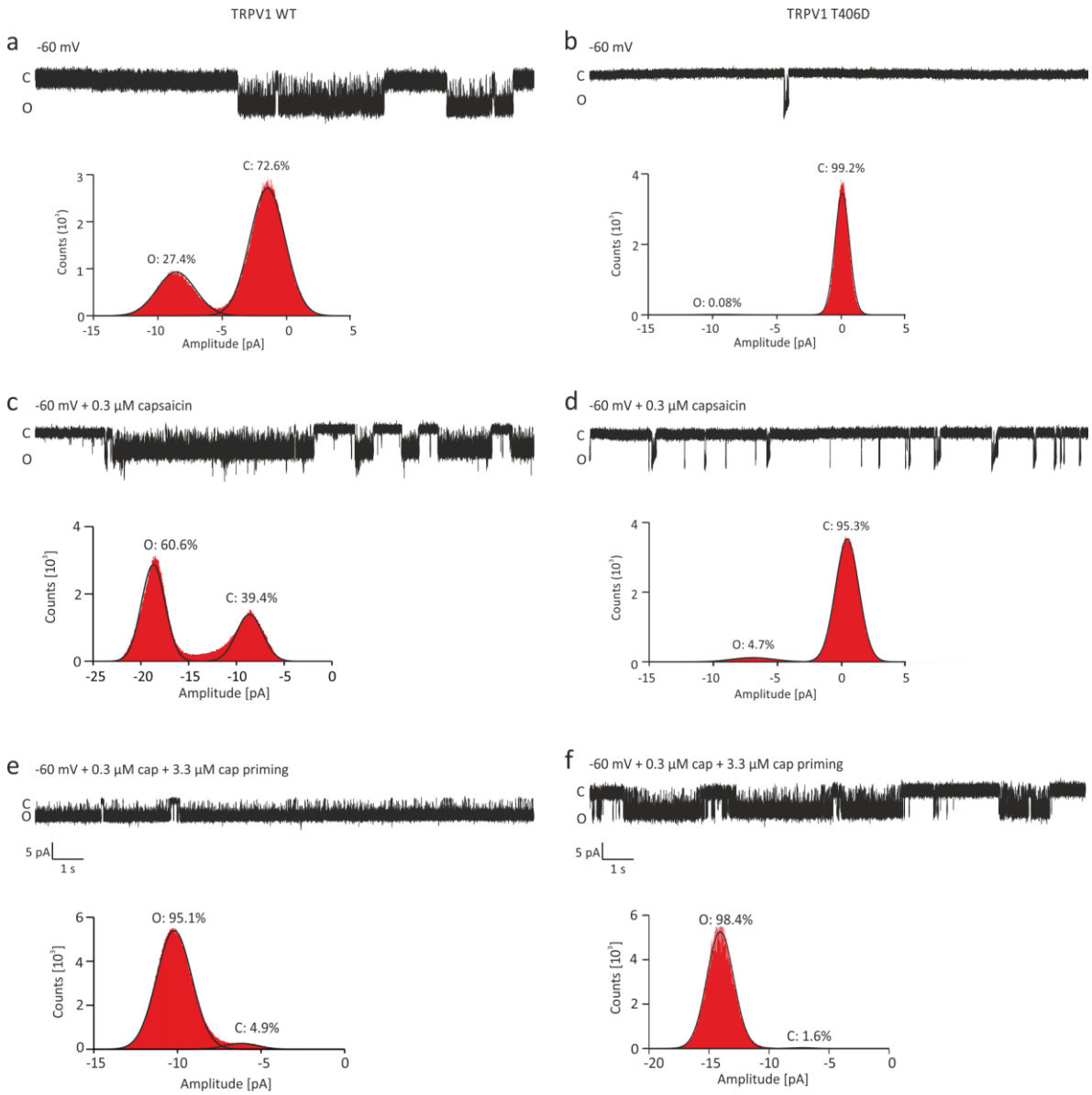

Figure 36. T406D mutagenesis affects the TRPV1 single channel characteristics. Single channel events were recorded in cell attached configuration at -60mV pipette potential for <2 min. A high [K^+] (140 mM) bath solution was used to equalize the membrane potential. The pipette solution contains Cs^+ and Ba^{2+} to block endogenous K^+ channels. Representative single channel traces and exemplary open probability of $TRPV1_{WT}$ and $TRPV1_{T406D}$ at (**a, b**) -60 mV, (**c, d**) -60 mV and 0.3 µM capsaicin, and (**e, f**) -60 mV, 0.3 µM capsaicin and priming with 3.3 µM capsaicin for 2 min. Interestingly, the current levels of $TRPV1_{T406D}$ were not constant, the conductance shifts from an initial high to lower state.

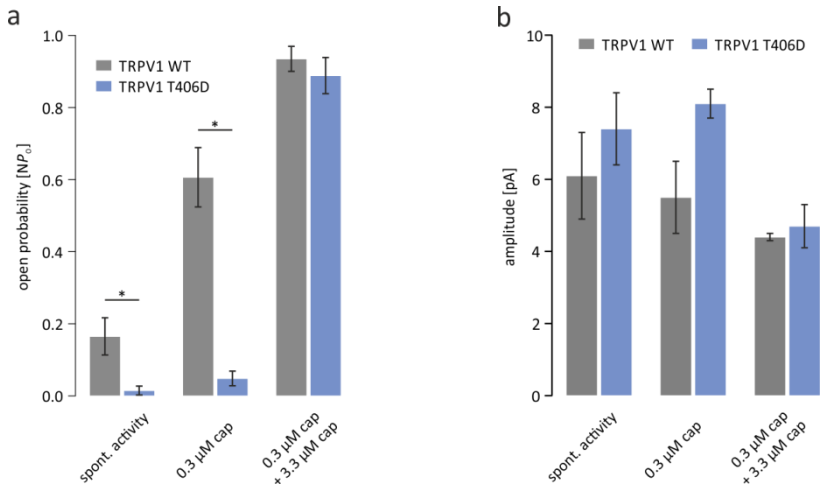

Figure 37. Open probability (NP_O) and single channel amplitude of TRPV1$_{WT}$ and TRPV1$_{T406D}$. (**a**) The NP_O of spontaneous and capsaicin (0.3 µM)-induced channel opening is significantly lower in TRPV1$_{T406D}$ than in TRPV1$_{WT}$ ($p < 0.05$). The open probabilities of TRPV1$_{T406D}$ and TRPV1$_{WT}$ become equal after priming with 3.3 µM capsaicin. (**b**) TRPV1$_{WT}$ and TRPV1$_{T406D}$ single channel amplitudes in cell-attached configuration at an approximate membrane potential of 0 and a pipette potential of -60 mV. Mean ± sem of n = 3-6 independent measurements (unpaired *WR-test* $p < 0.05$).

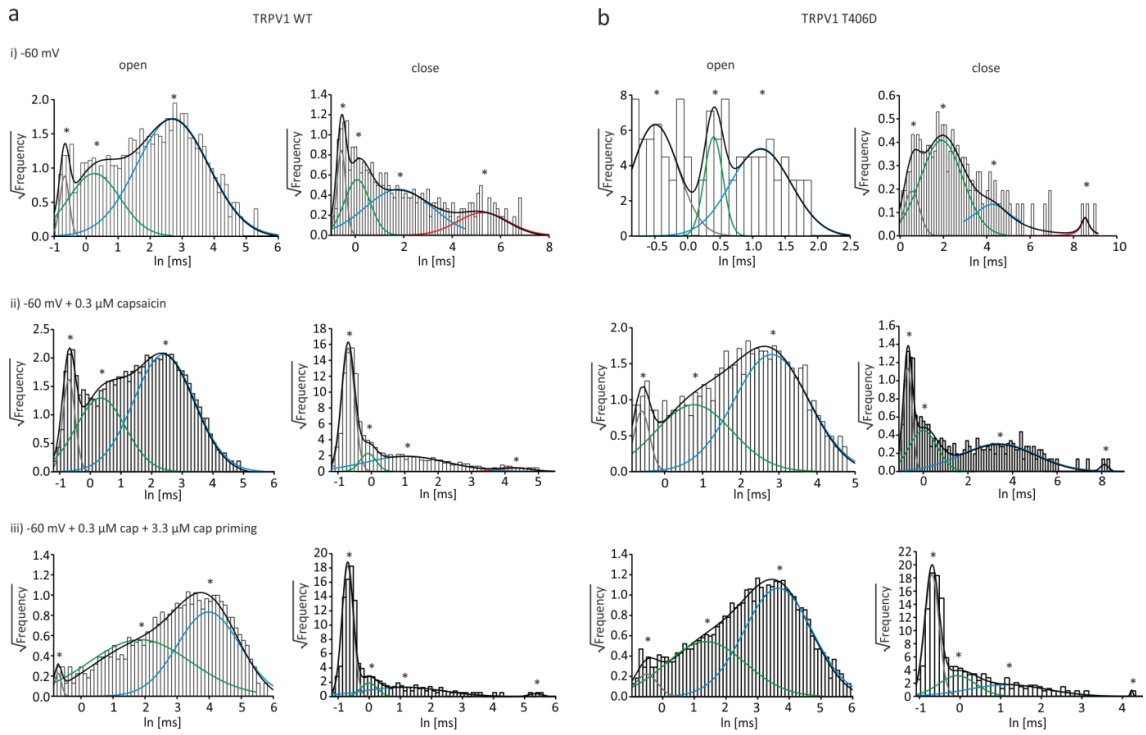

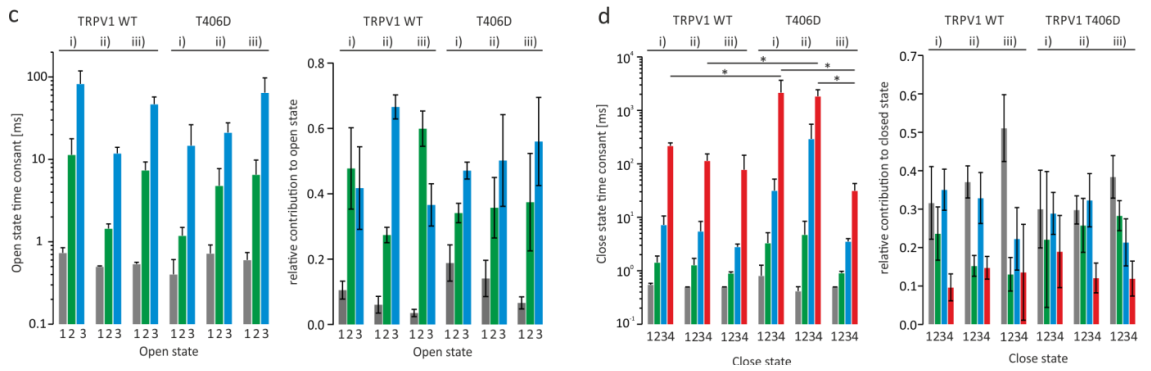

Figure 38. Dwell-time distribution analysis of $TRPV1_{WT}$ and $TRPV1_{T406D}$ single-channel recordings. Representative open and closed dwell-time histograms of (**a**) $TRPV1_{WT}$ and (**b**) $TRPV1_{T406D}$ at -60 mV (i), -60 mV + 0.3 µM capsaicin (ii), and -60 mV + 0.3 µM capsaicin after priming with 3.3 µM capsaicin (iii). The polymodal fit of $TRPV1_{WT}$ and $TRPV1_{T406D}$ dwell-time distributions revealed 3 open states (O1, O2, and O3) as well as 4 closed states (C1, C2, C3, and C4), marked as *. (**c**, **d**) The open state time constants and their relative contribution revealed no significant differences between $TRPV1_{WT}$ and $TRPV1_{T406D}$. However, the closed state C4 was significantly (*) higher under Ringer's condition, compared to the corresponding $TRPV1_{WT}$ C4 and the $TRPV1_{T406D}$ C4 after priming with 3.3 µM capsaicin (unpaired *WR-test* $p < 0.05$) (n = 3-10) (Jendryke et al. 2016).

6.12 What is the molecular mechanism that alters the ion channel gaiting?

The *in vivo* results revealed that the TRPV1-mediated responses to capsaicin and heat were modulated by the co-expression of Cdk5. Increasing the Cdk5 expression level in sensory neurons induces TRPV1-mediated hyperalgesia and allodynia, while a Cdk5 CoKo or a p35KO led to hypoalgesia. The *in vitro* experiments revealed that the co-expression of TRPV1, Cdk5, and p35 prevents the Ca^{2+} induced desensitization of $TRPV1_{WT}$. Mutagenesis of the Cdk5 phosphorylation site T406 enabled us to characterize the impact of that specific residue on TRPV1 function in detail. The exchange of T406 to the negatively charged aspartic acid had severe consequences for TRPV1 ion channel function. We could demonstrate that several biophysical properties were modulated in $TRPV1_{T406D}$. The activation kinetics were slowed, the voltage-dependence, the sensitivity to capsaicin, low pH or heat were modified and the Ca^{2+}-dependent desensitization was prevented. Finally, we found in single-channel experiments that the closed state C4 of the $TRPV1_{T406D}$ mutant is prolonged and is therefore the molecular parameter responsible for the modified $TRPV1_{T406D}$ function.

The question now is:

What is the structural/functional relationship that connects the Cdk5-dependent phosphorylation at position T406 to the TRPV1 gating mechanism?

In order to investigate position T406 with regard to the ion channel pore and gating mechanism, we made use of the high resolution structure of the TRPV1 and analyzed the 3D structure in cooperation with C. Ziegler (LS Biophysik, UR) (Fig. 39). The analysis showed that the membrane proximal domain (MPD), including T406, is relatively close to the TRP-domain, which is directly connected to the pore-forming transmembrane domain 6. Furthermore, we noticed that the conformational changes between the close and open state, comprise altered distances between the amino acid residues Y401, R499, and D707. We focused on these amino acids based on the assumption that they may participate in the gating process and might be involved in stabilizing the conformation of the respective states. Y401 is close to T406 and part of the flexible loop, R499 is located in the intracellular loop between TMD 2 and TMD 3 and close to the PKA phosphorylation site S501, and D707 is part of the TRP domain. Analyzing the distance between Y401 and D707 revealed that the distance of 3.1 Å in the closed state shortens to 2.6 Å in the open/intermediate state, allowing direct interaction of Y401 and D707 via hydrogen bridges. Assuming that the TRP-domain directly affects the ion channel gating by modulating the pore forming TMD 6, it may be possible that TRP-domain adjacent structures affect the ion channel gating by interacting with the TRP-domain. To investigate this hypothetical transition pathway, we generated together with M. Schladt several alanine mutants and performed a detailed electrophysiological characterization. We generated the following TRPV1 single mutants (Y401A, R499A, or D707A), and double mutant receptors (Y401A-T406D, Y401A-D707A, and T406D-D707A) (Schladt 2015). To investigate whether these amino acids are involved in the transition-pathway (TP) and influence TRPV1 gating properties, the various receptor mutants were functionally characterized in patch-clamp experiments regarding desensitization, voltage-dependence, and sensitivity to capsaicin or protons.

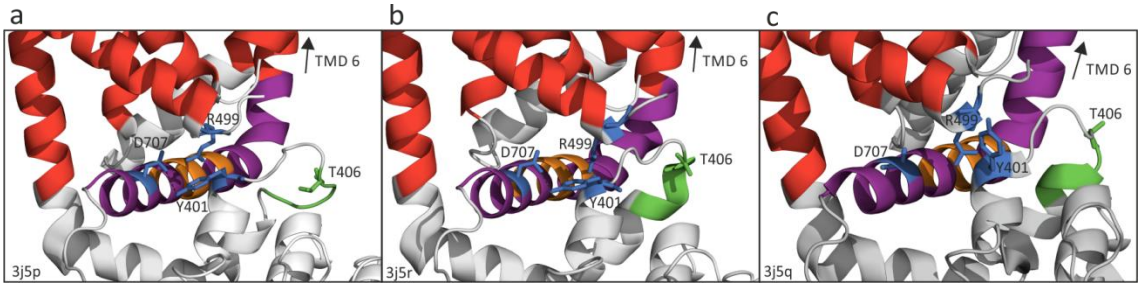

Figure 39. High resolution cryo-EM structures of TRPV1 (**a**) Apoprotein, (**b**) capsaicin bound and (**c**) RTX/DkTx bound. D707 and Y401 are close proximity in the closed and intermediate state, with distances of 3.1 Å (closed state) and 2.6 Å (intermediate state), which allow direct interactions via hydrogen bridges. R499 resides next to D707 and Y401, but due to distances larger than 2.6 Å, direct interactions are considered unlikely to occur. In the open state, the distance between D707 and Y401 is increased rendering direct interactions impossible. Relevant TRPV1 structures were color coded: **Red** transmembrane domain (TMD) 1-6, **Purple** TRP domain, **Orange** TRP box, **Green** Cdk5 consensus site, and **Blue** Transition pathway mutants.

6.13 Desensitization of transition pathway mutants

In order to investigate activation and desensitization kinetics of the transition pathway mutants, CHO cells expressing the TRPV1 double-mutants were recorded in whole-cell configuration in the presence of extracellular Ca^{2+}. Inward and outward currents were induced by the consecutive application of voltage-ramps (-100 mV to +100 mV) and TRPV1-mediated responses were induced by 3.3 µM capsaicin (Fig. 40). For analysis of ion channel desensitization, ratios of $I_{maximal}/I_{steady}$ were calculated and the activation kinetics was presented as time to half maximal response (t_{50}). The stimulation of $TRPV1_{WT}$ with 3.3 µM capsaicin induced fast TRPV1-mediated currents, characterized by a strong acute desensitization. In contrast, the transition pathway mutants lacked a Ca^{2+}-dependent desensitization. The maximal responses were presented in Figure 41a. The mean ± sem values indicate a high variability, which might be based on different expression rates. Analysis of the t_{50} values revealed that mutagenesis in the structures adjacent to the TRP-domain strongly reduced the activation kinetics of the response to the first application of capsaicin (Fig. 41b). In $TRPV1_{WT}$ and $TRPV1_{D707A}$ we found t_{50} values of 5 to 10 s for outward and inward currents, but the other TP-mutants showed significantly slowed activation kinetics with t_{50} values of 20 to 60 s at +100 mV and 30 to 70 s at -100 mV (*Tukey's test* $p < 0.05$).

Furthermore, we found that the Ca^{2+}-induced desensitization ($I_{steady}/I_{maximal}$) was prevented in the transition pathway mutants (*Tukey's test* $p < 0.05$) (Fig. 41c). Based on these data it can be concluded that TRP-domain residues (D707) as well as adjacent residues, such as Y401 and R499 modulate the activation kinetics and desensitization of TRPV1 ion channels.

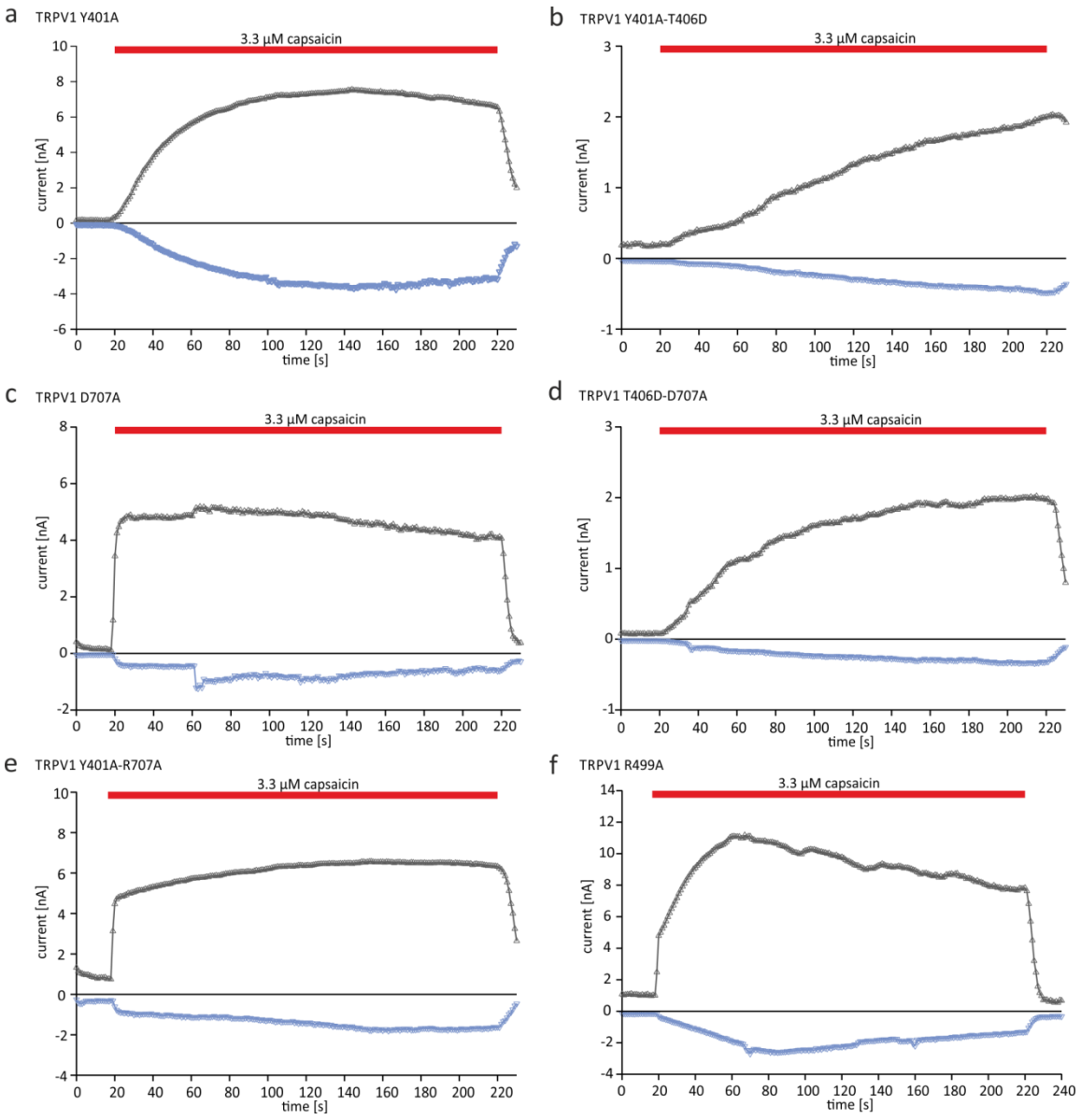

Figure 40. Desensitization of TRPV1 transition pathway mutants. TRPV1-mediated currents were evoked by applying 3.3 µM capsaicin in the presence of extracellular Ca^{2+}. Ca^{2+}-mediated desensitization was prevented in all TRPV1 transition pathway mutants. Additionally, the activation kinetics of TRPV1 mutants (**a**) Y401A, (**b**) Y401A-T406D, (**d**) T406D-D707A, and (**f**) R499A was reduced (n = 5–8).

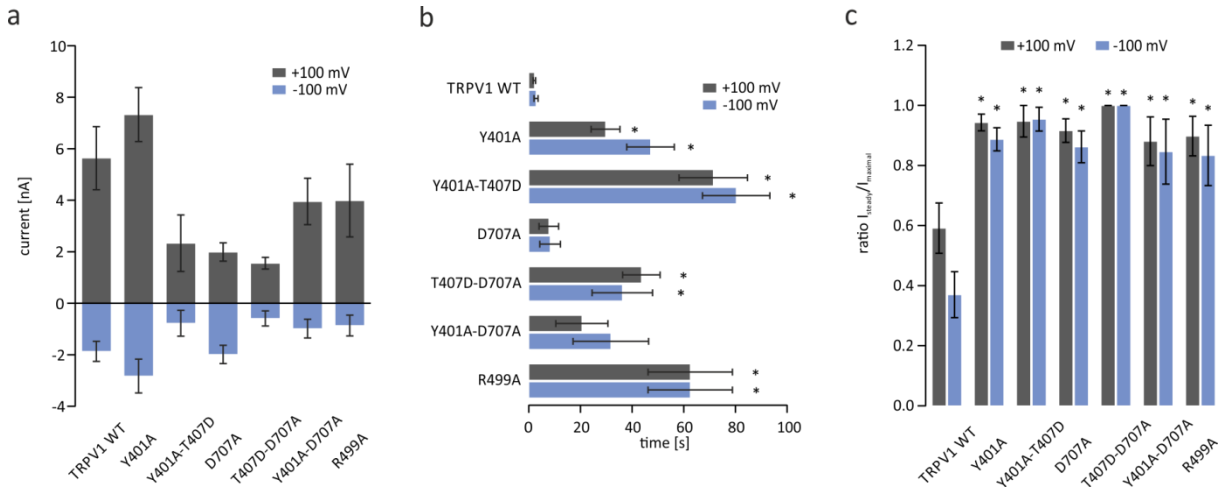

Figure 41. Analysis of TP pathway mutants. (**a**) TRPV1-mediated responses induced by 3.3 µM capsaicin were variable, but not significantly different (*Tukey's-test* n.s.). (**b**) Compared to the $TRPV1_{WT}$, activation kinetics of Y401A, Y401A-T406D, T406D-D707A, and R499A were significantly slowed (*Tukey's*-test $p < 0.05$). (**c**) The Ca^{2+}-dependent desensitization was prevented in TRPV1 transition pathway mutants (*Tukey's*-test:$p < 0.05$). Data is presented as mean ± sem of n = 5-8 independent measurements.

6.14 **TP-mutant capsaicin concentration/response-relationship**

Next we were interested in the capsaicin sensitivity of the transition pathway mutants. Therefore, CHO cells expressing the mutant TRPV1 receptors were challenged with various capsaicin concentrations (0.05 µM to 3.3 µM) in the absence of extracellular Ca^{2+}. As in the $TRPV1_{T406D}$ experiments, the concentration/response-relationship of the TP-mutants were analyzed before and after priming with 3.3 µM capsaicin (Fig. 42). In $TRPV1_{WT}$ measurements, the first and second concentration/response-relationship revealed the same response pattern with EC_{50} values of 1^{st} 0.34 ± 0.07, 2^{nd} 0.39 ± 0.12 µM at +100 mV; 1^{st} 0.65 ± 0.14, 2^{nd} 0.68 ± 0.14 µM at -100 mV, and similar Hill curves and EC_{50} values were determined for the $TRPV1_{D707A}$ mutant (Table 4). In TRPV1 Y401A, Y401A-T406D, T406D-D707A, and R499A mutants, the first application series of capsaicin evoked no or only weak TRPV1-mediated currents, which did not allow the calculation of EC_{50} values. After priming with 3.3 µM capsaicin, these TRPV1 TP-mutants gained full responsiveness and obtained EC_{50} values which were similar to those of $TRPV1_{WT}$ (Table 4). In the TRPV1 double-mutants Y401A-T406D and T406D-D707A, the first application series of capsaicin evoked no TRPV1-mediated currents.

However, in the second series of applications, capsaicin induced responses with significantly reduced EC_{50} values 0.09 ± 0.01 µM at +100 mV (*Tukey's test:* $p < 0.05$). These data show that the capsaicin sensitivity of TRPV1 receptors were unaffected in D707A mutants, but mutagenesis of adjacent residues such as Y401A, R499A and Y401A-D707A affects the capsaicin sensitivity before priming. Furthermore, data obtained from the double-mutants Y401A-T406D and T406D-D707A revealed that the aspartate at position T406 contributes to sensitization of the TRPV1 receptor to capsaicin.

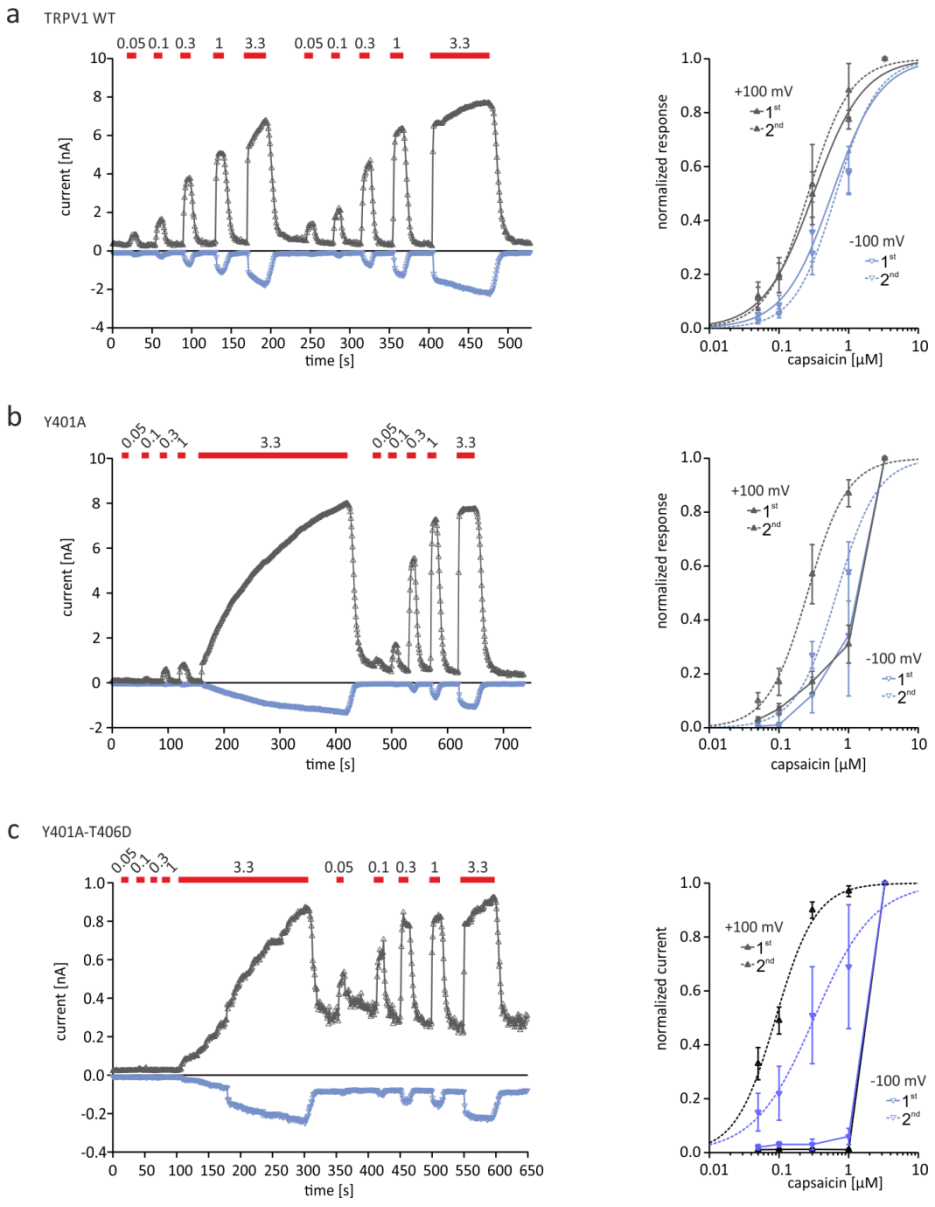

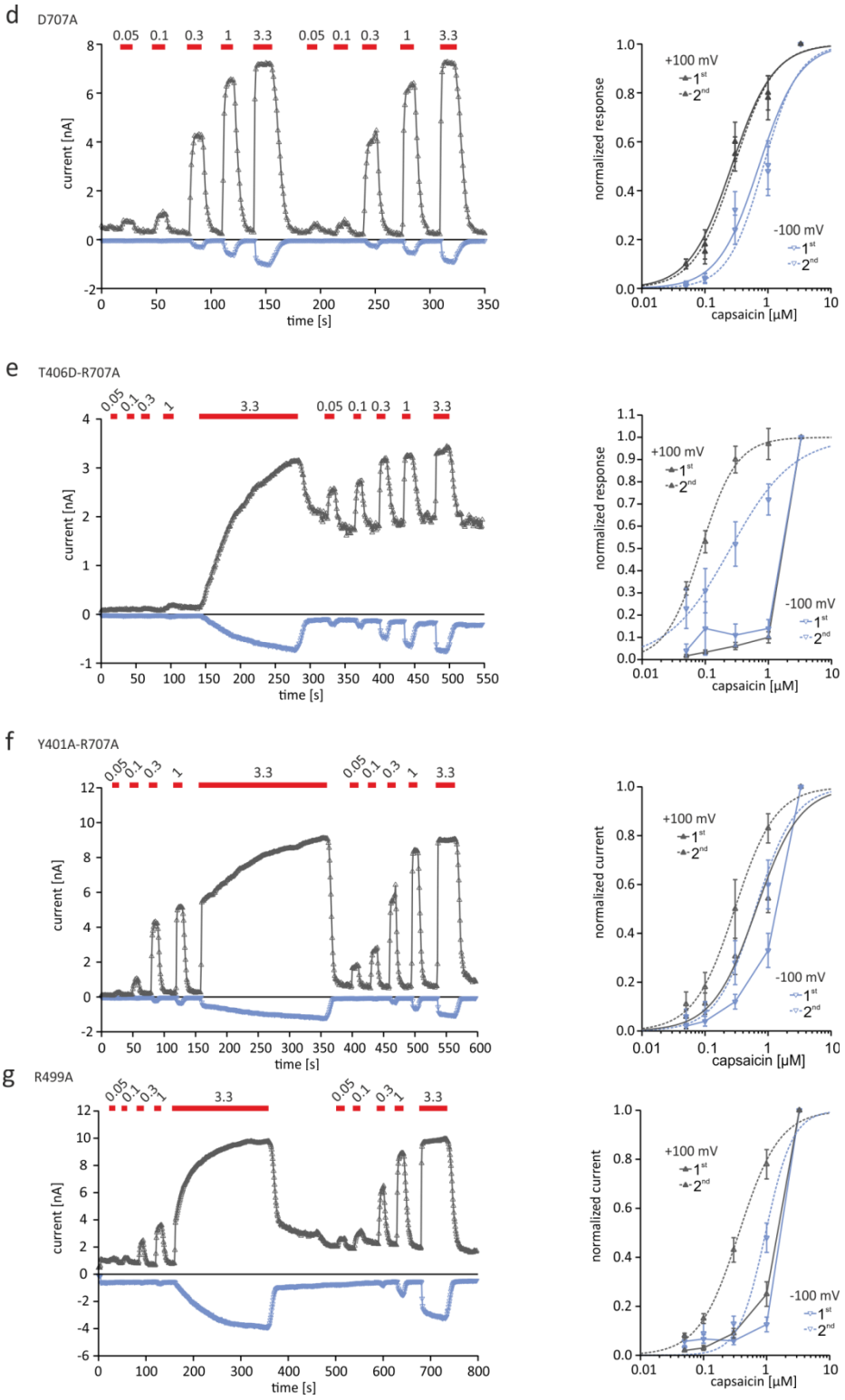

Figure 42. Capsaicin concentration/response-relationship of TRPV1 transition pathway mutants. Left panel: Representative inward and outward currents of $TRPV1_{WT}$ or TP mutants induced by increasing capsaicin concentrations (0.05 to 3.3 µM). Right panel: Corresponding normalized responses and Hill curves for the calculation of the EC_{50} values for 1st and 2nd inward and outward responses.

Weak or no responsiveness to capsaicin in some TP mutants prevents the calculation of EC_{50} values for the first application series n = 4-8.

	inward currrent (-100 mV)		outward currrent (+100 mV)	
	1st	2nd	1st	2nd
TRPV1	EC_{50} ± SEM	EC_{50} ± SEM	EC_{50} ± SEM	EC_{50} ± SEM
WT	0.65 ± 0.14	0.68 ± 0.14	0.34 ± 0.07	0.39 ± 0.12
Y401A	-	0.76 ± 0.14	-	0.29 ± 0.06
Y401A-T406D	-	0.53 ± 0.3	-	*0.09 ± 0.01
D707A	0.81 ± 0.16	0.86 ± 0.15	0.36 ± 0.13	0.33 ± 0.06
T406D-D707A	-	0.24 ± 0.06	-	*0.09 ± 0.01
Y401A-D707A	-	0.71 ± 0.17	0.7 ± 0.14	0.36 ± 0.12
R499A	-	0.91 ± 0.09	-	0.43 ± 0.09

Table 4. EC_{50} values of TP mutants. In the most of the TP mutants, the weak responsiveness to low concentrations of capsaicin did not allow the calculation of EC_{50} values. Interestingly, outward currents mediated by Y401A-T406D and T406D-D707A TRPV1 receptors during the 2nd application series showed a significantly (*) increased capsaicin sensitivity (*Tukey's*-test $p < 0.05$; n = 4-8).

6.15 **Voltage-dependence of transition pathway mutants**

Since the voltage dependence of $TRPV1_{T406D}$ is enhanced by priming the receptor with 3.3 µM capsaicin, we wanted to test whether the voltage-dependence of the transition pathway mutants is also subject to modulation. To this end, transiently transfected CHO cells were electrophysiologically characterized in the whole-cell configuration. In absence of extracellular Ca^{2+}, voltage steps (-120 to +160 mV) were applied before, during, and 60 s after washout of 3.3 µM capsaicin. Analyzing the voltage-dependence of $TRPV1_{WT}$ and TP-mutants revealed no significant differences (Fig. 43). In Ca^{2+}-free Ringer's solution, most of the mutants showed voltage-induced currents (0.1-0.3 nA/pF), which were increased by the application of 3.3 µM capsaicin (0.4-1 nA/pF). The current densities in the TRPV1 double mutants Y401A-T406D and T406D-D707A were too small (40-60 pA/pF). The conductance G was calculated and normalized to G_{max}, in order to estimate $V_{1/2}$ by means of a sigmoidal fit. The analysis of the conductance revealed that the TP-mutants did not show an altered voltage-dependence before and after the full activation of the TRPV1 receptor protein.

Under Ringer's condition, we found in all TP mutants a $V_{1/2}$ of +100 to +120 mV, which was reduced to -20 to -60 mV during capsaicin application. Interestingly, the Y401A-T406D and T406D-D707A mutants also showed no altered voltage-dependence after the washout of capsaicin. However, the $TRPV1_{T406D}$ mutant showed an increased voltage-dependence after the capsaicin washout, but the TP mutants did not showed an altered voltage-dependence after the washout of 3.3 µM capsaicin. Therefore, we conclude that the transition pathway mutants did not reproduce the altered voltage dependence of the $TRPV1_{T406D}$ mutant.

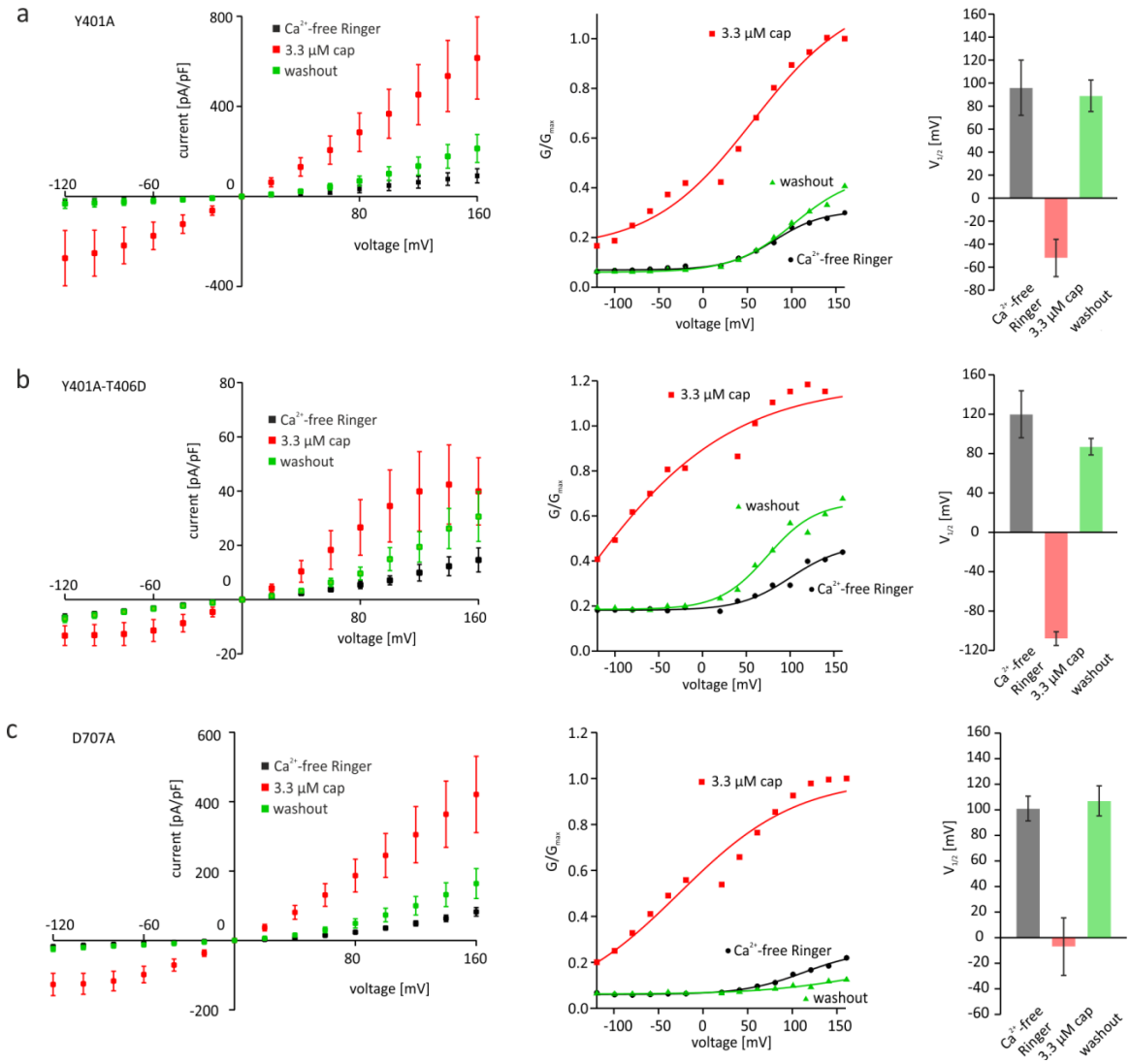

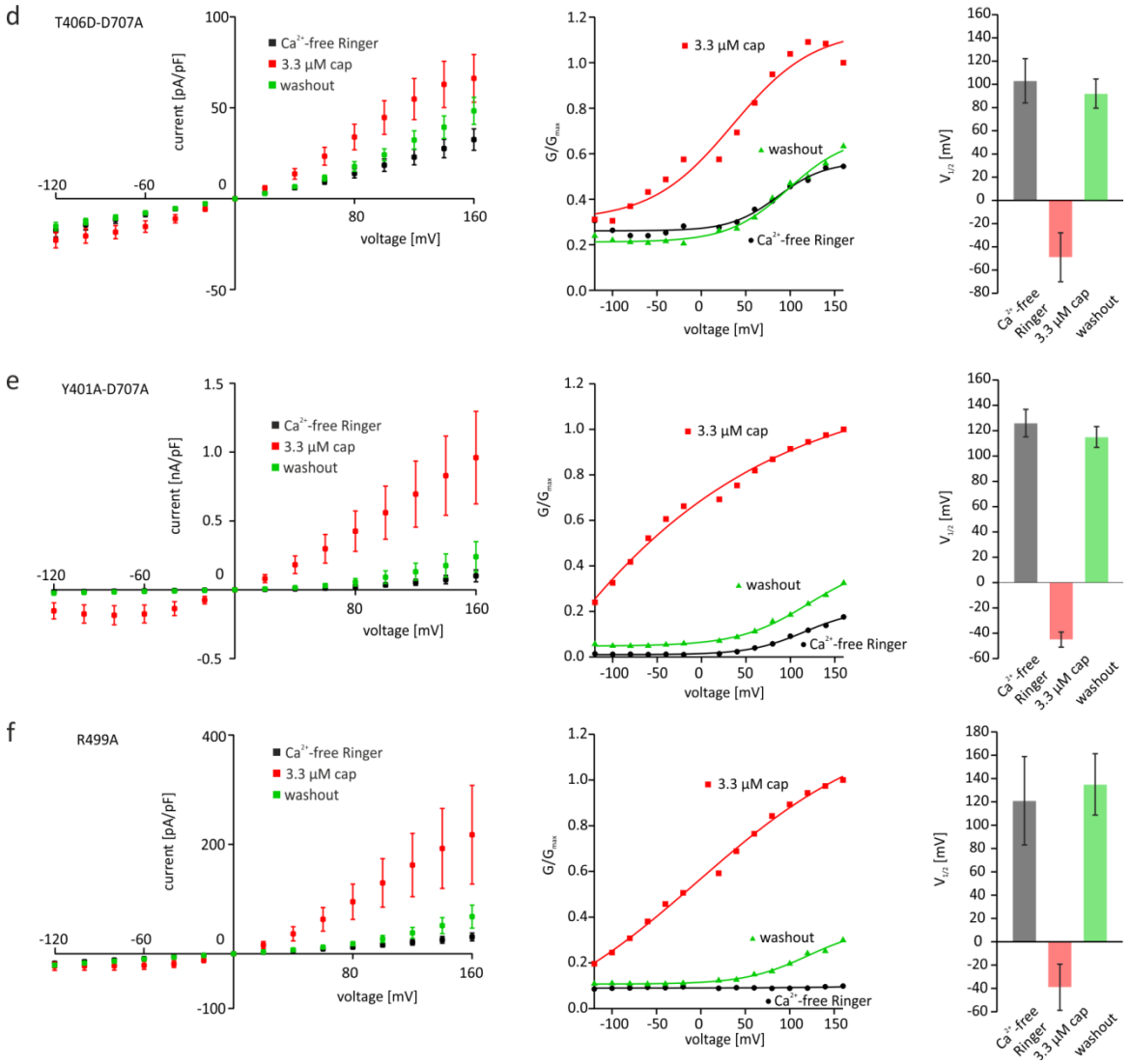

Figure 43. Voltage-dependence of TRPV1 transition pathway mutants. IV-relationships were measured in Ca^{2+}-free Ringer's solution using voltage-step protocols (-120 to 160 mV), before, during, and 1 min after washout of 3.3 µM capsaicin. n = 5-7

6.16 **Low pH activation of TRPV1 transition pathway mutants**

Finally, we were interested in the activation of TP mutants by pH 6, therefore the TRPV1 mutants Y401A, D707A, T406D-D707A, and Y401A-D707A were challenged in the absence of extracellular Ca^{2+} with two consecutive series of application of pH6, as well as 0.3 and 3.3 µM capsaicin. TRPV1-mediated currents were recorded in the whole-cell configuration applying voltage-ramps (-100 mV to +100 mV). Representative pH6 and capsaicin-induced TRPV1-mediated inward and outward currents as well as the corresponding ratio of 1st and 2nd responses were presented in Figure 44.

The analysis of the TRP domain mutant D707A revealed that pH6 and capsaicin induced similar responses in the 1st and 2nd application series, resulting in a ratio of about 1. Y401A-D707A TRPV1 receptor mutants showed slightly weaker responses in the first series of application of pH6 and 0.3 µM capsaicin, but gained full responsiveness after priming with 3.3 M µM capsaicin, resulting in ratios (1st vs. 2nd response) of 0.5 to 0.9, which indicates a slight sensitization to pH6 and 0.3 µM capsaicin. Moreover, Y401A and T406D-D707A also did not respond to pH6 and 0.3 µM capsaicin in the first application series, but again developed full responsiveness of the TRPV1 receptor after priming with 3.3 µM capsaicin. The calculated ratios were below 0.4, indicating a strong sensitization of the TRPV1 receptor variants. These data show again that the mutations of the amino acids T406D and Y401A which are adjacent to the TRP domain, have severe consequences on TRPV1 function. The lack of pH6 or 0.3 µM evoked responses before the priming supports the hypothesis that TRP-domain adjacent structures, including Y401 and T406, affect the TRPV1 ion channel gating.

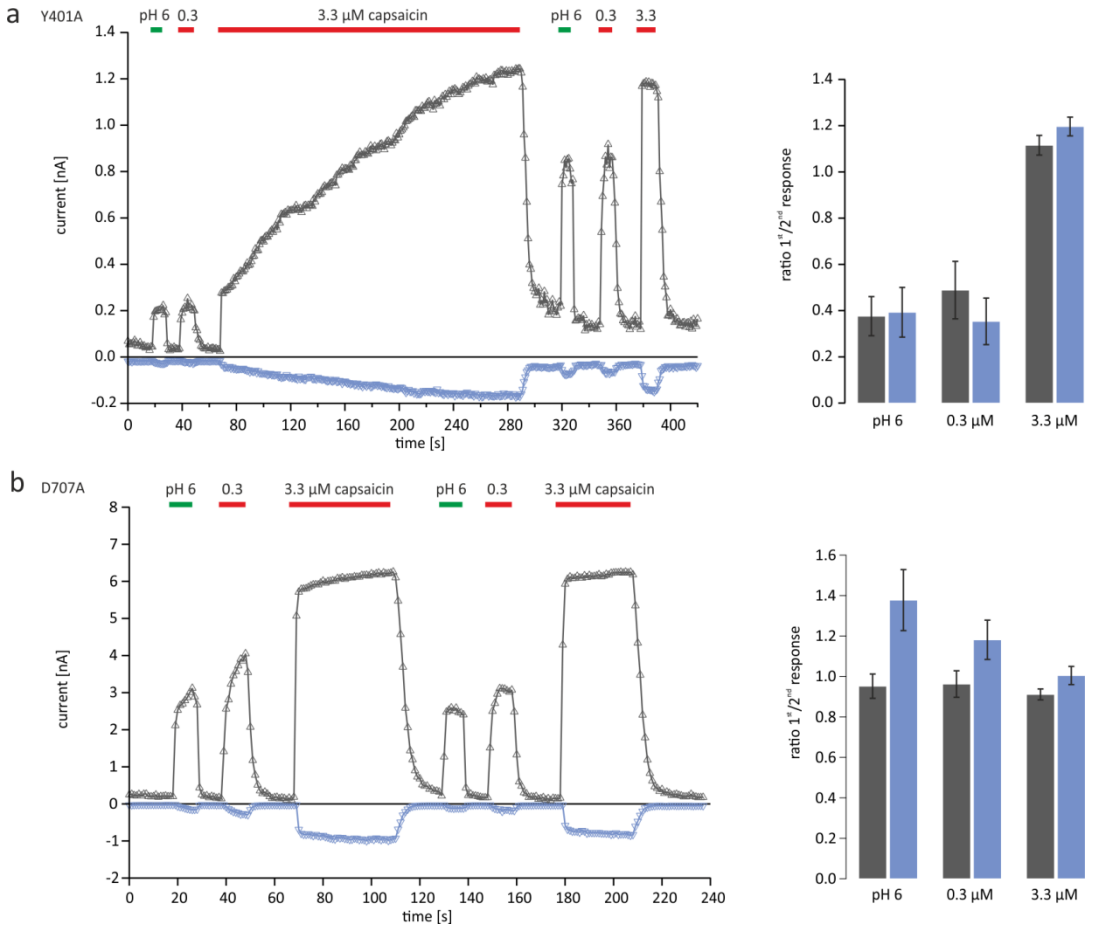

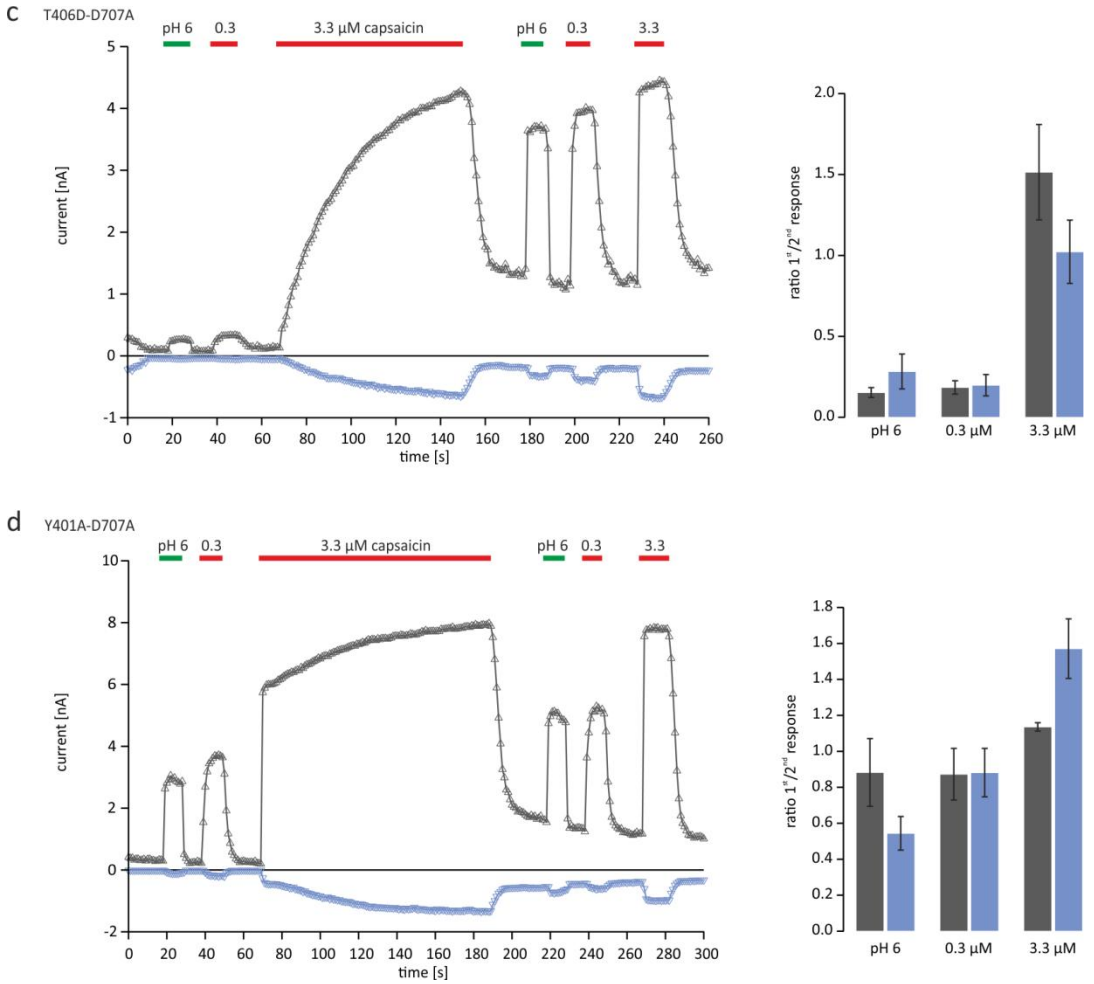

Figure 44. Proton-mediated activation of transition pathway mutants. Left panel: Representative inward (-100 mV) and outward (+100 mV) currents of (**a**) $TRPV1_{Y401A}$, (**b**) $TRPV1_{D707A}$, (**c**) $TRPV1_{T406D\text{-}D707A}$, and (**d**) $TRPV1_{Y401A\text{-}D707A}$. Low pH Ringer's solution, 0.3 µM, and 3.3 µM were applied in two consecutive series. Right panel: Ratio of 1st and 2nd response to the same stimuli. Ratios of about 1 indicated no sensitization or desensitization, whereas ratios >1 represent desensitization and ratios <1 receptor sensitization. Mean ± sem of n = 6-10 independent measurements.

In summary, the in vivo data demonstrated that the TRPV1-mediated nociception is highly modulated by the Cdk5 activity in sensory neurons. The behavioral study using the TRPV1 agonist capsaicin and heat revealed that increased Cdk5 activity led to hyperalgesia and allodynia, whereas decreased Cdk5 activity induces hypoalgesia. These in vivo findings were transferred into a recombinant expression system to characterize the underlying molecular mechanisms in detail. The key result of the electrophysiological characterization was that the co-expression of TRPV1, Cdk5, and p35 prevents the Ca^{2+}-mediated desensitization.

Since, the kinase Cdk5 is able to phosphorylate TRPV1 at position T406 we generated several $TRPV1_{T406}$ mutants to investigate the effect on receptor function. Particularly, we were interested in mimicking the phosphorylation of T406, by introducing a negatively charged amino acid. The key outcome was that the introduction of charged amino acids especially the negatively charged aspartic acid has severe consequences on TRPV1 activation kinetics, desensitization, voltage activation, and single channel properties. Additionally, we could demonstrate that the use-dependent activation pattern of $TRPV1_{T406D}$ is based on an altered gating mechanism, which affects the TRPV1-mediated responses to capsaicin, low pH, and heat. The single-channel experiments revealed that the $TRPV1_{T406D}$ mutant directly affects the gating mechanism of the ion channel by prolonging one of the closed states. In order to investigate the altered TRPV1 gating mechanism in detail, we analyzed the TRPV1 structure and investigated the potential transition pathway by mutagenesis and electrophysiological characterization of functional properties. These data suggest that the TRPV1 linker domain, including T406, affects the TRP domain, which is connected to the pore forming TMD 6. Therefore, we conclude that the Cdk5-mediated phosphorylation of TRPV1 at position T406 affects the ion channel gating, by modifying the conformation of the TRP-domain adjacent linker domain.

7 Discussion

The aim of this study was to improve the understanding of the signal transduction mechanisms in nociceptive neurons by characterizing the functional and conformational impact of Cdk5-mediated phosphorylation of the TRPV1 protein. To this end, we and our collaboration partners (NIH, Bethesda USA) performed several different experimental approaches such as behavioral testing of genetically engineered Cdk5 mice (Jendryke et al. 2016), as well as electrophysiological recordings, Ca^{2+} imaging experiments, and TIRF microscopy of transiently transfected CHO cells. The obtained data illustrate the impact of T406 phosphorylation or mutagenesis on the function of TRPV1 receptors. Moreover, the functional characterization of T406 mutants let us speculate on the conformational changes that could be involved in the gating mechanism of TRPV1 ion channels. Finally, we analyzed the potential transition pathway of TRPV1 activation and phosphorylation by investigating the effect of transition pathway mutants on TRPV1 function. The molecular mechanism of TRPV1 activation is of particular significance, since TRPV1 plays a key role in nociception. This modulation of TRPV1 contributes to the induction of hyperalgesia/allodynia or hypoalgesia and is a potential target for the future development of analgesic drugs.

7.1 TRPV1 phosphorylation and nociception

It is known that the kinase-mediated phosphorylation of TRPV1 induces hyperalgesia and allodynia *in vivo*. For instance, the studies of Caterina et al., and Davis et al. revealed that the PKA-mediated phosphorylation of the TRPV1 receptor has severe impact on the TRPV1 ion channel function and the TRPV1-mediated nociception *in vivo* (Caterina et al. 2000; Davis et al. 2000). Moreover, it is known that the PKA or PKC-mediated phosphorylation of the receptor protein led to an increased sensitivity to capsaicin and heat in genetically engineered mice (De Petrocellis et al. 2001; Rathee et al. 2002; Bhave et al. 2003; Premkumar et al. 2004; Rosenbaum & Simon 2004). The same was also true for the CaMKII-mediated phosphorylation of TRPV1 (Jung et al. 2004). Therefore, we assume that the Cdk5-mediated phosphorylation has similar effects on TRPV1 function like its phosphorylation by PKA, PKC, or CaMKII.

In our joint study, Kulkarni et al. extended their *in vivo* analysis (Jendryke et al. 2016). They investigated the TPRV1-mediated pain responses of genetically engineered mice by means of the specific TRPV1 agonist capsaicin or noxious heat (45 °C). In mice overexpressing p35, the neuronal activator of Cdk5, they observed an increased Cdk5 activity which induced hyperalgesia and/or allodynia. However, the conditional knockout of Cdk5 or the knockout of p35 in sensory neurons induced hypoalgesia. In conclusion, these results revealed that TRPV1-mediated nociception is modulated by the kinase Cdk5. We assume that the increased sensitivity to capsaicin or heat is due to the Cdk5-mediated phosphorylation of the TRPV1 receptor protein. This is in line with previous studies showing that the kinase-mediated phosphorylation of TRPV1 induces hyperalgesia and/or allodynia (Pareek et al. 2007; Pareek et al. 2006). Thus, we set out to investigate the TRPV1 function with regard to the Cdk5-mediated phosphorylation, by means of a detailed electrophysiological characterization of the TRPV1 receptor protein function.

7.2 The molecular mechanism of TRPV1 phosphorylation

The phosphorylation of TRPV1 receptors affects the ion channel function in different ways. The phosphorylation of TRPV1 increases the sensitivity and/or prevents the Ca^{2+}-dependent desensitization of the receptor protein. To the best of our knowledge, no *in vitro* data regarding the Cdk5-dependent phosphorylation of TRPV1 were available so far. Thus, we set out to analyze the TRPV1-mediated currents of transiently transfected CHO cells expressing TRPV1 or a combination of TRPV1, Cdk5, and the neuron specific Cdk5 activator p35. TRPV1-mediated currents and Ca^{2+}-dependent desensitization of TRPV1 was induced by challenging cells with saturating capsaicin concentrations in the presence of extracellular Ca^{2+}. Our data revealed that TRPV1-mediated currents strongly desensitize in presence of Ca^{2+}, whereas the co-expression of Cdk5 and p35 prevented the Ca^{2+}-induced acute desensitization of TRPV1-mediated currents. The analysis of the capsaicin concentration/response-relationship reveals that Cdk5 co-expression does not affect the TRPV1 sensitivity to capsaicin. Thus, we conclude that our findings were in line with the results of Mohapatra and Nau, the kinase-mediated phosphorylation of TRPV1 decreases the Ca^{2+}-dependent desensitization (Mohapatra & Nau 2003), and not in line with the results of Rathee et al. 2002 and Bhave et al. 2003 revealing that the PKC-mediated phosphorylation of TRPV1 sensitizes the receptor to capsaicin and heat (Rathee

et al. 2002; Bhave et al. 2003). In general, TRPV1 sensitization or prevention of receptor desensitization has severe consequences on the TRPV1-mediated nociception *in vivo*. The sensitization of the receptor protein reduces the activation threshold of TRPV1 receptors, whereas prevention of the Ca^{2+}-dependent desensitization reduces the decline of the stimuli induced responses. Both, receptor sensitization and prevention of receptor desensitization increases the net influx of cations through the TRPV1 pore, which leads to an intensified depolarization of the plasma membrane. Therefore, the TRPV1-mediated depolarization of the free nerve endings of the sensory neurons triggers the activation of voltage-gated Na channels. The subsequently increased influx of Na depolarizes the free nerve endings and initiates the formation of action potentials. In conclusion, the phosphorylation of TRPV1 increases the net influx of cations, which increases the depolarization of the free nerve endings, and leads to the increased generation of action potentials. Finally, the central nervous system can interpret the increased frequency of action potentials as pain. Moreover, the prolonged activation of sensory neurons and the increased influx of cations (Ca^{2+}) can also induce protein degradation and/or cytotoxic processes that led to axon decline of sensory neurons (Kim et al. 2006; Reilly et al. 2008; Agopyan et al. 2004). To prevent the excessive influx of cations trough the TRPV1 ion channel pore, the desensitization of the TRPV1 ion channel reduces the net influx of cations. The underlying mechanism may involve an increase in the rate of entries into a desensitized state or a decrease in the rate of exits from desensitized states. In order to investigate this aspect in more detail we set out to analyze the TRPV1 function of $TRPV1_{T406}$ receptor mutants.

7.3 $TRPV1_{T406}$ mutagenesis

In general, protein phosphorylation can be inhibited by removing serine or threonine residues at putative phosphorylation sites, or be mimicked by introducing a bulky and negatively charged amino acid (aspartate or glutamate) by site directed mutagenesis of the target protein. Some of the previous mentioned TRPV1 studies also made use of TRPV1 receptor mutants in order to identify the phosphorylation sites or to investigate the effect of altered amino acid residues on TRPV1 function. In order to identify the PKA phosphorylation sites in the TRPV1 receptor Bhave et al. mutated the potential consensus sites (S6, S116, T144, T370, S502, S774, and S820) in the TRPV1 receptor with alanine.

They revealed that the PKA-mediated phosphorylation of TRPV1 at amino acid S116 is functionally relevant and prevents the Ca^{2+}-dependent desensitization (Bhave et al. 2002). This was supported by the studies of Mohapatra and Nau, which showed that the PKA-dependent phosphorylation can be mimicked by the introduction of negatively charged amino acids (Mohapatra & Nau 2003). Similarly, site-directed mutagenesis studies of TRPV1 were used to identiy the phosphorylation sites for CaMKII and Src kinase (Zhang et al. 2005; Jung et al. 2004). Numazaki et al. replaced the Ser residues S502 and S800 with alanine, in order to inhibit the PKC-mediated phosphorylation (Numazaki et al. 2002). In conclusion, these studies revealed that the mutagenesis of the TRPV1 phosphorylation sites into alanine prevent the kianse-mediated phosphorylation, whereas the introduction of aspartate mimics the phosphorylation. The TRPV1 consensus sites for kinase-mediated phosphorylation are far from the ion channel pore in the TRPV1 N- and C-terminus as well as in intracellular loops. However, the consensus sites are located in structures such as ankyrin repeats, linker domains and the TRP domain, which are part of the TRPV1 gating mechanism. In order to investigate this, we set out to generate several TRPV1 mutants in order to mimic or inhibit the Cdk5-mediated phosphorylation of the receptor protein. We replaced threonine 406 by the amino acids aspartate or alanine, respectively. Moreover, we were interested in the effect of amino acid residues such as histidine and proline on TRPV1 function, since these residues were characterized by different size and/or charge. Our data revealed that the introduction of both, negatively (Asp or Glu) as well as positively (Arg, His or Lys) charged amino acid residues, but also proline, inhibits the Ca^{2+}-dependent desensitization of TRPV1 receptors. Moreover, we found in $TRPV1_{T406D}$ and $TRPV1_{T406E}$ mutants an initially low stimulus sensitivity and very slow activation kinetics. In order to investigate the $TRPV1_{T406D}$ receptor variant in more detail, we analyzed also the initial TRPV1-mediated current as well as a second response to the same stimulus after priming the receptor protein. The data revealed that the prolonged activation of $TRPV1_{T406D}$ with capsaicin induces a markedly increased sensitivity and acceleration of TRPV1 activation kinetics. To the best of our knowledge, this use-dependent behavior of TRPV1 mutants was not yet described. Neither the kinase-mediated phosphorylation of TRPV1 nor the introduction of amino acid residues such as alanine leads to a slowed activation kinetics as we found in $TRPV1_{T406D}$ mutants.

Therefore, we suggest that in $TRPV1_{T406D}$ the protein conformation is altered, which affects the gating mechanism of the receptor protein and induces the use-dependent behavior. More precisely, we suggest that the aspartate at position 406 alters the conformation of the four TRPV1 subunits and that the binding of capsaicin to all four subunits is necessary to rearrange these conformational changes. Alternatively, during the maximal activation, the mutagenesis of amino acid T406 might increase the translocation of the TRPV1 receptor protein into the plasma membrane. Interestingly, Xing et al. and Liu et al. found that Cdk5 positively regulates the TRPV1 membrane trafficking in sensory neurons. Their studies revealed that Cdk5 is able to phosphorylate the motor protein KIF13B, which then promotes the trafficking process of TRPV1 to the plasma membrane. Furthermore, they found that this regulatory mechanism is connected to inflammatory heat-induced hyperalgesia (Liu et al. 2015; Xing et al. 2012). In order to address this, we investigated the stimulus-dependent receptor translocation by means of TIRF microscopy. We analyzed the fluorescence of GFP tagged $TRPV1_{WT}$ and $TRPV1_{T406}$ mutants in the plasma membrane of CHO cells. The data revealed that the GFP-fluorescence of cells expressing GFP-$TRPV1_{WT}$ or GFP-$TRPV1_{T406D}$ is unaffected by challenging cells with a supramaximal concentration of capsaicin. Thus, we conclude that the slowed activation kinetics of $TRPV1_{T406D}$ is not due to an increased membrane trafficking of the receptor, but most likely due to functional and structural changes in the TRPV1 receptor protein.

7.4 $TRPV1_{T406D}$ voltage-dependence

The kinase-dependent phosphorylation of TRPV1 increases the voltage-dependence of the receptor protein (Matta & Ahern 2007; Premkumar & Ahern 2000). Thus, we set out to investigate the voltage-dependence of $TRPV1_{WT}$, $TRPV1_{T406A}$, and $TRPV1_{T406D}$ in detail by means of voltage-step protocols. Interestingly, hardly any voltage-dependent $TRPV1_{T406D}$-mediated currents could be recorded before the initial application of capsaicin. A prolonged application of capsaicin significantly enhances the voltage-dependence, which was also present up to 5 minutes after the capsaicin washout. To the best of our knowledge, this effect on the voltage-dependence of TRPV1 receptor was unknown. The introduction of negatively charged residues into the TRPV1 receptor, in order to mimic the PKA, PKC, or CaMKII mediated phosphorylation, induced the same

functional characteristics as the kinase-mediated phosphorylation. The mutated TRPV1 receptors in the PKA, PKC, or CaMKII-kinase studies neither showed the use-dependent behavior nor the altered voltage-dependence we found in $TRPV1_{T406D}$ mutants. The analysis of $TRPV1_{T406D}$ revealed that the introduction of a negative residue (Asp) at amino acid T406 does not mimic the Cdk5-mediated phosphorylation of TRPV1. Thus, we assume that the mutagenesis of TRPV1 at residue T406 affects the gating mechanism of the ion channel in a different way than the Cdk5-mediated phosphorylation of TRPV1. In general, the phosphorylation of proteins is a dynamic process, which depends on several factors such as kinase activity or access to the consensus site. For instance, the Cdk5-mediated phosphorylation of TRPV1 depends not only on the Cdk5 function but also on the functionality of the Cdk5 activator p35. Additionally, the Cdk5-mediated phosphorylation only affects the folded TRPV1 protein in the plasma membrane, whereas, the mutagenesis of the TRPV1 receptor could also affect the folding process of the four TRPV1 subunits. Notably is also that the voltage-dependent activation of TRPV1, which is probably the primary molecular mechanism that induces the opening of the ion channel pore, is affected by the T406D mutagenesis. The agonist-mediated activation such as binding of capsaicin or protons simply modulates the voltage-dependence of the TRPV1 receptors. Therefore, we assume that the introduction of aspartic acid at position T406 directly affects the gating mechanism that is potentially linked to the voltage sensor of the TRPV1 receptor protein.

7.5 The TRPV1 ion channel sensitivity to capsaicin

Capsaicin activates the TRPV1 receptor by binding to an intracellular binding site, which is formed by transmembrane domain 3 and 4 in each of the four subunits of the TRPV1 receptor. We suggest that the binding of capsaicin induces conformational changes in the adjacent structures, which most likely facilitate the opening of the TRPV1 pore. The priming of the $TRPV1_{T406D}$ receptor work best at high concentrations of capsaicin. Therefore, we assume that the binding of capsaicin to the four binding sites of one TRPV1 receptor is necessary to induce the conformational changes, which reverses the $TRPV1_{T406D}$ function. Since, the PKC-mediated phosphorylation of TRPV1 increases the receptor sensitivity to capsaicin (Bhave et al. 2003), we set out to investigate the impact of $TRPV1_{T406}$ mutagenesis on the sensitivity to capsaicin.

The TRPV1 receptor protein sensitivity to capsaicin was investigated by analyzing the capsaicin concentration-response relationship before and after priming with 3.3 µM capsaicin. To prevent the Ca^{2+}-dependent desensitization of TRPV1 receptors we recorded in absence of extracellular Ca^{2+}. The data revealed that the sensitivity to capsaicin of $TRPV1_{WT}$ and most of the $TRPV1_{T406}$ mutants was equal before and after the prolonged application of capsaicin. However, in $TRPV1_{T406D}$ and $TRPV1_{T406E}$ measurements, we found hardly any responses to capsaicin before the prolonged application of 3.3 µM capsaicin. But, after the priming of $TRPV1_{T406D}$ and $TRPV1_{T406E}$ receptors, we observed a significantly increased responsiveness to low capsaicin concentrations, which indicates a sensitization of these receptor proteins. The sensitization of TRPV1 by introducing negatively charged amino acids is in line with the previous mentioned studies. As mentioned before, the PKC-mediated phosphorylation of TRPV1 can be mimicked by replacing the PKC-consensus site with alanine, which prevents the receptor protein sensitization (Mohapatra & Nau 2003; Studer & McNaughton 2010). The use-dependent concentration/response-relationship of $TRPV1_{T406D}$ does not correlate to the observations we made in the TRPV1, Cdk5, p35 co-expression measurements. This supports the hypothesis that the introduction of aspartic acid at residue T406 affects the TRPV1 function in a different way than the Cdk5-dependent phosphorylation. As mentioned before, the mutagenesis of TRPV1 affects every subunit of every receptor protein, whereas the Cdk5-dependent phosphorylation of TRPV1 is more variable.

7.6 Proton and heat induced activation of $TRPV1_{T406}$ mutants

Since $TRPV1_{T406D}$ affects the capsaicin-induced gating mechanism of the TRPV1 receptor protein, we set out to investigate alternative activation mechanisms. Therefore, we investigated the proton and heat-mediated activation of $TRPV1_{T406}$ mutants. The proton binding site is extracellularly located at the outer pore (Aneiros et al. 2011), thus we suggest that the proton-mediated activation of TRPV1 has a different activation mechanism than capsaicin. The analysis of the proton or heat-induced TRPV1-mediated currents revealed that the $TRPV1_{T406}$ mutants carrying a negatively charged amino acid residue showed again a use-dependent behavior. Hardly any TRPV1-mediated response could be evoked in $TRPV1_{T406D}$ expressing cells by the initial stimulation with hot temperatures or low pH.

However, the prolonged activation of the $TRPV1_{T406D}$ with 3.3 µM capsaicin induced an increased responsiveness to heat and low pH. Therefore, we conclude that the introduction of aspartic acid at residue T406 does not directly affect the heat, low pH or capsaicin-mediated activation of TRPV1, but supports the hypothesis that the T406D mutation affects the TRPV1 gating mechanism.

7.7 Single channel properties of $TRPV1_{T406D}$ receptors

In order to investigate the gating mechanism of TRPV1 and $TRPV1_{T406D}$ in detail, we analyzed the single-channel properties. The analysis of single-channel properties is the most accurate method of ion channel characterization, since the function of one receptor protein is observed. The analysis of Studer and McNaughten revealed that the TRPV1 gaiting has different open and closed states, which indicates a complex gating mechanism that includes several conformational changes. Based on their model, the TRPV1 gating is subdivided in three open and four closed states, which were changed by agonist mediated activation, phosphorylation or dephosphorylation (Studer & McNaughton 2010). These findings were in line with our single-channel analysis. We found also three open and four closed states in $TRPV1_{WT}$ and $TRPV1_{T406D}$. Additionally, we found that the low open probability of $TRPV1_{T406D}$, before priming the receptor, is based on the increased length of closed state C4. In conclusion, the $TRPV1_{T406D}$ single-channel properties are in line with our previous electrophysiological results and support the hypothesis that the gating mechanism of $TRPV1_{T406D}$ is modulated. All $TRPV1_{T406D}$ experiments revealed that the initial non-liganded $TRPV1_{T406D}$ conformation shows a limited ion channel function, whereas the priming of the receptor led to wild-type (sensitized) like ion channel characteristics. Therefore, we suggest that the introduction of aspartic acid at position T406 induces conformational changes in the TRPV1 protein, which affect the ion channel gating mechanism.

7.8 The high resolution structure of TRPV1

Our data demonstrate that one amino acid in the intracellular N-terminus of the TRPV1 can affect the ion channel gating mechanism. Position T406 of the TRPV1 sequence is neither located within the capsaicin binding site or ion channel pore, nor directly related to the voltage sensor or another identified region of the protein responsible for heat or proton activation (Choi et al. 2014). Therefore, to shed light on the TRPV1 gating mechanism we made use of the recently published high resolution (3-4 Å) structures of rTRPV1 (Cao et al. 2013). Three distinct rTRPV1 structures are available in the data bases representing the closed, intermediate, and open state. Comparing these structures with focus on T406 revealed interesting details in the protein conformation. It appears that T406 is located in a flexible linker in close proximity to the TRP-domain, and the conformation of this linker seems to differ between the closed and open state. In the closed state T406 is part of the flexible linker, whereas in the open state T406 is integrated into a α-helix. Furthermore, to scrutinize the putative role of T406 in the gating process of the pore, we looked at the all-atom simulation of TRPV1 by Zheng and Qin (Zheng & Qin 2015), which is based on the high resolution structure of rTRPV1 by (Cao et al. 2013). Based on their model the transition pathway includes four functional parts listed in the motional order: i) ankyrin repeats domain (ARD) residue 110-357 ⇨ membrane proximal domain (MPD) residue 358-439 (contains T406) ⇨ C-terminal domain (CTD) 691-719 (including TRP-box) ⇨ Transmembrane domain (TMD) 5-6 (Zheng & Qin 2015). Additionally, the authors analyzed the van der Waals (vdW) energy of the intracellular domains in the closed and open state. Within the intracellular domain, they found that several amino acids have higher vdW energy in the open state than in the closed state. Particularly T406, R409 and M412 showed high vdW energy differences and are strategic positioned interfacing the MPD, the CTD and the TMD. In conclusion these findings support the hypothesis that T406 participates in TRPV1 ion channel gating.

In order to investigate a potential transition pathway we (in cooperation with Prof. C. Ziegler (Department of Biophysics, University of Regensburg)) analyzed the TRPV1 3D structures provided by Cao et al., and Liao et al.

The aim was to identify potential structures or residues of the TRPV1 receptor protein, which connect the Cdk5-mediated phosphorylation or mutagenesis at position T406 to the gating mechanism of TRPV1 ion channels. Therefore, we analyzed the relative distance between the linker domain, including T406, and the TRP domain, which is connected to the pore forming TMD 6. The analysis revealed that the distance between amino acid Y401 (linker domain) and D707 (TRP domain) is different in the open or closed ion channel. In the closed state we measured 3.1 Å between these amino acid residues, whereas, in the intermediate and open state we found a distance of 2.6 Å, which is a distance that facilitates hydrogen bounds. Thus, we assumed that the phosphorylation or mutagenesis of T406 affects the potential interaction between the linker domain (Y401) and the TRP-domain (D707). Moreover, the analysis revealed that residue R499 is in close proximity to the residues of D707 and Y401. Interestingly, R499 is close to the PKA phosphorylation site S501, in the intracellular loop between transmembrane domain 2 and 3, thus we assume that the PKA-dependent phosphorylation of S501 may induce similar functional and conformational changes as the Cdk5-mediated phosphorylation at T406.

7.9 **The TRPV1 transition pathway of Cdk5-mediated phosphorylation**

In order to investigate the TRPV1 gating mechanism, which is affected by the phosphorylation and/or mutagenesis of amino acid T406, we set out to analyze the potential transition pathway in detail. Thus, we generated several TRPV1 receptor protein mutants and characterized the ion channel function by means of electrophysiological recordings. We assume that the potential transition pathway of $TRPV1_{WT}$ or $TRPV1_{T406D}$ receptor proteins is interrupted by introducing alanine at amino acid residue Y401, R499, and D707. The charge or polarity of amino acid residues facilitates the formation of hydrogen bounds, which is necessary for the organization of tertiary structures of proteins. However, the amino acid characteristics of alanine prevent the formation of hydrogen bounds, which might induce an altered protein conformation. Thus, we assume that the mutagenesis of the transition pathway affects the functional properties of TRPV1 and $TRPV1_{T406D}$. Interestingly, we found in all transition pathway mutants a significantly reduced desensitization, in particular in the D707A, Y401A mutants as well as in the double mutant Y401A-D707A.

These results supports our hypothesis that the membrane proximal domain (MPD) and the TRP-domain directly interact and that the interruption of the suggested hydrogen bounds affect the ion channel gating. Moreover, we assume that the close proximity of T406 to Y401 affects the interaction of Y401 and D707. However, the mutagenesis of R499A also prevents the Ca^{2+}-dependent desensitization of TRPV1 receptors. Therefore, we suggest that not only the direct interaction via hydrogen bounds between Y401 and D707 are essential for the TRPV1 ion channel gating, but also the electrostatic properties of the adjacent amino acid residue R499. The close proximity of the phosphorylation sites S501 (PKA) to R499 might indicate that the PKA-mediated phosphorylation of TRPV1 also affects the gating mechanism. The interaction of R499, which resides in the intracellular loop between TMD 2 and 3, with the TRP-domain could be modified. In conclusion, we suggest that the phosphorylation of T406 or S501 has severe consequences on the flexibility of the TRP-domain. Since the TRP-domain is directly connected to the pore forming TMD6, we suggest this transition pathway has severe consequences for the opening and/or closing of the lower gate of the TRPV1 ion channel pore. This hypothesis is supported by the functional characterization of transition-pathway mutants D707A and R499A, revealing the same use-dependent activation as $TRPV1_{T406D}$. Analyzing the sensitivity of transition pathway mutants to capsaicin or protons revealed that these receptor variants were insensitive to the stimulus before priming the receptor protein, whereas the maximal activation increases the responsiveness. However, the analysis of the current-voltage relationship revealed that the mutagenesis of the transition pathway did not change the voltage-dependence of the TRPV1 receptors. In conclusion, the mutagenesis of the transition pathway revealed that the gating mechanism of the TRPV1 receptor protein highly depends on the conformational changes and interactions that occur between the membrane proximal domain (MPD) and the TRP-domain. These conformational changes affect in particular the activation and desensitization kinetics of TRPV1 receptor proteins.

7.10 **The Ca^{2+}-dependent desensitization of TRPV1 mutants**

The Ca^{2+}-dependent desensitization of TRPV1 receptor proteins is important for ion channel modulation, since, the unregulated influx of Ca^{2+} into cells provokes cell death (Studer & McNaughton 2010; Kim et al. 2006; Agopyan et al. 2004; Reilly et al. 2008).

As described before, the TRPV1 desensitization is due to the calcineurin-dependent dephosphorylation of the receptor protein. However, we know very little about the conformational changes that are induced by dephosphorylation or phosphorylation of TRPV1 receptor proteins. Since, calcineurin is activated by the Ca^{2+}/calmodulin complex the accurate interaction between these molecules is required. The N- and C-termini of the TRPV1 receptor are important players in TRPV1 desensitization. Numazaki et al. found that calmodulin binds at the C-terminus (amino acid 765-800) of TRPV1. They revealed that disruption of the calmodulin binding site prevents the Ca^{2+}-dependent receptor desensitization (Numazaki et al. 2003). Similar results were found by Joseph et al. by analyzing the Ca^{2+} dependent desensitization of TRPV1-TRPV3 chimera. They replaced the C-terminus of TRPV1 with the C-terminus of the TRPV3 receptor protein, and found that the chimeric receptor does not desensitize during heat activation (Joseph et al. 2013). Additionally, it is known that the N-terminal binding of ATP to the TRPV1 receptor at amino acid K155 prevents the Ca^{2+}-dependent desensitization (Lau et al. 2012). Since we found a strong Ca^{2+}-dependent desensitization in $TRPV1_{WT}$ and $TRPV1_{T406}$ mutants, we suggest that our TRPV1 mutations did not affect the ATP or calmodulin binding to the N- and C–terminus. Thus, we assume that the Ca^{2+}-dependent dephosphorylation is active in all $TRPV1_{T406}$ and transition pathway mutants, but the conformational changes in the TRPV1 transition pathway prevents the ion channel desensitization. As discussed before, the prevention of Ca^{2+}-dependent desensitization has severe consequence for the TRPV1-mediated nociception. The prolonged influx of cations would initially increase the depolarization, which facilitates the action potential generation, but the unregulated influx of Ca^{2+} could induce axon decline or cell death.

8 Conclusion

The $TRPV1_{T406D}$ and the transition pathway mutants not only showed a reduced desensitization but also a use-dependent activation. Even though the TRPV1 voltage sensing mechanism is not fully understood yet, we suggest that the use-dependent activation and the altered voltage-dependence of $TRPV1_{T406D}$ are based on an altered ion channel structure. The structural and electrophysiological analysis indicates that the mutagenesis of TRPV1 at residue T406D or at the transition pathway induces several conformational changes in the receptor protein. These changes affect the voltage-dependence and other ion channel properties by interrupting the transition pathway of the gating mechanism of the TRPV1 receptor protein. Moreover, we suggest that the prolonged activation of $TRPV1_{T406D}$ with capsaicin induces structural rearrangements of the receptor protein, which led to receptor function that is similar to the $TRPV1_{WT}$. To shed light on the conformational changes that occur during the priming of $TRPV1_{T406D}$ it would be necessary to resolve the structure of the receptor protein before and after priming. These structures would clearly demonstrate the effect of the T406D mutation on the TRPV1 structure. By means of such high resolution 3D structures we would be able to identify potential hydrogen bounds and/or conformational alterations of the TRPV1 receptor. It would be also interesting to investigate the effect of $TRPV1_{T406D}$ on the signal transduction in sensory neurons. We would assume that the initially prevented influx of cations trough the $TRPV1_{T406D}$ ion channel pore would result in neurons that were less excitable. However, the prolonged activation with high concentrations of capsaicin would increase the cation influx and would result in neurons that were more excitable. Moreover, we would assume that the expression of $TRPV1_{T406D}$ in the free nerve endings of sensory neurons induce a complex TRPV1-mediated nociceptive behavior *in vivo*. The phenotype could have an initially low responsiveness to TRPV1-mediated noxious stimuli (hypoalgesia), but the prolonged activation would induce hyperalgesia or allodyina.

9 Materials

9.1 Consumables

Borosilicate glass pipette	GB150EFT-10	Science Products GmbH, Hofheim, Germany
Cell culture dish	Ø 10 cm	TPP, Trasadingen, Switzerland
	Ø 3.5 cm	Sarstedt AG & Co, Nümbrecht, Germany
Cell scraper		TPP, Trasadingen, Switzerland
Centrifuge tube	15 and 50 ml	Corning, Tweksbury, USA
Coverslip	Ø 12, 25 mm	VWR International, Radnor, USA
Eppendorf tube	0.5, 1.5, 2 ml	Eppendorf, Hamburg, Germany
Object slide	76 x 26 mm	Paul Marienfeld GmbH, Königshofen, Germany
sterile filter	0.2 µM	Sarstedt AG & Co, Nümbrecht, Germany
	70 µM	BD Bioscience, Franklin Lakes, USA

9.2 Chemicals

Acrylamide	Carl Roth GmbH & Co KG, Karlsruhe, Germany
Agarose	Peqlab Biotechnologie GmbH, Erlangen, Germany
$BaCl_2$	Merck, Darmstadt, Germany
$CaCl_2$	Carl Roth GmbH & Co KG, Karlsruhe, Germany
Capsaicin	Alomone labs, Jerusalem, Israel
Capsazepine	Cayman Chemical, Michigan, USA
DMSO	Sigma-Aldrich Co., Irvine, UK

dNTP	Bioline GmbH, Luckenwalde, Germany
EDTA	Sigma-Aldrich Co., Steinheim, Germany
EGTA	AppliChem, Darmstadt, Germany
Ethidium bromide	Sigma-Aldrich Co., Steinheim, Germany
Glycerol	Sigma-Aldrich Co., St. Louis, USA
HEPES	Sigma-Aldrich Co., Steinheim, Germany
KCl	Carl Roth GmbH & Co KG, Karlsruhe, Germany
$MgCl_2$	Carl Roth GmbH & Co KG, Karlsruhe, Germany
NaCl	Carl Roth GmbH & Co KG, Karlsruhe, Germany
Orange DNA loading Dye	Peqlab Biotechnologie GmbH, Erlangen, Germany
Penicillin-streptomycin	Sigma-Aldrich Co., St. Louis, USA
Trypsin-EDTA	Life technologies GmbH, Darmstadt, Germany

9.3 **Enzymes and buffers**

Restriction enzyms	New England Biolabs GmbH, Frankfurt a.M., Germany
Buffer 2	New England Biolabs GmbH, Frankfurt a.M., Germany
Buffer Red	Qiagen, Hilden, Germany
CutSmart Buffer	New England Biolabs GmbH, Frankfurt a.M., Germany
Ligase Buffer	Promega GmbH, Mannheim, Germany
Phosphate-buffered saline	Sigma-Aldrich Co., St. Louis, USA

PFUltra HF Polymerase	Aglient Technologies, Santa Clara, USA
PFUltra HF Reaction Buffer	Aglient Technologies, Santa Clara, USA
RKT Buffer	Quiagen GmbH, Hilden, Germany
T4 Ligase	Promega GmbH, Mannheim, Germany
T4 Ligase buffer	New England Biolabs GmbH, Frankfurt a.M., Germany
Taq Polymerase	Roche, Basel, Switzerland

9.4 **Cell culture media**

Alpha MEM Eagle	PAN-Biotech GmbH, Aidenbach, Germany
DMEM	Life technologies GmbH, Darmstadt, Germany
Fetal calf serum	Sigma-Aldrich Co., St. Louis, USA
LB Medium	Carl Roth GmbH & Co KG, Karlsruhe, Germany
Opti-MEM	Life technologies GmbH, Darmstadt, Germany

9.5 **Solutions**

Ampicilin stock solution	100 mg/ml in H_2O
Ca^{2+}- Ringer's extracellular solution:	140 mM NaCl
(pH 7.35) 290 ± 10 mosmol/kg	5 mM KCl
	2 mM $CaCl_2$
	2 mM $MgCl_2$
	10 mM HEPES
Ringer's extracellular solution:	140 mM NaCl
Ca^{2+}-free 290 ± 10 mosmol/kg	5 mM KCl
(pH 7.35)	5 mM EGTA
	2 mM $MgCl_2$
	10 mM HEPES
Pipette Solution A:	140 mM CsCl
(pH 7.35) 300 ± 10 mosmol/kg	1 mM $MgCl_2$
	0.1 mM $CaCl_2$
	5 mM EGTA
	10 mM HEPES
Pipette Solution B:	145 mM CsCl
(pH 7.35) 300 ± 10 mosmol/kg	1 mM $CaCl_2$
	2 mM $MgCl_2$
	11 mM EGTA
	2 mM HEPES
LB-Agar	15 g Agar pro 1 L LB-Medium
LB (Luria-Bertani)-Medium:	10 g/l Trypton
(pH 7.4)	5 g/l Yeast extract
	10 g/l NaCl

TBE buffer:	0.9 M Tris
	0.9 M Borsäure
	4 mM EDTA
Trypsin-EDTA-Solution:	0.5 g/l Trypsin
	0.2 g/l EDTA
SOC medium	10 mM NaCl
	10 mM $MgCl_2$
	10 mM $MgSO_4$
	20 mM glucose
	2% tryptone
	0.5% yeast extract

9.6 **Devices**

Cell culture microscope	Olympus IX70	Olympus, Tokyo, Japan
4x Objective	UPlanFI 0.13 Ph1	Olympus, Tokyo, Japan
10x Objective	0.30 Ph2	Olympus, Tokyo, Japan
20x Objective	LCPlan 0.4	Olympus, Tokyo, Japan
Patch-clamp microscope 1	Axio VertA1	Carl Zeiss GmbH, Jena, Germany
10x Objective	A-Plan 0.25 Ph1	Carl Zeiss GmbH, Jena, Germany
40x Objective	LD-Plan-Neofluar 0.6 Ph2 Korr	Carl Zeiss GmbH, Jena, Germany
63x Objective	LD-Plan-Neofluar 0.75 Korr	Carl Zeiss GmbH, Jena, German
Patch-clamp microscope 2	Axiovert 35M	Carl Zeiss GmbH, Jena, Germany
5x Objective	CP-Acromat 0.12	Carl Zeiss GmbH, Jena, Germany
10x Objective	LD-Plan-Neofluar 0.3	Carl Zeiss GmbH, Jena, Germany
32x Objective	Acrosigmat 0.4 Ph1	Carl Zeiss GmbH, Jena, Germany

Light source	HXP 75W	Osram GmbH, Munich, Germany
	XBO 75W/2	Osram GmbH, Munich, Germany
Patch-clamp amplifier	EPC-10	HEKA Electronic, Lamprecht, Germany
Micromanipulator:	1U RACK	Scientifica, Uckfield, UK
	MHW-103	Narishige, London, UK
Perfusion system:	VM8 perfusion	Ala Sientific Instruments, Farmigdale, USA
Faraday cage		AMETEK GmbH, Meerbusch, Germany
Vibration damping table		TMC, Peabody, USA
Centrifuges:	Biofuge pico	Thermo Scientific, Rockford, USA
	Centrifuge 5415R	Eppendorf, Hamburg, Germany
	Megafuge 1.0	Thermo Scientific, Rockford, USA
	Megafuge 2.0 R	Thermo Scientific, Rockford, USA
DMZ universal puller		Zeitz-Instruments GmbH, Munich, Germany
Incubator Heracell 150		Thermo Scientific, Rockford, USA
Nanodrop		Nanodrop Technologies Inc., Wilmington, USA
Neubauer chamber		Brand GmbH & Co. KG, Wertheim, Germany
ThermoCycler		Bio-Rad, Laboratories, GmbH, Munich, Germany
Sterile work bench		Herasafe KS12 ThermoScientific, Waltham, USA

9.7 Software

IGOR Pro	WaveMetrics, Oregon, USA
PatchMaster	HEKA Electronic, Lamprecht, Germany
Pulse	HEKA Electronic, Lamprecht, Germany
PulseFit	HEKA Electronic, Lamprecht, Germany
SnapGene	GSL Biotech, Chicago, USA
PyMol 1.6	Schrödinger, LLC, Mannheim/Munich, Germany

9.8 DNA Oligonucleotides:

9.8.1 Overlap extension PCR primer

Forward primer A:	5’-CTC TGG CTA ACT AGA GAA CCC ACT GC-3’
Reverse primer B:	5’-CTG ATC AGC GAG CTC TAG CAT TTA GG-3’

TRPV1 T406A:

Reverse primer A:	5’-CAT GTC ATG ACG GTT AGG GGC-3’
Forward primer B:	5’-ATC GCT TAC AGC AGC AGT GAG GC-3’

TRPV1 A406D:

Reverse primer A:	5’-CAT GTC ATG ACG GTT AGG GTC-3’
Forward primer B:	5’-AT CGC TTA CAG CAG CAG TGA GGA-3’

TRPV1 D406E:

Reverse primer A:	5’-CAT GTC ATG ACG GTT AGG TTC-3’
Forward primer B:	5’-G CTT ACA GCA GCA GTG AGG AAC-3’

9.8.2 pGEM-T Vector cloning primer

Restriction site primer

BstEII forward:	5‘-CTG GTG ACC CTC TTG GTG GAG-3’
SacII reverse:	5‘-GTA GGC AGC CGC GGT GAA GAT GAT C-3’
SacII forward:	5‘-GAT CAT CTT CAC CGC GGC TG-3’
Xba reverse:	5‘-CAC TAT AGA ATA GGG CCC TCT AGA TGC ATG-3’

Mutagenesis primer

TRPV1 T406R:

Reverse primer A: 5’-GTC ATG ACG GTT AGG TCT CTC ACT GCT GCT GTA-3’

Forward primer B: 5’-TAC AGC AGC AGT GAG AGA CCT AAC CGT CAT GAC-3’

TRPV1 T406Y:

Reverse primer A: 5’-GTC ATG ACG GTT AGG GTA CTC ACT GCT GCT GTA-3’

Forward primer B: 5’-TAC AGC AGC AGT GAG TAC CCT AAC CGT CAT GAC-3’

TRPV1 T406H:

Reverse primer A: 5’-GTC ATG ACG GTT AGG GTG CTC ACT GCT GCT GTA-3’

Forward primer B: 5’-TAC AGC AGC AGT GAG CAC CCT AAC CGT CAT GAC-3’

TRPV1 T406K:

Reverse primer A: 5’-GTC ATG ACG GTT AGG TTT CTC ACT GCT GCT GTA-3’

Forward primer B: 5’-TAC AGC AGC AGT GAG AAA CCT AAC CGT CAT GAC-3’

TRPV1 T406I:

Reverse primer A: 5’-GTC ATG ACG GTT AGG TAT CTC ACT GCT GCT GTA-3’

Forward primer B: 5’-TAC AGC AGC AGT GAG ATA CCT AAC CGT CAT GAC-3’

TRPV1 T406P:

Reverse primer A: 5’-GTC ATG ACG GTT AGG GGG CTC ACT GCT GCT GTA-3’

Forward primer B: 5’-TAC AGC AGC AGT GAG CCC CCT AAC CGT CAT GAC-3’

TRPV1 T406M:

Reverse primer A: 5’-GTC ATG ACG GTT AGG CAT CTC ACT GCT GCT GTA -3’

Forward primer B: 5’-TAC AGC AGC AGT GAG ATG CCT AAC CGT CAT GAC -3’

TRPV1 T406F:

Reverse primer A: 5’-GTC ATG ACG GTT AGG GAA CTC ACT GCT GCT GTA -3’

Forward primer B: 5’-TAC AGC AGC AGT GAG TTC CCT AAC CGT CAT GAC -3’

TRPV1 P407A:

Reverse primer A: 5’-CAT GTC ATG ACG GTT AGC GGT CTC ACT GCT GCT -3’

Forward primer B: 5’-AGC AGC AGT GAG ACC GCT AAC CGT CAT GAC ATG -3’

TRPV1 D707A:

Reverse primer A:	5‘-AGC TCT TCT CTG TAG CCA GGA TGG TG-3’
Forward primer B:	5‘-CAC CAT CCT GGC TAC AGA GAA GAG CT-3’

TRPV1 R499A:

Reverse primer A:	5‘-GG TCG CGC CTG CAG GAA ATA TTG AAT CC-3’
Forward primer B:	5‘-CAA TAT TTC CTG CAG GCG CGA CCA TCC CTC-3’

TRPV1 Y401A:

Reverse primer A:	5‘-C ACT GCT GCT GGC AGC GAT CAC CTC C-3’
Forward primer B:	5‘-G GAG GTG ATC GCT GCC AGC AGC AGT G-3’

9.8.3 **TRPV1-GFP fusion protein Primer**

rTRPV1-AfeI-F:	5‘-AAA AGC GCT AGG ATG GAA CAA CGG GCT-3’
rTRPV1-ApaI-R:	5’- A AAG GGC CCT CTC CCC TGG GAC CAT GGA A-3’

9.8.4 **Sequencing Primer**

pGEM-T sequencing primer

Reverse M13:	5’-AGC GGA TAA CAA TTT CAC ACA GGA-3’
Forward M13:	5’-CGC CAG GGT TTT CCC AGT CAC GAC-3’

pCDNA3 sequencing primer

Forward pCDNA3 T7:	5’-TAA TAC GAC TCA CTA TAG GG-3’
Reverse pCDNA BGH:	5’-TAG AAG GCA CAG TCG AGG-3’
TRPV1_550:	5'-GTC TGC TAA AAG CCA TGC TCA A -3'
TRPV1_1550:	5'-CCC TAT AAG CTG AAA AAC ACC -3'

TRPV1-GFP sequencing primer

rV1-Y401_B:	5‘-C ACT GCT GCT GGC AGC GAT CAC CTC C-3’
rV1-Y401_F:	5’-G GAG GTG ATC GCT GCC AGC AGC AGT G-3’
eGFP-50-R:	5’-TT GCC GGT GGT GCA GAT G-3’
eGFP-200-F:	5’-CAC TAC CTG AGC ACC CAG T-3’
SV40-R:	5’- GAT GCT ATT GCT TTA TTT GTA ACC ATT A-3’

10 Bibliography

Agopyan, N. et al., **2004**. TRPV1 receptors mediate particulate matter-induced apoptosis. *Am J Physiol Lung Cell Mol Physiol.*, 286, pp.563–572.

Aneiros, E. et al., **2011**. The biophysical and molecular basis of TRPV1 proton gating. *The EMBO journal*, 30(6), pp.994–1002.

Bhave, G. et al., **2002**. cAMP-dependent protein kinase regulates desensitization of the capsaicin receptor (VR1) by direct phosphorylation. *Neuron*, 35(4), pp.721–731.

Bhave, G. et al., **2003**. Protein kinase C phosphorylation sensitizes but does not activate the capsaicin receptor transient receptor potential vanilloid 1 (TRPV1). *PNAS*, 100(21), pp.12480–12485.

Bölcskei, K. et al., **2005**. Investigation of the role of TRPV1 receptors in acute and chronic nociceptive processes using gene-deficient mice. *Pain*, 117(3), pp.368–376.

Cao, E. et al., **2013**. TRPV1 structures in distinct conformations reveal activation mechanisms. *Nature*, 504(7478), pp.113–8.

Caterina, M.J. et al., **2000**. Impaired Nocicieption and Pain Sensation in Mice Lacking the Capsaicin Receptor. *Science*, 288, pp.306–313.

Caterina, M.J. et al., **1997**. The capsaicin receptor: a heat-activated ion channel in the pain pathway. *Nature*, 389(6653), pp.816–824.

Cesare, P. et al., **1999**. Specific involvement of PKC-ϵ in sensitization of the neuronal response to painful heat. *Neuron*, 23(3), pp.617–624.

Choi, S.-I. et al., **2014**. Are Sensory TRP Channels Biological Alarms for Lipid Peroxidation? *International Journal of Molecular Sciences*, 15(9), pp.16430–16457.

Christoph, T. et al., **2006**. Silencing of vanilloid receptor TRPV1 by RNAi reduces neuropathic and visceral pain in vivo. *Biochemical and Biophysical Research Communications*, 350(1), pp.238–243.

Chuang, H.H. et al., **2001**. Bradykinin and nerve growth factor release the capsaicin receptor from PtdIns(4,5)P2-mediated inhibition. *Nature*, 411(6840), pp.957–962.

Chung, M.-K., Güler, A.D. & Caterina, M.J., **2008**. TRPV1 shows dynamic ionic selectivity during agonist stimulation. *Nature neuroscience*, 11(5), pp.555–564.

Clapham, D.E., **2003**. TRP channels as cellular sensors. *Nature*, 426(6966), pp.517–524.

Cortright, D.W. & Szallasi, A., **2004**. Biochemical pharmacology of the vanilloid receptor TRPV1. *European Journal of Biochemistry*, 271(10), pp.1814–1819.

Cosens, D.J. & Manning, a, **1969**. Abnormal electroretinogram from a Drosophila mutant. *Nature*, 224(5216), pp.285–287.

Culshaw, A.J. et al., **2006**. Identification and biological characterization of 6-aryl-7-isopropylquinazolinones as novel TRPV1 antagonists that are effective in models of chronic pain. *Journal of medicinal chemistry*, 49(2), pp.471–474.

Davis, J.B. et al., **2000**. Vanilloid receptor-1 is essential for inflammatory thermal hyperalgesia. *Nature*, 405, pp.183–187.

Dedov, V.N. et al., **2002**. Gingerols: a novel class of vanilloid receptor (VR1) agonists. *British journal of pharmacology*, 137(6), pp.793–798.

Dessaint, J. et al., **2004**. Yohimbine inhibits firing activities of rat dorsal root ganglion neurons by blocking Na+ channels and vanilloid VR1 receptors. *European Journal of Pharmacology*, 485(1-3), pp.11–20.

Dhaka, A., Viswanath, V. & Patapoutian, A., **2006**. Trp ion channels and temperature sensation. *Annual review of neuroscience*, 29, pp.135–161.

Docherty, R.J., Yeats, J.C. & Piper, a S., **1997**. Capsazepine block of voltage-activated calcium channels in adult rat dorsal root ganglion neurones in culture. *British journal of pharmacology*, 121(7), pp.1461–1467.

Erler, I. et al., **2004**. Ca2+-selective Transient Receptor Potential V Channel Architecture and Function Require a Specific Ankyrin Repeat. *Journal of Biological Chemistry*, 279(33), pp.34456–34463.

Gees, M., Colsoul, B. & Nilius, B., **2010**. The role of transient receptor potential cation channels in Ca2+ signaling. *Cold Spring Ahrb Perspect Biol*, p.a003962.

Gorman, C., Padmanabhan, R. & Howard, B.H., **1983**. High efficiency DNA-mediated transformation of primate cells. *Science*, 221(4610), pp.551–553.

Gregorio-Teruel, L. et al., **2014**. Mutation of I696 and W697 in the TRP box of vanilloid receptor subtype I modulates allosteric channel activation. *The Journal of general physiology*, 143(3), pp.361–75.

Gunthorpe, M.J. et al., **2002**. The diversity in the vanilloid (TRPV) receptor family of ion channels. *Trends in Pharmacological Sciences*, 23(4), pp.183–191.

Gunthorpe, M.J. et al., **2000**. Voltage- and time-dependent properties of the recombinant rat vanilloid receptor (rVR1). *The Journal of Physiology*, 525, pp.747–759.

Haslwanter, T. et al., **2013**. Ch: 6 Somatosensory System. In *Sensory Systems*. Free Software Foundation, Inc., pp. 141–149.

Hellwig, N., **2005**. Homo- and heteromeric assembly of TRPV channel subunits. *Journal of Cell Science*, 118(5), pp.917–928.

Higuchi, R., Krummel, B. & Saiki, R.K., **1988**. A general method of in vitro preparation and specific mutagenesis of DNA fragments: study of protein and DNA interactions. *Nucleic acids research*, 16(15), pp.7351–7367.

Ho, K.W., Ward, N.J. & Calkins, D.J., **2012**. TRPV1: a stress response protein in the central nervous system. *American journal of neurodegenerative disease*, 1(1), pp.1–14.

Hwang, S.W. et al., **2000**. Direct activation of capsaicin receptors by products of lipoxygenases: endogenous capsaicin-like substances. *PNAS*, 97(11), pp.6155–6160.

Jara-Oseguera, A., Simon, S. a & Rosenbaum, T., **2008**. TRPV1: on the road to pain relief. *Current molecular pharmacology*, 1(3), pp.255–269.

Jendryke, T. et al., **2016**. TRPV1 function is modulated by Cdk5-mediated phosphorylation: insights into the molecular mechanism of nociception. *Scientific Reports*, p.6:srep22007.

Jin, X. et al., **2004**. Modulation of TRPV1 by nonreceptor tyrosine kinase, c-Src kinase. *Am J of Cell physiology*, 287(2), pp.558–563.

Johnson, L.N. & Barford, D., **1993**. The effects of phosphorylation on the structure and function of proteins. *Annual Review of Biophysics and Biomolecular Structure*, 22, pp.199–232.

Jordt, S.E. & Julius, D., **2002**. Molecular basis for species-specific sensitivity to “hot” chili peppers. *Cell*, 108(3), pp.421–430.

Jordt, S.E., Tominaga, M. & Julius, D., **2000**. Acid potentiation of the capsaicin receptor determined by a key extracellular site. *PNAS*, 97(14), pp.8134–8139.

Joseph, J. et al., **2013**. Carboxyl-terminal Domain of Transient Receptor Potential Vanilloid 1 Contains Distinct Segments Differentially Involved in Capsaicin- and Heat-induced Desensitization. *J Biol Chem.*, 288(50), pp.35690–35702.

Jung, J. et al., **2002**. Agonist Recognition Sites in the Cytosolic Tails of Vanilloid Receptor 1. *Journal of Biological Chemistry*, 277(46), pp.44448–44454.

Jung, J. et al., **2004**. Phosphorylation of Vanilloid Receptor 1 by Ca 2+/Calmodulin-dependent Kinase II Regulates Its Vanilloid Binding. *Journal of Biological Chemistry*, 279(8), pp.7048–7054.

Kandel, E.R. et al., **2000**. Ch: 22 The Bodily Senses. In *Principles of neuronal science*. McGraw-Hill Companies, pp. 431–435.

Kim, S.R. et al., **2006**. Transient receptor potential vanilloid subtype 1 mediates microglial cell death in vivo and in vitro via Ca2+-mediated mitochondrial damage and cytochrome c release. *J Immunol.*, (177), pp.4322–4329.

Koplas, P.A., Rosenberg, R.L. & Oxford, G.S., **1997**. The role of calcium in the desensitization of capsaicin responses in rat dorsal root ganglion neurons. *The Journal of neuroscience*, 17(10), pp.3525–3537.

Latorre, R., Zaelzer, C. & Brauchi, S., **2009**. Structure–functional intimacies of transient receptor potential channels. *Quarterly Reviews of Biophysics*, 42(03), p.201.

Lau, S.-Y., Procko, E. & Gaudet, R., **2012**. Distinct properties of Ca2+-calmodulin binding to N- and C-terminal regulatory regions of the TRPV1 channel. *The Journal of General Physiology*, 140(5), pp.541–555.

Liao, M. et al., **2013**. Structure of the TRPV1 ion channel determined by electron cryo-microscopy. *Nature*, 504(7478), pp.107–12.

Lishko, P. V. et al., **2007**. The Ankyrin Repeats of TRPV1 Bind Multiple Ligands and Modulate Channel Sensitivity. *Neuron*, 54(6), pp.905–918.

Liu, J. et al., **2015**. Phosphorylation of TRPV1 by cyclin-dependent kinase 5 promotes TRPV1 surface localization, leading to inflammatory thermal hyperalgesia. *Experimental Neurology*, 273, pp.253–262.

Liu, L. & Simon, S. a, **1997**. Capsazepine, a vanilloid receptor antagonist, inhibits nicotinic acetylcholine receptors in rat trigeminal ganglia. *Neuroscience letters*, 228(1), pp.29–32.

Liu, L. & Simon, S. a, **1996**. Similarities and differences in the currents activated by capsaicin, piperine, and zingerone in rat trigeminal ganglion cells. *Journal of neurophysiology*, 76(3), pp.1858–1869.

Lopshire, J.C. & Nicol, G.D., **1998**. The cAMP transduction cascade mediates the prostaglandin E2 enhancement of the capsaicin-elicited current in rat sensory neurons: whole-cell and single-channel studies. *The Journal of neuroscience*, 18(16), pp.6081–6092.

Lukacs, V. et al., **2007**. Dual Regulation of TRPV1 by Phosphoinositides. *Journal of Neuroscience*, 27(26), pp.7070–7080.

Ma, W. & Quirion, R., **2007**. Inflammatory mediators modulating the transient receptor potential vanilloid 1 receptor: therapeutic targets to treat inflammatory and neuropathic pain. *Expert Opin. Ther. Targets*, 11(3), pp.307–320.

Matta, J. a., Miyares, R.L. & Ahern, G.P., **2007**. TRPV1 is a novel target for omega-3 polyunsaturated fatty acids. *The Journal of Physiology*, 578(2), pp.397–411.

Matta, J.A. & Ahern, G.P., **2007**. Voltage is a partial activator of rat thermosensitive TRP channels. *The Journal of Physiology*, 2, pp.469–482.

McNamara, F.N., Randall, A. & Gunthorpe, M.J., **2005**. Effects of piperine, the pungent component of black pepper, at the human vanilloid receptor (TRPV1). *British journal of pharmacology*, 144(6), pp.781–790.

Minke, B. & Cook, B., **2002**. TRP channel proteins and signal transduction. *Physiological reviews*, 82(2), pp.429–472.

Mohapatra, D.P. & Nau, C., **2003**. Desensitization of Capsaicin-activated Currents in the Vanilloid Receptor TRPV1 Is Decreased by the Cyclic AMP-dependent Protein Kinase Pathway. *Journal of Biological Chemistry*, 278(50), pp.50080–50090.

Moiseenkova-Bell, V.Y. et al., **2008**. Structure of TRPV1 channel revealed by electron cryomicroscopy. *PNAS*, 105(21), pp.7451–7455.

Montell, C. & Rubin, G.M., **1989**. Molecular characterization of the Drosophila trp locus: a putative integral membrane protein required for phototransduction. *Neuron*, 2(4), pp.1313–1323.

Neher, E. & Sakmann, B., **1976**. Single-channel currents recorded from membrane of denervated frog muscle fibres. *Nature*, 260, pp.799 – 802.

Nordmann, G.C., **2015**. *The TRPV1 ion channel: Reconstitution in giant unilamellar vesicles and characterization of heat-evoked responses of T406D mutants, Master Thesis, Department of Psychiatry and Psychotherapy, University of Regensburg*.

Numazaki, M. et al., **2002**. Direct phosphorylation of capsaicin receptor VR1 by protein kinase Cε and identification of two target serine residues. *Journal of Biological Chemistry*, 277(16), pp.13375–13378.

Numazaki, M. et al., **2003**. Structural determinant of TRPV1 desensitization interacts with calmodulin. *PNAS*, 100(13), pp.8002–8006.

Oseguera, A.J. et al., **2007**. On the Mechanism of TBA Block of the TRPV1 Channel. *Biophysical Journal*, 92(11), pp.3901–3914.

Pareek, T.K. et al., **2006**. Cyclin-dependent kinase 5 activity regulates pain signaling. *PNAS*, 103(3), pp.791–796.

Pareek, T.K. et al., **2007**. Cyclin-dependent kinase 5 modulates nociceptive signaling through direct phosphorylation of transient receptor potential vanilloid 1. *PNAS*, 104(2), pp.660–665.

Patapoutian, A. et al., **2003**. Sensory systems: ThermoTRP channels and beyond: mechanisms of temperature sensation. *Nature Reviews Neuroscience*, 4(7), pp.529–539.

Pearce, L. V et al., **2004**. Evodiamine functions as an agonist for the vanilloid receptor TRPV1. *Organic & biomolecular chemistry*, 2(16), pp.2281–2286.

De Petrocellis, L. et al., **2001**. The vanilloid receptor (VR1)-mediated effects of anandamide are potently enhanced by the cAMP-dependent protein kinase. *Journal of Neurochemistry*, 77(6), pp.1660–1663.

Premkumar, L.S. et al., **2004**. Enhancement of potency and efficacy of NADA by PKC-mediated phosphorylation of vanilloid receptor. *Journal of neurophysiology*, 91(3), pp.1442–1449.

Premkumar, L.S. & Ahern, G.P., **2000**. Induction of vanilloid receptor channel activity by protein kinase C. *Nature*, 408, pp.985–90.

Prescott, E.D. & Julius, D., **2003**. A modular PIP2 binding site as a determinant of capsaicin receptor sensitivity. *Science*, 300(16), pp.1284–1288.

Price, T.J. et al., **2004**. Modulation of trigeminal sensory neuron activity by the dual cannabinoid-vanilloid agonists anandamide, N-arachidonoyl-dopamine and arachidonyl-2-chloroethylamide. *British journal of pharmacology*, 141(7), pp.1118–1130.

Puntambekar, P., **2004**. Direct Interaction of Adenosine with the TRPV1 Channel Protein. *Journal of Neuroscience*, 24(14), pp.3663–3671.

Rathee, P.K. et al., **2002**. PKA/AKAP/VR-1 module: A common link of Gs-mediated signaling to thermal hyperalgesia. *The Journal of neuroscience*, 22(11), pp.4740–4745.

Reilly, C.A. et al., **2008**. Calcium-dependent and independent mechanisms of capsaicin receptor (TRPV1)-mediated cytokine production and cell death in human bronchial epithelial cells. *J Biochem Mol Toxicol.*, 19(4), pp.266–275.

Rosenbaum, T. et al., **2004**. Ca2+/calmodulin modulates TRPV1 activation by capsaicin. *The Journal of general physiology*, 123(1), pp.53–62.

Rosenbaum, T. & Simon, S.A., **2004**. Chapter 5: TRPV1 Receptors and Signal Transduction. In *TRP Ion Channel Function in Sensory Transduction and Cellular Signaling Cascades.* Liedtke WB, Heller S, editors.

Ross, R. a, **2003**. Anandamide and vanilloid TRPV1 receptors. *British journal of pharmacology*, 140(5), pp.790–801.

Saiki, R.K. et al., **1988**. Primer-directed enzymatic amplification of DNA with a thermostable DNA polymerase. *Science*, 239(4839), pp.487–491.

Schladt, M., **2015**. *Biophysical and pharmacological characterization of TRPV1 wild type- and ion channels. Master Thesis, Department of Psychiatry and Psychotherapy, University of Regensburg*.

Stein, A.T. et al., **2006**. Phosphoinositide 3-kinase binds to TRPV1 and mediates NGF-stimulated TRPV1 trafficking to the plasma membrane. *The Journal of general physiology*, 128(5), pp.509–522.

Studer, M. & McNaughton, P. a, **2010**. Modulation of single-channel properties of TRPV1 by phosphorylation. *The Journal of physiology*, 588(Pt 19), pp.3743–3756.

Szallasi, a & Blumberg, P.M., **1989**. Resiniferatoxin, a phorbol-related diterpene, acts as an ultrapotent analog of capsaicin, the irritant constituent in red pepper. *Neuroscience*, 30(2), pp.515–520.

Tóth, A. et al., **2002**. Thapsigargin binds to and inhibits the cloned vanilloid receptor-1. *Biochemical and Biophysical Research Communications*, 293, pp.777–782.

Ufret-Vincenty, C. a. et al., **2011**. Localization of the PIP2 sensor of TRPV1 ion channels. *Journal of Biological Chemistry*, 286(11), pp.9688–9698.

Utreras, E. et al., **2013**. TGF-β1 sensitizes TRPV1 through Cdk5 signaling in odontoblast-like cells. *Molecular pain*, 9, pp.1–14.

Varga, A. et al., **2006**. Relative roles of protein kinase A and protein kinase C in modulation of transient receptor potential vanilloid type 1 receptor responsiveness in rat sensory neurons in vitro and peripheral nociceptors in vivo. *Neuroscience*, 140(2), pp.645–657.

Vellani, V. et al., **2001**. Protein kinase C activation potentiates gating of the vanilloid receptor VR1 by capsaicin, protons, heat and anandamide. *Journal of Physiology*, 534(3), pp.813–825.

Venkatachalam, K. & Montell, C., **2007**. TRP channels. *Annual review of biochemistry*, 76, pp.387–417.

Vennekens, R. et al., **2000**. Permeation and gating properties of the novel epithelial Ca2+ channel. *Journal of Biological Chemistry*, 275(6), pp.3963–3969.

Voets, T. et al., **2004**. The principle of temperature-dependent gating in cold- and heat-sensitive TRP channels. *Nature*, 430(7001), pp.748–754.

Vriens J., A.G.N.B. et al., **2009**. Pharmacology of Vanilloid Transient Receptor Potential Cation Channels. *Mol. Pharmacol.*, 75(6), pp.1262–1279.

Xing, B.-M. et al., **2012**. Cyclin-Dependent Kinase 5 Controls TRPV1 Membrane Trafficking and the Heat Sensitivity of Nociceptors through KIF13B. *Journal of Neuroscience*, 32(42), pp.14709–14721.

Xu, S. et al., **2008**. 17beta-Estradiol Activates Estrogen Receptor beta-Signalling and Inhibits Transient Receptor Potential Vanilloid Receptor 1 Activation By Capsaicin in Adult Rat Nociceptor Neurons. *Endocrinology*, 149(11), pp.5540–5548.

Yang, B.H. et al., **2003**. Activation of vanilloid receptor 1 (VR1) by eugenol. *Journal of dental research*, 82(10), pp.781–785.

Yang, Y.R. et al., **2007**. Activation of cyclin-dependent kinase 5 (Cdk5) in primary sensory and dorsal horn neurons by peripheral inflammation contributes to heat hyperalgesia. *Pain*, 127(1-2), pp.109–120.

Yao, J. & Qin, F., **2009**. Interaction with phosphoinositides confers adaptation onto the TRPV1 pain receptor. *PLoS Biology*, 7(2), pp.0350–0363.

Yue, L. et al., **2001**. CaT1 manifests the pore properties of the calcium-release-activated calcium channel. *Nature*, 410(6829), pp.705–709.

Zhang, X., Huang, J. & McNaughton, P.A., **2005**. NGF rapidly increases membrane expression of TRPV1 heat-gated ion channels. *The EMBO journal*, 24(24), pp.4211–4223.

Zheng, W. & Qin, F., **2015**. A combined coarse-grained and all-atom simulation of TRPV1 channel gating and heat activation. *The Journal of General Physiology*, 145(5), pp.443–456.

11 Appendix

11.1 Publications

TRPV1 function is modulated by Cdk5-mediated phosphorylation: insights into the molecular mechanism of nociception.
Jendryke T, Prochazkova M, Hall BE, Nordmann GC, Schladt M, Milenkovic VM, Kulkarni AB, Wetzel CH.
Scientific Reports. 2016 Feb 23;6:22007.
doi: 10.1038/srep22007.

Bestrophin 1 is indispensable for volume regulation in human retinal pigment epithelium cells.
Milenkovic A, Brandl C, Milenkovic VM, **Jendryke T**, Sirianant L, Wanitchakool P, Zimmermann S, Reiff CM, Horling F, Schrewe H, Schreiber R, Kunzelmann K, Wetzel CH, Weber BH.
Proc Natl Acad Sci U S A. 2015 May 19;112(20):E2630-9.
doi: 10.1073/pnas.1418840112. Epub 2015 May 4.

11.2 Poster

TRPV1 is sensitized by CDK5-dependent phosphorylation

Thomas Jendryke, Christian Wetzel

International Workshop on Transient Receptor Potential (TRP) Channels,

Valencia (Spanien), 2012

Functional characterization of the CDK5-dependent TRPV1 phosphorylation

Thomas Jendryke, Christian Wetzel

The 10th Göttingen Meeting of the German Neuroscience Society,

Göttingen (Deutschland), 2013

11.3 **Danksagung**

Zu guter Letzt möchte ich mich bei allen bedanken, die direkt oder indirekt zum Gelingen dieser Arbeit beigetragen haben.

Ganz herzlich bedanke ich mich bei Herrn Prof. Dr. C. Wetzel für die Möglichkeit an diesem spannenden Thema zu arbeiten. Vielen Dank auch für die hervorragende Betreuung und die vielen interessanten Diskussionen auch abseits der Wissenschaft.

Prof. Dr. R. Warth danke ich für die freundliche Übernahme des Korreferates

Prof. Dr. R. Rupprecht und Prof. Dr. Dr. Dr. H. Hatt danke ich für die Förderung, sowie für das Interesse an meiner Arbeit.

Ganz besonders danke ich Vladimir, Tatjana und Angelika für die tolle Zusammenarbeit und für alle wissenschaftlichen und nicht wissenschaftlichen Diskussionen. Es hat mir viel Freude bereitet mit euch im Labor zu arbeiten.

Dem gesamten Forschungsteam des Lehrstuhls für Psychiatrie und Psychotherapie danke ich für die tolle Arbeitsatmosphäre und für die großartige und zuverlässige Unterstützung.

Ich möchte mich auch bei allen Studenten bedanken, die ich im Verlauf meiner Promotion betreut habe. Insbesondere bei Moritz und Gregory für die tolle Zeit im und außerhalb des Labors.

Danken möchte ich auch den Mitarbeitern des Lehrstuhls für Zellphysiologie der Ruhr-Universität Bochum für die tolle Arbeitsatmosphäre und die tolle Zeit die wir hatten.

Ein ganz besonderer Dank gilt meiner Familie die immer an mich geglaubt und mich jederzeit Unterstützt hat. Insbesondere danke ich auch bei meiner Freundin Miriam für die Geduld und Unterstützung.